REMOTE SENSING OF MICRO POLLUTANTS IN WATER USING A FIBRE OPTIC ANALYSIS SYSTEM

Kieran Higgins, B.Sc. (Applied Physics)

A thesis submitted to Dublin City University
in candidacy for the Degree of Master of Science

July 1993

I hereby declare that none of the material contained in this thesis has been used in any other submission for any other award. Further, that the contents of this thesis are the sole work of the author except where an acknowledgement has been made for any assistance received.

Supervisor: Dr. Vincent Ruddy
School of Applied Physical Sciences
Dublin City University

Dedication

I dedicate this work to my parents, Evelyn and Micheál who have always been supportive of everything I have attempted; shared my enjoyment when I have succeeded, my dissapointment when I have not and who have put up with my impatience in between times. I would like also to dedicate this work to my sister Ethna who helped me more than I could ever help her this summer.

Declaration

I hereby certify that this material, which I now submit for assessment on the programme of study leading to the award of Master of Science, is entirely my own work and has not been taken from the work of others save and to the extent that such work has been cited and acknowledged within the text of my work.

Signed: _____ Date: 6/9/93

Candidate

Acknowledgement

But for the efforts of a large number of people this work would never have seen the light of day. I would like to take this opportunity to thank some of them. Where to start ?...

To my brother Ger and sister Sinéad for always being there.
To little Dee.
To all the boys in the lab; Simon, Dave, Ferg, Kieran, Gerry B, Jude and also everyone in "Optronics Ireland", DCU.
To Ger, Charles, Kev and Brian.
To all the residents of 41 Walnut Court and "Rossio".
To Des and Cian, for constructive ideas, excellent workmanship and continuous dedication to quality.
To Willie and Geraldine for helping me put it together.
To Joe, Al and Mike for all their help.
To all the members of the Physics Staff, DCU for 6 great years.
To my external examiner Dr. A Scott, U.C.D.
To Dr.Brian McCraith for all his help and support and his keen interest.
Above all, thanks to Dr. Vince Ruddy, whose help and advice was invaluable, and who was generous to a fault with his time during the course of this work.

Before I proceed, I would like to thank anyone else who should be on this page but is not.

Go raibh míle maith agaibh go léir.

ABSTRACT

The real-time detection of phenols in groundwater using a fibre optic fluorescent sensor system is discussed. Two sensor designs are discussed, modelled and experimentally evaluated. One, consisting of a single source fibre and nine 'return' fibres used with a deuterium lamp source, double monochromator and photomultiplier detector is compared to a dual fibre device which is excited by a frequency quadrupled Nd-Yag laser source, narrow pass band optical filter and photomultiplier detector. The latter system has a reference channel to compensate for temporal variations in laser output optical power. Phenol resolution of less than 1 ppb was achieved with the laser based sensor operating over a source-sample distance of 15 metres.

LIST OF FIGURES

LIST OF TABLES

TABLE OF CONTENTS.

CHAPTER 1

CHAPTER 1.

INTRODUCTION TO OPTICAL FIBRES AND OPTICAL FIBRE SENSORS.

1.1 Introduction.

Optical fibres are typically associated with long-haul telecommunications systems. These fibres have been established in recent times as the best medium for high density information interchange over long and short distances using high quality single-mode fibres which can be manufactured relatively inexpensively. However the range of fibres, and indeed the range of applications where optical fibres can be used, is much more extensive. Optical fibre sensors have, and are being used to measure and monitor many physical parameters in a number of different work areas not least of which is environmental sensing. Over 20 years have elapsed since the concept of combining optical fibre technology with environmental sensing was first suggested. During this interval the underlying building blocks, comprising fibre-optic and related components, have evolved from very simple light-guiding bundles of glass fibres into a range of extremely elegant, rugged and relatively inexpensive devices[1]. These, in turn, have stimulated an ever increasing interest in the exploration of fibre-optic techniques for sensing media which has generated a number of proven devices and subsystems. The work reported here is concerned with the development of a fibre optic based sensor for the remote detection and concentration determination of phenol in water.

1.2 Optical Fibres.

The transmission of light via a dielectric waveguide structure was first proposed and investigated at the beginning of the twentieth century. However it was not until the mid 1950's that the dielectric structure we know as the optical fibre was developed[2]. This structure consists of a transparent waveguiding cylindrical core of high refractive index surrounded by a transparent cladding of slightly lower refractive index which supports the

waveguiding core whilst also reducing the radiation loss into the surrounding medium. The core size ranges from a few microns (single mode telecommunications fibre) up to millimetres in diameter The dielectric used is generally silica but developments in glass technology now enable enhanced transmission in the U.V. and I.R. regions. The propagation of light through an optical fibre is governed by a number of parameters which cover almost every aspect of guided wave and classical optics. For the purpose of the work in this thesis however, fibres are used simply as transmission/collection media to and from a remote location and thus the parameters of most interest are those of Spectral Attenuation and Numerical Aperture.

1.2.1 Numerical Aperture.

Fig. 1.1 shows a cross sectional view of a step index optical fibre. The refractive index of the cladding, n_{cl} is less than that for the core, n_{core}. Light striking the cladding from the core will be totally internally reflected if the angle of incidence is greater than the critical angle, Θ_c. The critical angle occurs at the angle of incidence where the transmitted ray is refracted along the surface of the core-cladding interface. The critical angle is given by:

$$Sm(\Theta_c) = n_{cl}/n_{core} \qquad 1.2.1.(i)$$

As the refractive index changes abruptly at the core-cladding interface, a step refractive index profile results.

Equation 1.2.1 (i) can be used to find the size of the cone of light which will be accepted by this optical fibre. If a ray is incident on the core-cladding interface at the critical angle then it will have a corresponding angle Θ_{max} associated with it[3], which is dependent on the refractive index of the medium from which the ray was launched, n_1. If the cone angle is Θ_{max} then by Snells Law:

$$\begin{aligned} n_1 Sin\Theta_{max} &= n_{core} Sin\Theta_t \\ &= n_{core} Sin(90°-\Theta_c) \\ &= n_{core} Cos(\Theta_c) \\ &= n_{core}[1-Sin^2(\Theta_c)]^{½} \end{aligned}$$

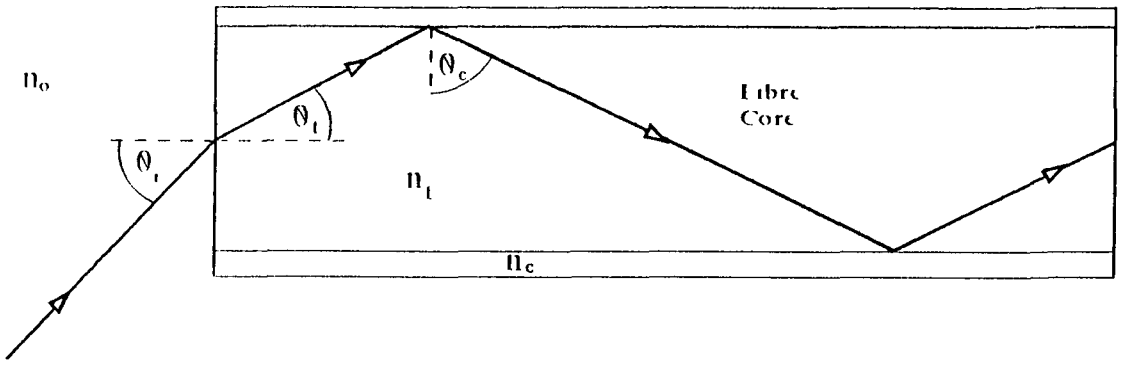

$$\theta_i = \theta_{max}$$

$$NA = n_o \text{Sin}\, \theta_{max}$$

$$f/\# = 1/2(NA)$$

Figure 1.1: Light Ray approach to Definition of NA

From Eqn. 1.2.1 (i) $Sin(\Theta_c) = n_{cl}/n_{core}$, thus

$$n_1 Sin\Theta_{max} = (n_{core}^2 - n_{clad}^2)^{1/2} \qquad 1.2.1 \text{ (ii)}.$$

This value is known as the numerical aperture, NA, and is a measure of how much light can be collected by an optical system.

1.2.2 Spectral Attenuation.

The total attenuation of light passing along a fibre depends on three main factors namely, absorption due to impurities introduced at manufacture (such as water vapour), microbending (loss induced by mechanical effects on the fibre), and Rayleigh scattering.

Microbending, as it is a mechanical effect is not specifically spectrally dependent. Absorption lines due to the presence of impurities in silica are most pronounced in the case of the water or OH absorption peak present at 1.38 microns. By keeping impurity levels low ($1:10^9$) this absorption peak can be kept to the same order as Rayleigh scattering[4].

In a well constructed optical fibre Rayleigh scattering will dominate the loss process and imposes the lower limit on achievable attenuation. Unlike absorption processes where impurity atoms capture and convert the light energy to thermal energy, Rayleigh scattering is a spatial redistribution of light incident on minute discontinuities in the core glass structure. These discontinuities are a direct consequence of the cooling process during the drawing of the optical fibre from the glass preform. Rayleigh scattering varies as $1/\lambda^4$, and so increases dramatically as the wavelength decreases.

1.3 Optical Fibre Chemical Sensors(and their advantages).

Optical fibre sensors are essentially a means whereby light guided within an optical fibre can be modified in response to an external physical, chemical, biological, biomedical or similar influence. In the case of optical fibre chemical sensors light from an optical source whose relevant optical properties remain constant is launched into a fibre via a stable coupling mechanism and guided to the point at which the measurement is to take place. At this point either the light can be allowed to exit the fibre and be modulated in a separate zone

before being relaunched into the same or a different fibre (extrinsic fibre sensor), or the light can continue within the fibre and be modulated in response to the parameter being sensed (intrinsic fibre sensor)[5].

Optical fibre chemical sensors offer a number of notable features and advantages over other sensing techniques. Optical spectroscopy and optical techniques are widely used in conventional chemical analysis employing bulk-optical systems. The adaptation of these conventional instruments to optical fibre systems enables analysis to be carried out at a remote location in real time.

Optically excited transitions of an atom or molecule between various allowed quantum states are highly specific and have potential to yield considerable information regarding the molecule and its coupling to the surrounding medium. This information regarding the chemical structures can be obtained by absorption measurements, fluorescence, or Raman spectroscopy. The work in this thesis deals mainly with the fluorescence of a volatile chemical namely phenol in water.

Optical fibres allow remote sensing in that the source and analysing system (spectrometer,detector,datalogger etc.) can be located in a clean dry environment away from the sample; no grab sampling is required.

Fibre probes are small and inert and waveguided signals are free from electromagnetic interference making them suitable for use in inaccessible locations and in the environs of large motors and high current switch gear.

Optical fibre sensors do not always require a separate reference probe as is the case for many electrical probes (eg differential potentiometric probes) and if they do it is usually present at the analytical end of the sensor.

Finally, the components used in optical fibre sensors have been developed by the well established optoelectronics/telecommunications industries, and offer low cost , high performance fibres, sources and integrated detectors. These components offer possibilities for the use of disposable sensors, as well as more sophisticated, permanently deployed, cost effective sensors for use in chemical instrumentation and environmental monitoring industries.

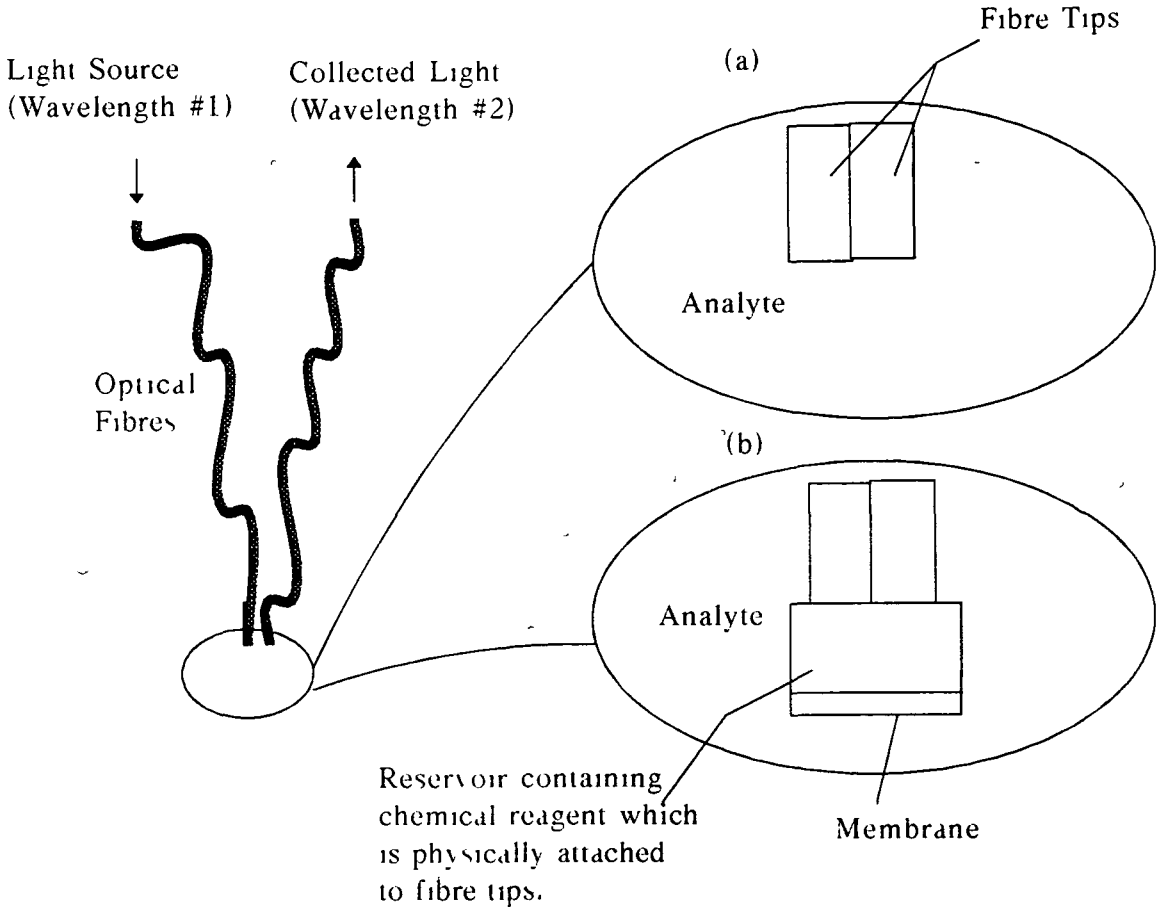

Figure 1.2 (a): Remote Fibre Spectroscopy.
(b): Fibre Optic Optrode.

1.4 Classification of Optical Fibre Chemical Sensors.

There are two main approaches to detection when using optical fibres as chemical sensors, namely remote fibre spectroscopy and fibre optic optrodes[6].(See Fig.1.2.(a) and (b)).

In the case of remote fibre spectroscopy the fibre acts as a simple light guide which enables direct spectral analysis (absorption/fluorescence) over a long distance[3].This type of sensor by virtue of its simplicity suffers few if any disadvantages.

With fibre optic optrodes the optical fibre is combined with a specific chemical reagent at the distal (sensing) end of the fibre. Reagents are chosen to react to specific analytes and the resultant spectral absorbance/fluorescence yield is a measure of analyte concentration. The reagents are contained in a reservoir attached to the fibre tip which can be accessed through a semi-permeable membrane, or the reagents may be immobilised directly on to the fibre tip. Such an optrode is shown in Fig 1.2.(a).

1.5 Thesis Outline.

This thesis describes an investigation of the design, construction, and testing of both a lab-based and a transportable system for the determination of the concentration of the volatile organic chemical *phenol* in groundwater.

Chapter 2 outlines the impetus for the project, a description of groundwater, phenol (characteristics,sources and environmental effects), and a description of recognised conventional methods used for determining the concentration of phenol in drinking water. Also discussed is the method employed in this work and a discussion of its relative merits over conventional detection techniques.

Chapter 3 describes the characteristics of the optical fibre probe used, mathematical modelling of its design and finally its characterisation.

Chapter 4 is concerned with the lab-based multiple-fibre experimental system used. The system design- the source, optics, detector, photon counting, and data collection are discussed. Sample preparation procedures and a discussion of the results achieved with this system are also included.

Chapter 5 outlines the construction and testing of the prototype transportable system using a miniature Nd:YAG pulsed laser source, and examines the results obtained with this system

Chapter 6, in conclusion, is an overall discussion and analysis of the work and a proposal for possible future developments.

References

1. J.P. Dakın, B. Culshaw: "Optıcal Fıbre Sensors: Prıncıples and Components", Artech House, (1988).

2. J.M. Senıor: "Optıcal Fıbre Communıcatıons: Prıncıples and Practıce", Prentıce Hall, (1985).

3. E. Hecht: "Optıcs" 2nd Edıtıon, Addıson-Wesley, (1987).

4. B. Culshaw: "Optıcal Fıbre Sensıng and Sıgnal Processıng", Peter Perıgrınus Ltd., (1984).

5. J.P. Dakin, B. Culshaw: "Optıcal Fıbre Sensors", Chp.2, p10. Artech House, (1988).

6. M.J. Sepanıak, B.J. Tromberg, T. Vo-Dınh: "Fıbre Optıc Affınıty Sensors ın Chemıcal Analysıs", Prog. Analytıcal Spectroscopy, Vol.11, pp. 481-509, (1988).

CHAPTER 2

CHAPTER 2.

PHENOLS AND GROUNDWATER POLLUTION.

2.1 Introduction. (Groundwater Pollution).

99.5% of the world's water cannot be used because it is either saline or locked up in glaciers and ice sheets. Less than 0.01% is present in rivers and lakes and the remainder is contained in rocks as groundwater [1]. Groundwater is part of the hydrological or water cycle. On top of the rainwater which is evaporated, used by plants and which is drained into rivers and streams, some percolates through the soil and into the underlying rocks: Groundwater. A body of rock containing an appreciable amount of water is known as an *aquifier*, and the water-table in an aquifier is the level below which the pores or cracks in the rock are completely saturated and can be accessed by a well or borehole. In Ireland 25% of the water we use comes from groundwater and this figure will undoubtedly rise as the country becomes more developed[2].

In general the quality of Irish groundwater is considered to be good possibly due to the slow percolation of rainwater, but as there is no national survey it is difficult to accurately assess groundwater quality. This, coupled with the fact that pesticides and commercial agricultural fertilizers can lead to contaminated groundwater (and affect human health) has led to the need for groundwater pollutant measurements not previously required.

2.2 Phenols: Characteristics, Sources and Environmental Effects.

Phenols are characterised by benzene rings substituted with a hydroxyl group. The family or series of phenolic compounds results from the variety of substitutions available for the hydrogen atoms on the basic benzene ring. These phenolic compounds include a wide variety of organic chemicals classified into monohydric, dihydric and polyhydric phenols depending on the number of hydroxyl groups attached. Phenol itself, which has but one hydroxyl group, is the most typical of these organic compounds and is often used as a model compound as the properties of phenol, with certain modifications (depending

on the nature of the substituents on the benzene ring), are shared by other phenolic compounds [3].

Phenolic compounds arise from the distillation of coal and wood; from oil refineries, chemical plants, livestock dips, human and other organic wastes, hydrolysis, chemical oxidation, and from naturally occurring sources and substances. Phenols and cresols (phenol with a single methyl group $-CH_3$ attached) have always been available in crude form from distillates of wood, coal and petroleum tars under the names cresote, cresylic acids and tar acids, and have been used for functions varying from treatment of telephone poles, to antiseptics, to food flavouring ingredients. Phenols are the precursors of pharmaceuticals, pesticides, fibres (Nylon-6), resins (Bakelite, Formica and Epoxies), antioxidants, photographic developers and numerous dyes [4]. A study of phenolic effluents from various industries in the U.S. [5] shows that in most, if not all case, simple phenol is the major constituent. The lowest-molecular-weight, or simplest phenols (phenol, cresols and xylenols) are volatile substances, having characteristically pungent, antiseptic odour and taste in dilute solutions (e.g. mg/L) and are poisonous in gram quantities [5].

Trace amounts (<1mg/L) of phenolic compounds can have significant detrimental effects on water quality [6]. Simple phenolic compounds, such as phenol are often biocidal and lower forms of life (especially aquatic) tend to be more severely affected. Acute or even chronic toxicity is seldom a problem for land animals: they avoid drinking water contaminated with phenols because of its objectionable taste. Also many phenols when ingested are rapidly expelled from the body. Aquatic species however cannot escape such pollution and so their poisoning is more serious. Phenol can taint the flavour of fish used for food with concentrations of 0 1 to 25µg/L (0.1-25 parts per billion) depending on the species of fish adding a particular off-flavour. Besides tainting of fish flesh phenols are also toxic to fish. Toxic effects are usually described in terms of *lethal concentrations which kill 50%* of the test species within 96 hours (LC_{50}) and depends on the particular biotic species. As an example, freshwater trout have an LC_{50} of 5000µg/L (5 parts per million) [7] It must be taken in context though that the LC_{50} is an indication of acute toxicity, representing

minimum conditions for survival rather than acceptable conditions for livelihood.

As phenols impart an objectionable taste to food and water toxic exposure seldom occurs in humans and so criteria for human public water supplies are based on taste thresholds. Chlorination is a standard method for the treatment of public water supplies. The advantage of chlorination, on top of disinfecting the water, is that it generally oxidizes the objectionable tasting or smelling organic substances into more innocuous compounds. However the reverse is true for simple phenols. Phenol has a taste objectionable to humans at the 10-100µg/L (10-100ppb) level whereas its chlorinated derivative has a taste threshold ranging from 1µg (1ppb) or less [8]. Thus the U.S. Environmental Protection Agency, the E.C., the Irish E P.A. and most other international agencies recommend a maximum of (1µg/L) of total phenols in domestic water supplies and the following criteria for other water supplies [9],[10]:

Irrigation	50 mg/L
Livestock Water	1000 mg/L
Aquatic Life	0.2 mg/L

2.3 Current Methods for Phenol Determination.

In a recent examination of the effect of organics on groundwater pollution by the International Association on Water Pollution Research and Control (IAWPRC) an impact assessment found that releases from *point* sources (waste tips, spills or leakages), although absorbed by soil will sooner or later contaminate groundwater. Additionally *diffuse* sources (pesticide applications etc)- although less severe in the short term- will lead to a continuous degradation of groundwater in the long term [11]. This refers in particular to the more water soluble organics (simple phenols) and so monitoring phenol levels in drinking water sources has become necessary and now requires sensitive (µg/L) analytical methods. There are numerous techniques used to determine concentration of phenols in water, many of which have recently been outdated during a re-examination of analytical techniques by the U.S. E.P.A. [12]. However, the following is a number of methods approved by the U.S. E.P.A. and their corresponding automated systems. Each is considered briefly

in comparison with the remote fibre spectroscopy technique used in this work, with respect to the nature of phenol as described in Section 2.2 as well as the instrumentation and sample preparation techniques involved.

Four basic instrumental techniques are currently used for the determination of phenols:

2.3.1 Colorimetric Method.

Colorimetry is a well established technique for analysing specific chemical content in an analyte where a reaction with a specific reagent causes a colour variation which in turn can be related to specific information on concentration. 4-Aminoantipyrine (4-AAP) forms a reddish-brown dye at a specific pH when it reacts with Phenols and the concentration is then determined by measuring absorbance at 510nm and 460nm. The automated versions of this method (eg. Technicon Instruments Corp.) claim a resolution of about 2µg/L [13]. However this system involves many distillation stages and requires complex and rigorous preparation of a number of chemicals, gases and samples. Not all phenols react with 4-AAP to form the dye, however there is another colorimetric method used in conjunction the 4-AAP method. Phenols have an oxidative reaction with 3-Methyl-2-Benzothiazolinone (MBTH) which offers comparable sensitivity to the 4-AAP method but with some extra phenol family members. Neither method is capable of distinguishing between specific phenols as is Gas Chromatography, and both are lab-based systems requiring grab sampling and extensive chemical and sample preparation which increases the chance of error and is monotonous and time consuming even when automated.

2.3.2 Gas Chromatography.

Gas Chromatography (GC) can be used to separate and determine phenol levels. This is a complex process which uses extraction and evaporation of the phenols prior to analysis. Concentration or pretreatment to form derivatives is also required after which samples are processed through a number of columns to sift off individual components. Analysis is carried out on retention times in the individual columns. In optimum conditions this system is sensitive to between 2 and 10µg/L (2-10ppb) depending on the specific phenol.

Gas chromatographic separation of sample components coupled with direct mass spectrometric determination is a powerful analytical tool for organic

compounds including phenols. GC-MS systems are very expensive analytical instruments usually only used in the case of unusual pollution incidents or extremely difficult samples where GC alone is not effective. This technique also suffers from the disadvantages listed in 2.3.1 above for the lab-based colorimetric analysis method.

2.3.3 UV Absorption at Different pH.

A phenol or a mixture of phenols may be determined in water samples by measuring the difference in absorption of UV light as the pH is changed from slightly acid (pH 5) to strongly alkaline (pH 12). The spectrum of the phenolate ion is displaced towards longer wavelengths at pH 12 compared to free phenol; this is termed the *bathochromic shift* effect. In practice the instruments implementing this effect to analyze phenols use either two light sources or two filtered beams one of which is a reference and the other a sample interrogating beam. All photometric measurements must be made using the same sample cell in the same sampling position each time requiring precise alignment. Comparisons carried out by the American Chemical Society [14] show a similar limit of detection to the 4-AAP method but a greater degree of accuracy using this UV ratio method.

2.3.4 Molecular Fluorescence Spectroscopy.

Upon UV irradiation, phenols absorb some of the UV energy through excitation processes. A portion of the absorbed energy is re-emitted spontaneously by excited phenol molecules at a longer wavelength. An excitation wavelength, λ_{exc} is selected, (usually this approximates the max absorption - in the UV for phenols) and fixed, while the wavelength of the UV emission is scanned. In cases where only a single, known phenol is present, this method is reasonably fast, simple and accurate down to µg/L (ppb) phenolic concentrations. This method is however occasionally used to monitor several phenols at once as many phenols fluoresce in the wavelength region between 290 and 330nm [15] as shown in Figure 2.2 and thus the concentration can be determined as an aggregate. This method is usually implemented using a standard laboratory fluorometer. With regard to the work in this thesis this technique is of particular interest as the systems developed and tested in Chapters 4 and 5 both use this technique incorporated with optical fibre spectroscopy.

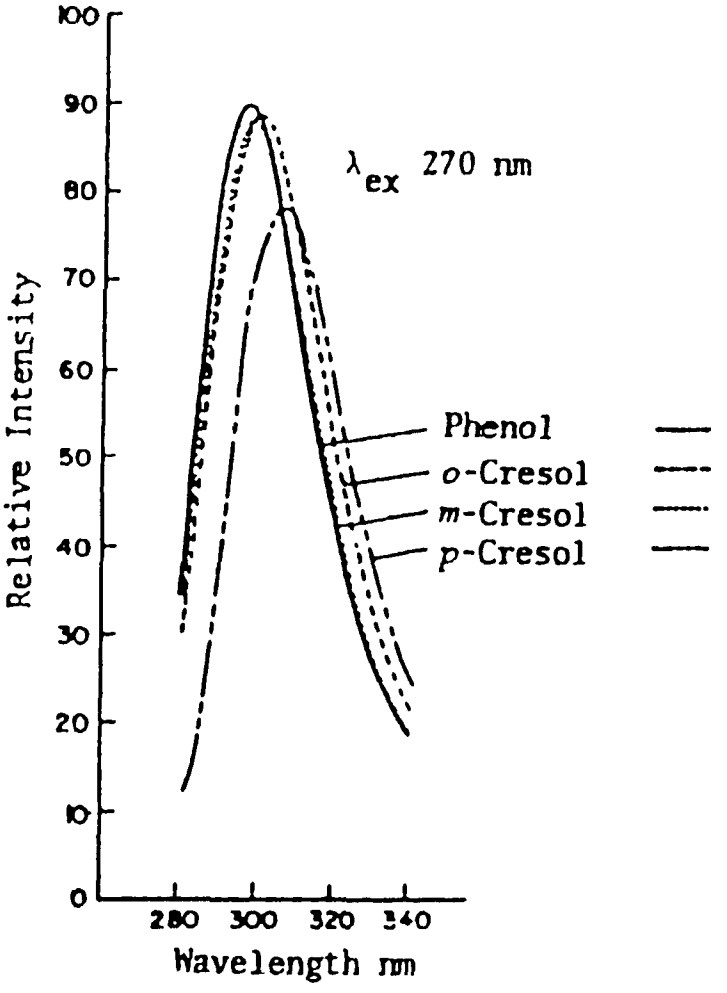

Figure 2.1: Fluorescence of various phenols in the UV.[1]

[1] See Ref [15]

2.4 Conclusions.

Groundwater is increasingly becoming a major source of drinking water worldwide. However it may suffer pollution from many sources including phenols. If so, because of the nature of groundwater (present in rocks) it is difficult, if not impossible to treat and restore to normal - unlike surface waters. Thus, the monitoring of groundwater is particularly important. Phenols are particularly soluble in water and are toxic to fish and taint fish flesh as well as having an objectionable taste to humans at low levels. Phenol concentration m water is, at present, monitored using a number of automated systems all of which have advantages and disadvantages as discussed above. They are all lab-based systems however and because they involve the use of grab sampling they have a number of obvious flaws when they are examined as groundwater monitoring techniques:

Firstly the very nature of grab-sampling is a totally random technique unless it is carried out on a continuous basis which would be impractical.

Phenols are volatile chemicals and the removal and transportation of samples from groundwater sources (wells,boreholes etc) may change the composition of the samples and thus give inaccurate pollution level readings.

Tedious and time-consuming sample preparation (and in some cases chemical reagent preparation) is required.

Because most of the equipment is bulky and in most cases very expensive it would be impractical to have it dedicated, on-site and in any case, access to the groundwater would be difficult, if not impossible

The system proposed in Chapter 4, using optical fibre spectrometry and photon-counting techniques is an experimental lab-based system which, unlike many of the systems outlined above requires very little sample preparation and has few components, is relatively inexpensive and can produce comparable detection limits. In Chapter 5, a transportable, on-line system is proposed which involves no sample preparation, and can continuously monitor phenol content in groundwater, to a maximum depth of 15m and so, has implications for concentration monitoring of groundwater on-site in boreholes and wells.

References

1. R. Thorn· **"Groundwater"**, Envıronmental Informatıon Servıce (ENFO), Brıefıng Sheet #3. (1989).

2. B.G.W. Wasserstatıstık,1986. Stats. Reprınted ın **"WATERSHED '89"** Conference Publıcatıon",1990 , Vol.1, p.40.

3. R.E. Tram: **"Quality Criteria For Water"**, p.183, E.P.A. Washıngton DC. (1972).

4. Mary S. Quınby-Hunt: **"Instrumentation for Environmental Monitoring - Lawrence Berkeley Lab. Environmental Instrumentation Study"**, Vol.2, Chp 12 (Water), pp 497-538 , J. Wıley and Sons, (1986).

5. Amerıcan Publıc Health Assoc. et al.: **"Standard Methods for the Examination of Water and Wastewater"**, 15th ed., Amerıcan Publıc Health Assoc., Washıngton DC. (1981).

6. T. R. Crompton: **"Determination of Organic Substances in Water"**,Vol.2, pp 149-189, Wıley & Sons, (1980).

7. A. L. Wılson: **"The Chemical Analysis of Water: General Principles and Techniques"**,Chp7, pp 399-404, London Royal Socıety of Chemıstry, (1988).

8. U.S. Envıronmental Protectıon Agency: **"Ambient Water Quality Criteria for Phenol/Chlorinated Phenols"**, Reports EPA-440/5-80-066 and EPA-440/5-80-032, Washıngton DC. (Oct 1980).

9. U.S. Envıronmental Protectıon Agency: **"Quality Criteria for Water"**, Washington DC. (1986).

10. P. J. Flanagan: **"Parameters of Water Quality-Interpretation and Standards"**, Irish Environmental Research Unit. (1988).

11. J. P. G. Loch et al. **"Organics in Groundwater"**, Presented at *International Assoc. on Water Pollution and Control (IAWPRC) Symposium, Watershed 1989.*

12. R. A. Hites, W. L. Budde: **"EPA's Analytical Methods for Water: The Next Generation"**, *Vol 25, No. 6, pp 998-1006, Environmental Science and Technology*,(1991).

13. M. E. Gales, Jr. and R. L. Booth: **"Automated 4-AAP Phenolic Method"**, *Jour. Amer. Water Works Assoc.* 68, 540, (1976).

14. J. E. Fountaine et al.: **"New Ultraviolet Ratio Spectrophotometric System for the Determination of Trace Amounts of Phenolic Compounds"**, *Analytical Chemistry,* 46, 62, (1974).

15. S. D. Kullbom et al.: **"Fluorescence Spectroscopy in the Study and Control of Water Pollution"**,Paper #288, Presented at Pittsburgh *Conference on Analytical Chem. and Applied Spectroscopy*, by the Perkin-Elmer Corp.,(1970).

CHAPTER 3

CHAPTER 3.

OPTICAL FIBRE SENSOR: DESIGN, MODELLING AND PROOF TESTING.

3.1 Introduction.

In any low-light optical system the problem perhaps most often encountered is that of coupling the maximum amount of light into the optical detector. This is especially true in the case of optical fibres and optical fibre sensor systems. Both the lab-based and portable sensor systems[1] designed and examined in this thesis involve the use of remote fibre spectroscopy and extrinsic sensors[2]. For this reason both systems are reliant on the intensity of fluorescent light from the analyte. Excitation light of specific wavelength is guided down one fibre and into the analyte and the fluorescent light (at a longer wavelength) is collected by one or more fibres and is guided towards the detector for analysis; See Fig. 3.1. The first part of this chapter is concerned with the nature of molecular fluorescence and its use in fibre optic fluorescent sensing particularly with respect to phenol fluorescence. The latter part describes the factors which govern the coupling of this fluorescent light into the collection fibre/s and describes the approach taken in designing and mathematically modelling a fibre optic probe which can capitalise on these factors and couple the maximum amount of light into the detection system.

3.2 Fluorescence Spectrometry and Fibre Optic Fluorescence Sensing as a Chemical Analytical Tool.

Fluorescence Spectrometry is becoming increasingly popular in many branches of chemical and biological science. It is used in studies of molecular structures and interactions and in the localisation of molecules (biological systems) as well as in many types of trace analysis[1]. As mentioned briefly above the essence of fluorescence spectrometry is that a molecular sample illuminated by an external source absorbs light energy of a certain wavelength and is *excited* into

---

[1] See Chapters 4 and 5 for more detail.

[2] See Chapter 1, Section 1.2

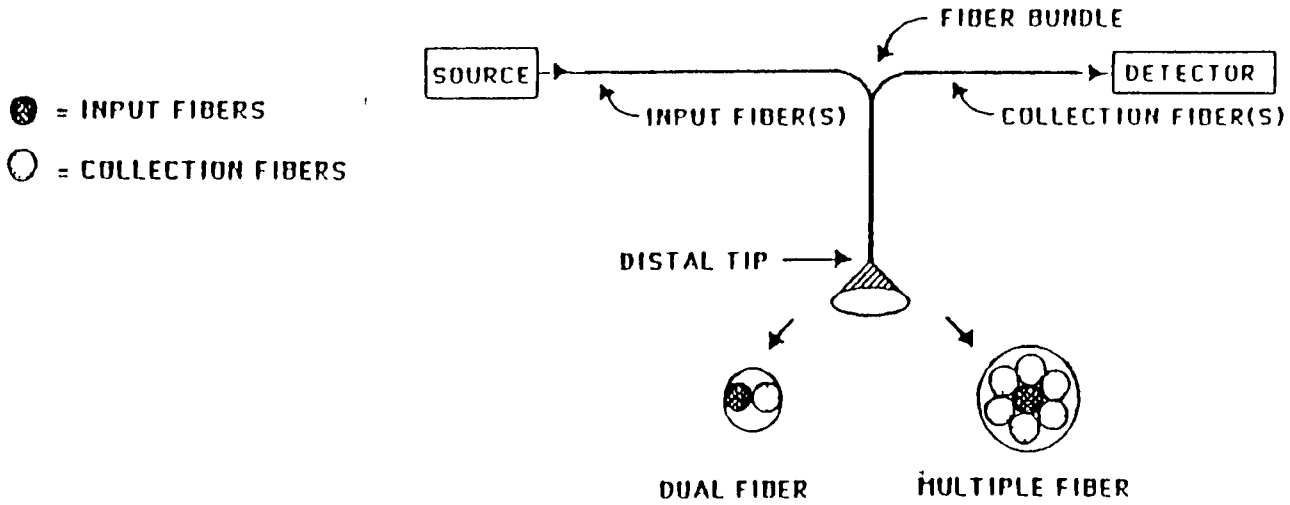

Figure 3.1: Principle of chemical fluorescence collection using optical fibres.

a higher state. The sample then emits light of a different wavelength (generally longer than that of the excitation light). The principal advantages of the technique are as follows:

(a) Sensitivity; where picogram quantities of material can frequently be studied.

(b) Selectivity; deriving in part from the two characteristic wavelengths (λ_{exc},λ_{emis}) of each compound, and

(c) The variety of sampling methods available; dilute and concentrated solutions, suspensions and solid surfaces, can all readily be studied and combinations of fluorescence spectroscopy and chromatography can also be used.

The usefulness of fluorescence spectrometry is widely documented. However, lab-based fluorometry systems are generally cumbersome with large light sources, monochromators and detection systems, which do not lend themselves to chemical analysis in the field. The advent of miniature high-performance detectors and compact high power sources coupled with advances in optical fibre technology has made viable portable chemical analysis, through optical fibres and fluorescence methods, a reality.

Most phenols and in particular, phenol itself both absorb and fluoresce in the Ultra-Violet region[3]. Fundamental attenuation due to Rayleigh Scattering which increases as $1/\lambda^4$ drastically reduces U.V. light power delivered over traditional optical fibres. Developments in the manufacturing process however have increased the transmission capabilities of fused silica fibres[4]. Both Plastic Clad Silica (PCS) and All Silica versions of this high quality step-mdex fibre were used in the assembly of the sensors assessed in the course of this work. Due to the limited transmission, even with this specialist fibre maximising the coupling of the optical components became critical. Thus the design of the distal end of the sensor was investigated so as to maximize the light gathering efficiency.

---

[3] See Chapter 2, Section 2 3 3/2 3 4

[4] See Chapter 4

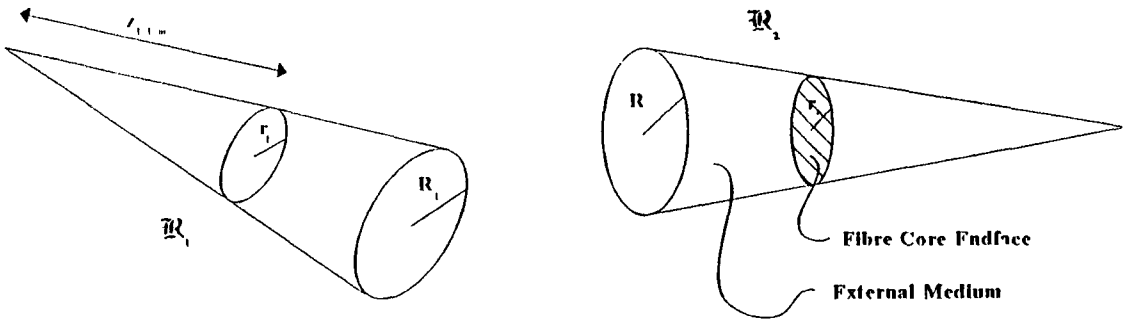

Figure 3 2 Emission/Collection cones (Basis $\mathfrak{R}_1$ and Basis $\mathfrak{R}_2$).

3.3 Fibre Orientation (Angular Considerations).

Previous work by others in the area of UV laser-induced fluorescence using optical fibres [2] concentrated on using parallel fibres at the distal end of the probe and parameters governing this type of measurement have been well characterised. However, in more recent work [3] various angular orientations have been used in examining fluorescence from soluble chemical species. A theory governing the performance of probes with angular dependence has been suggested [4] and the model used for collection of fluorescence in this work is related to this theory.

3.4 Mathematical Model (Software Prediction).

In order to construct the most efficient probe it was decided to both model and verify experimentally the effect of using various fibres at various angles to one another. A full description of the mathematical model is given in Appendix (A) however the following is an outline of the idea involved and the software written to examine the model.

3.4.1 Mathematical Model. (Outline)

In any system as complex as one which involves propagation of light in three different media where two are varying spatially with respect to the third it is essential to define a Basis or number of Bases and to find the relationship between them, before attempting to simulate the phenomenon taking place. Diagram 3.2 shows the Basis $\mathbb{R}_1$ describing the ideal cone of emission of light from the excitation fibre which is identical, in form, to that of the cone of collection $\mathbb{R}_2$. Thus any point in either Basis in the common medium outside the fibre face can be described in Carthesian Co-ordinates as follows:

Cone_1: Emitter

$$x_1^2+y_1^2 \le z_1^2 \tan\alpha_1 \qquad x_1=r_1\cos\theta_1$$
$$y_1=r_1\sin\theta_1$$
$$z_{1_{lim}} \le z_1 \qquad 0\le\theta_1\le 2\pi \qquad \text{3.4.1}$$
$$with;$$
$$z_1\text{lim}=r_1\tan\alpha_1 \qquad z_1\text{lim}\le z_1\le z_1\text{max}$$

Cone_2:Collector

$$x_2^2+y_2^2 \le z_2^2\tan^2\alpha_2 \qquad x_2=r_2 Cos\theta_2$$
$$y_2=r_2 Sin\theta_2$$
$$z_2\text{lim}\le z_2\le z_2\text{max} \qquad 0\le\theta_2\le 2\pi \qquad \text{3.4.2}$$
$$with;$$
$$z_2\ge z_2\text{lim}=r_2/\tan\alpha_2 \qquad 0\le r_2\le z_2\tan\alpha_2$$

In the case of multimode fibre and especially with large core diameters the inhomogeneity of the beam emitted from the fibre face must be taken into account [4]. Thus it is assumed that all of the points of the end face of the fibre are as point sources illuminating a core of max half-angle α_1. The irradiance due to each of these sources , of co-ordinates $(r\mathrm{Cos}\theta, r\mathrm{Sin}\theta, z_{1lm})$ in the coordinate system $\mathbb{R}_1$ with surface r,dr,dθ is;

$$dI_o = \frac{P_o}{\pi r_1^2} \frac{r dr d\theta}{2\pi [1-Cos\alpha_1]\rho_1^2}$$

$$with \quad \rho^{2_1} = (x_1 - rCos\theta)^2 + (y - rSin\theta)^2 + (z_1 - z_{1lm})^2 \qquad 3.4.3$$

[5]

Thus, at the point $M(x_1,y_1,z_1)\mathbb{R}_1$ (Exit face of illuminating fibre core) the total irradiance is given by;

$$I_o = \oint_{FibreFace_1} dI_o \qquad 3.4.4$$

Obviously the integration must only be made over that part of the fibre endface which may illuminate the point $M(x_1,y_1,z_1)\mathbb{R}_1$ i.e.$(Core_1)$. Thus for ease of programming

$$I_o = \int_{r=0}^{r_1} \int_{\theta=0}^{2\pi} Test_1(r,\theta)\, dI_o \qquad 3.4.5$$

where $Test_1$ is the condition that the slope between the point on the fibre face and the point $M(x_1,y_1,z_1)\mathbb{R}_1$ is less than or equal to the tan of the N.A. α_1

$$\alpha_1 = Tan^{-1}\left[\frac{y_{11}-y_{10}}{x_{11}-x_{10}}\right] \qquad 3.4.6$$

($Test_1$ is either 0 or 1)

Similarly for the collection of the fluorescent light the Raman Intensity dI_R (W/sr) given by an element of volume $dx_1,dy_1,dz_1)$ centred on the point $M(x_1,y_1,z_1)\mathbb{R}_1$ is given by

$$P_c = \iiint_{\substack{Intersection \\ of NA Cones}} dI_o \quad \Omega(M) \qquad 3.4.7$$

[5] See Appendix A

DUAL FIBRE MATHEMATICAL MODEL.

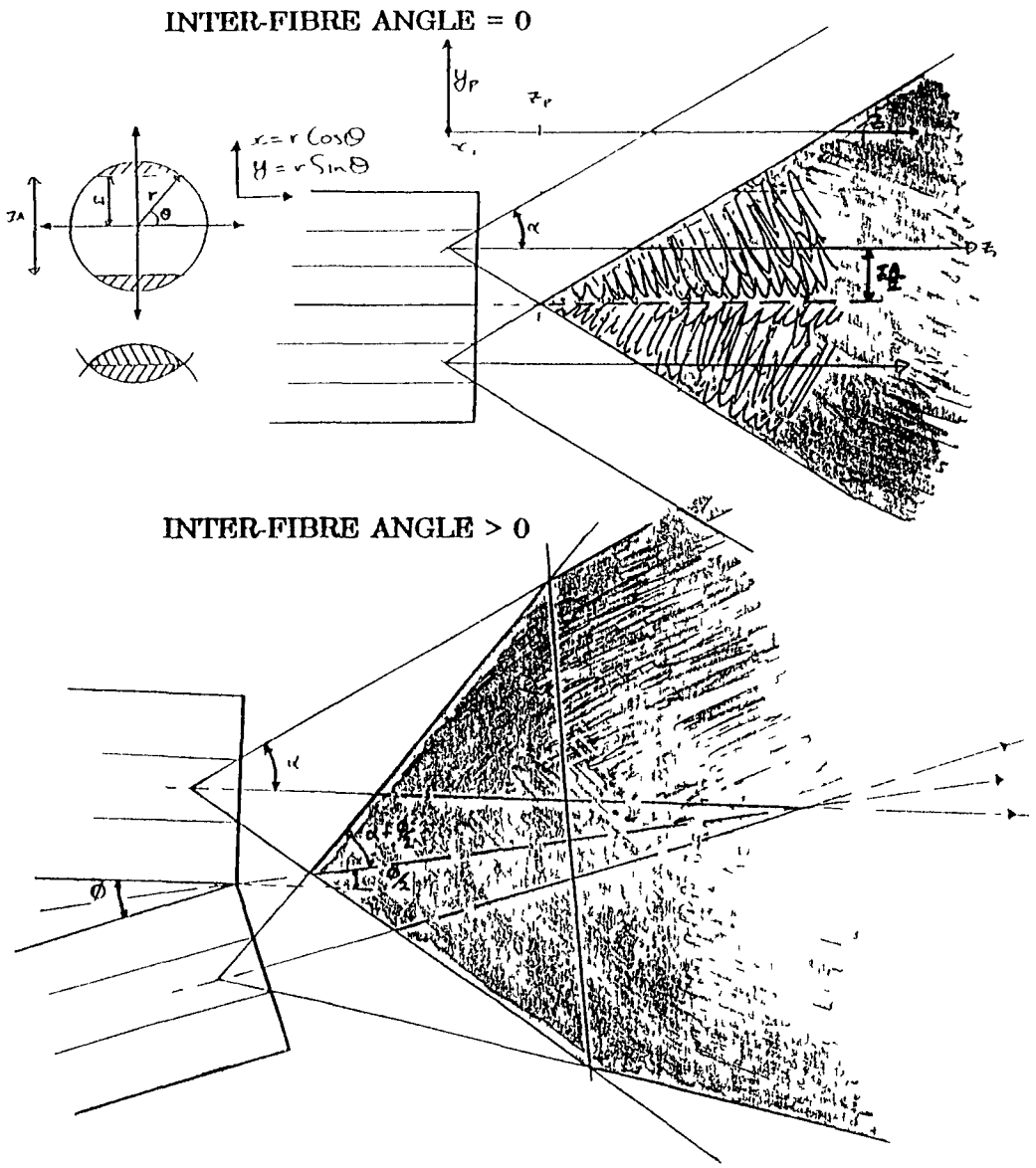

Figure 3.3 Side view of overlap of emission and collection cones with
(a) Inter fibre angle = 0.
(b) Inter fibre angle > 0.

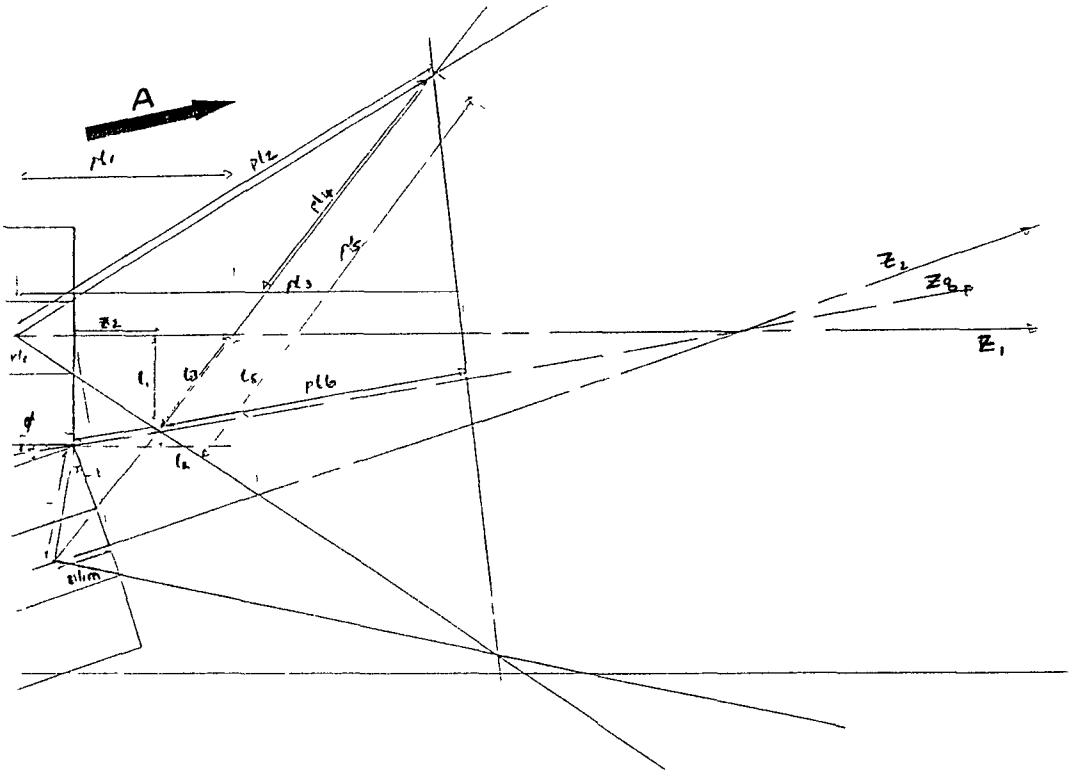

Figure 3 4 Labeled diagram of parameters used in Test$_a$c Software.[6]

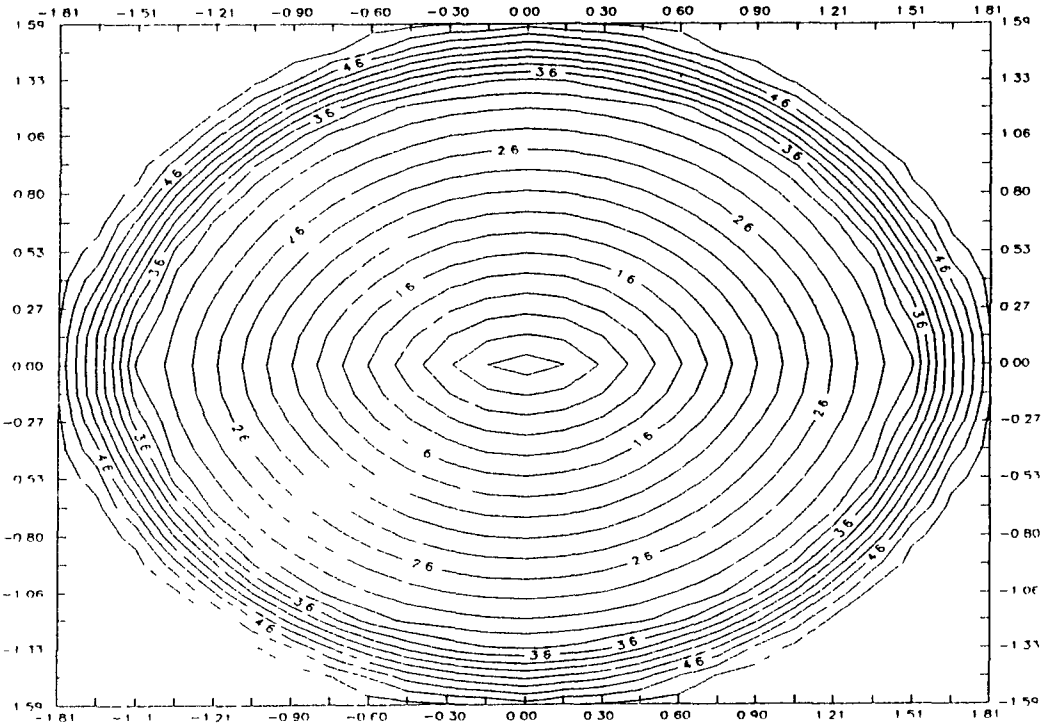

Figure 3 5 View of Test$_a$c volume in direction of arrow A from point z_q=0 Interfibre Angle = 20° |pl6| = 3.6mm.

[6] Appendix B

where Ω(M) is the divergent solid angle given by the point $M(x_2,y_2,z_2)\mathbb{R}_2$ and arriving on the surface of the collecting fibre;

$$\Omega(M) = \int_{r=0}^{r_2} \int_{\theta=0}^{2\pi} Test_2(r,\theta) \frac{Cos\psi}{\rho_2^2} \, r dr d\theta \qquad 3.4.8$$

with

$$\rho_2^2 = (x_2 - r_2 Cos\Theta_2)^2 + (y_2 - r_2 Sin\Theta_2)^2 + (z_2 l:$$
$$Cos\psi = (z_2 - z_2 lim)/\rho$$

There are a number of approaches which one can use in the analysis of the collection of fluorescent light but all depend on being able to characterise the overlap volume of both the emission and collection cones defined outlined above in the limits of Equation 3.4.7. Much of the work concerning the modelling of the collection efficiency of the fibre probe in this chapter was involved in defining this volume and how it alters with change in angle between the two fibres. This concept is illustrated diagrammatically in Figure 3.3 (a) and (b) and a mathematical description of the volume involving the parameters and variables in Figure 3.4 is available in Appendix B. The software programme written to characterise this volume is known as "$Test_0$.c" and a copy of both itself and a flowchart describing how it works are also included in Appendix B. This software was written in both TurboC and AnsiC languages and were run on both an "Enigma" 386 pc and on HP workstations . Figures 3.5 shows a topographical view of the $Test_0$ volume at an inter fibre angle of 20° from the point of contact of two fibres looking directly into the analyte (400µm core, 850µm total diameter). From this figure the change in shape of the interaction volume after only 3.5mm into the liquid can be observed. Figures 3.6 and 3.7 show topographical views of the same volume from the axis of both the excitation and collection fibres respectively. Figures 3.8 (a)(b)(c) and (d) show surface area grid drawings of $Test_0$ volumes for various inter-fibre angles between two 400µm core diameter fibres of NA 0 4. These profiles were all constructed from data generated by the $Test_0$ modelling program which generated the points lying on and inside the $Test_0$ volume. The software

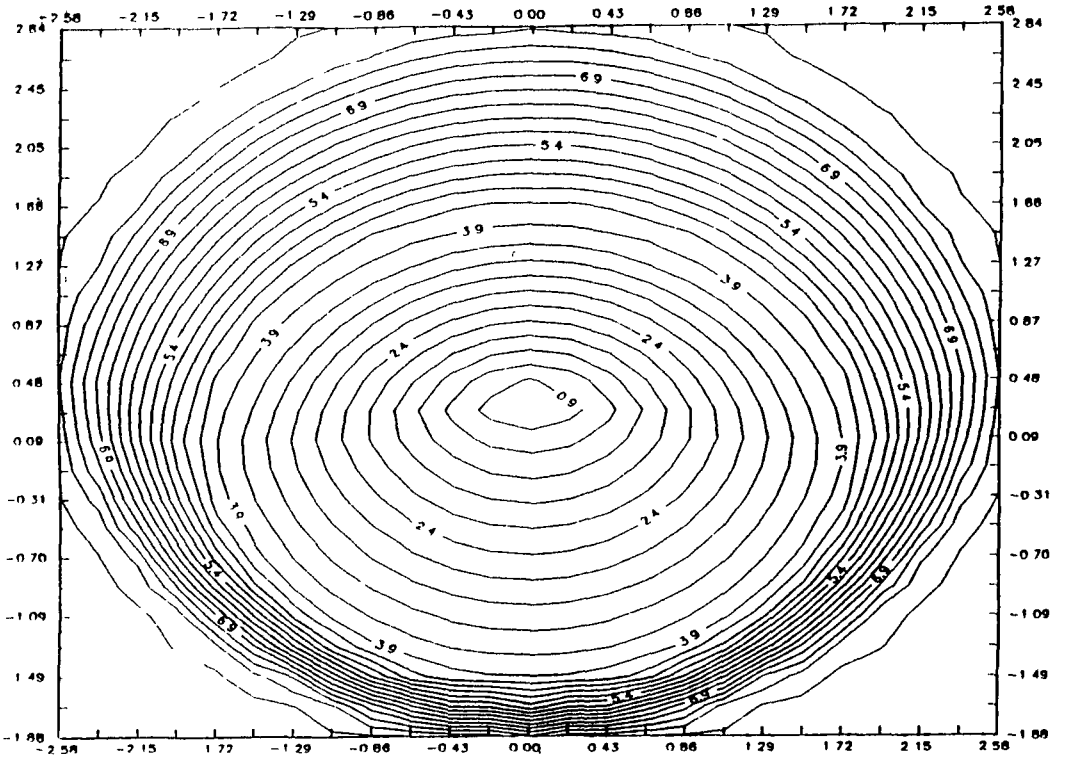

Figure 3.6: Topographical view of Test$_o$.c volume as would be observed from excitation fibre.

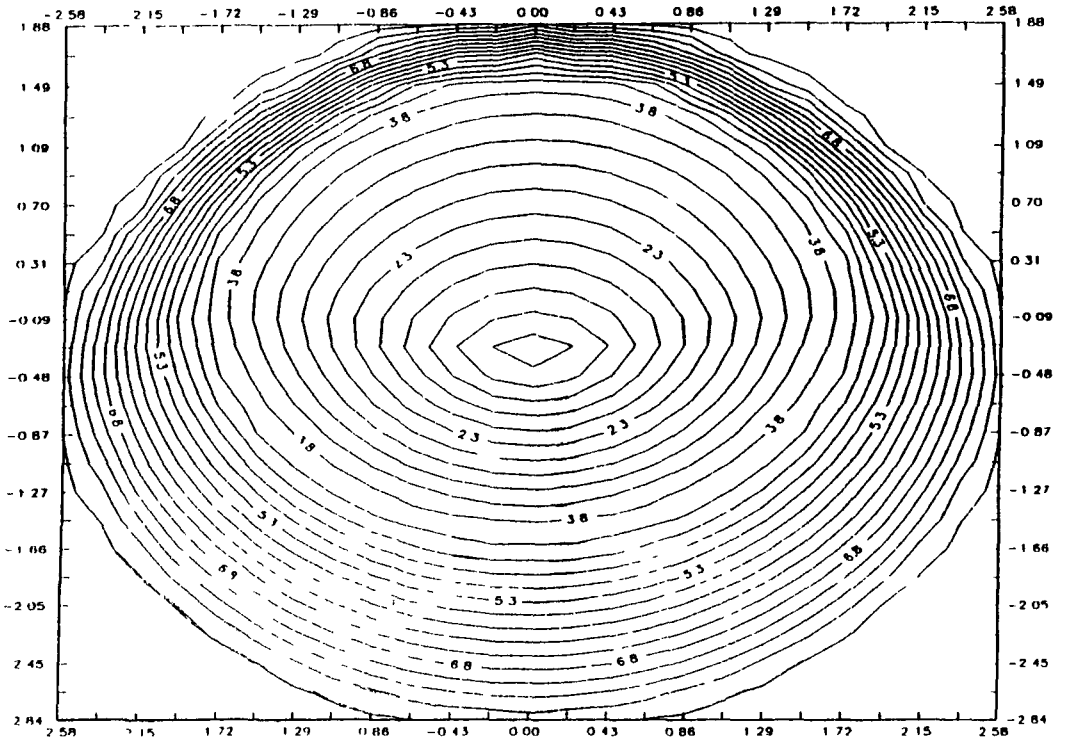

Figure 3 7: Topographical view of Test$_o$.c volume as would be seen from axis of collection fibre.

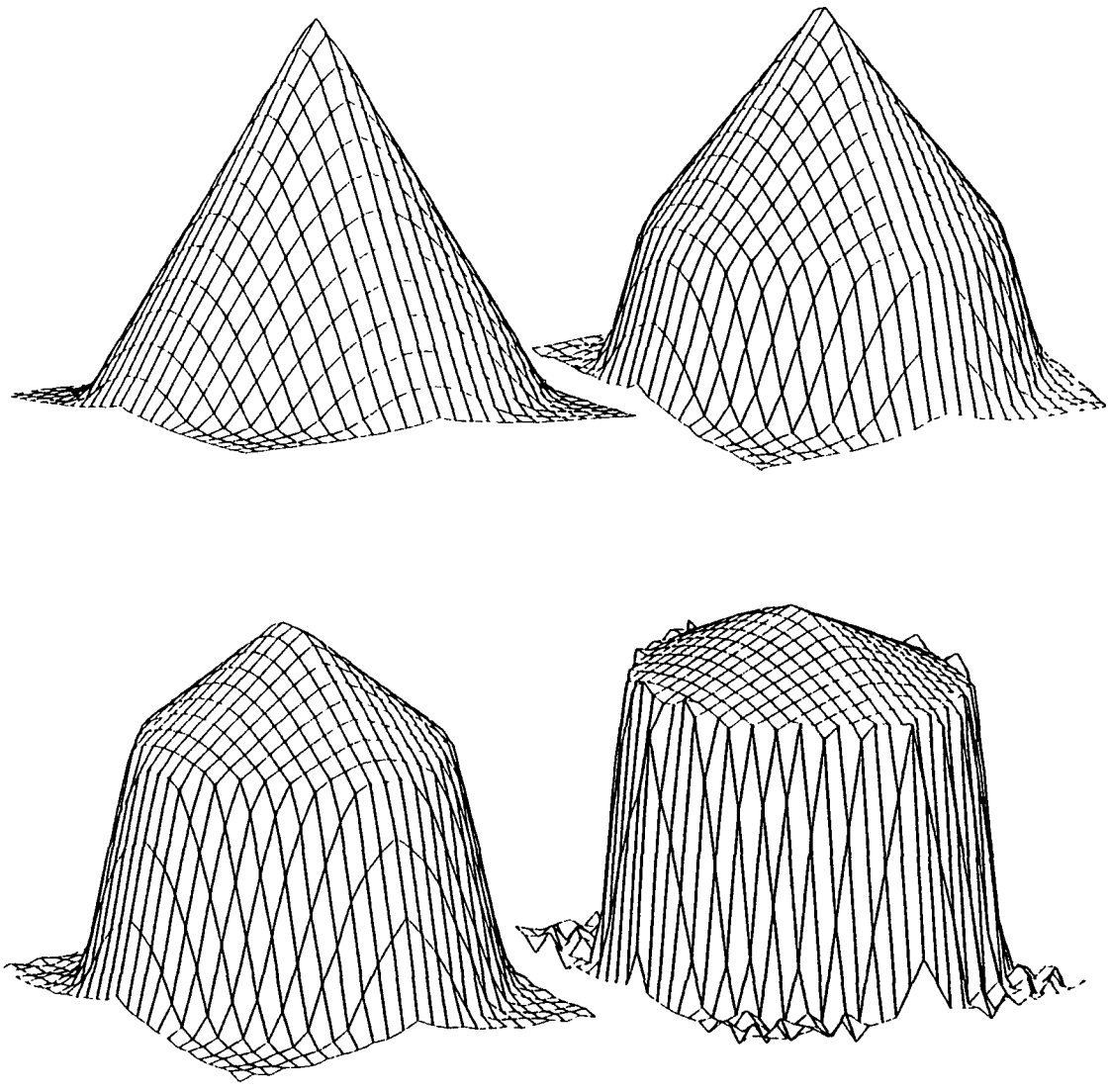

Figure 3.8: Surface profile of overlap volume of emission and collection cones

(a) Inter fibre angle = 2°. Depth of profile z_q = 10mm.

(b) Inter fibre angle = 16°. Depth of profile z_q = 5mm.

(c) Inter fibre angle = 24°. Depth of profile z_q = 5mm.

(d) Inter fibre angle = 32°. Depth of profile z_q = 5mm.

which was used to estimate the collection efficiency of various configurations. "Eff.c" is also described in detail in Appendix C.

3.5 Experimental Verification and Results.

3.5.1 Experimental Setup.

The model discussed is based on the assumption of a number of setup conditions. The experimental system used to verify this model was an attempt to recreate these conditions in a real experimental situation and to examine the effect on collection efficiency while varying the angle between the emission and collection fibres. The light source used initially was the 488nm line of a 3W Argon-Ion laser (Cathodeon), which was used to excite a Rhodamine 6G dye solution. This gave very varied results perhaps due to the power instability in the laser. This, coupled with the fact that the prototype system would involve using a Deuterium lamp[7] led us to use the discrete 488 line which is characteristic to the D_2 spectrum. An added factor is that this was a better simulation of the final detection setup in which the probe was to be used. Two 1m lengths of Fibreguide Ind. "Superguide" SPC 400B, with a N.A.= 0.4 and a core diameter of 400µm were prepared. After cleaving fibre end preparation was carried out by hand using four grades of aluminium oxide grit paper (Grit: 30µm to 3µm). Fibre chucks were used to clamp the fibre during polishing and the endfaces were visually inspected at regular intervals with a low power microscope. Water was used as an anti-friction agent while a "figure of eight" polishing technique was used on a small hand-polishing rig. The radiation from the lamp (described in greater detail in Chapter 4) was focused onto the fibre end-face via an f/2 lens. The fibre was positioned by using an xy positioner which was clamped to the lamp housing by a specially designed fitting. The fibre ends in contact with the analyte were mounted on a specially constructed jig as in Figure 3.9. The fibres were waxed in place until the optimum position was found and then bonded in that position with epoxy. The jig allowed the angles to be varied without varying any of the other parameters governing the

[7] Deuterium Lamps are noted as high UV output sources (Phenol excitation).

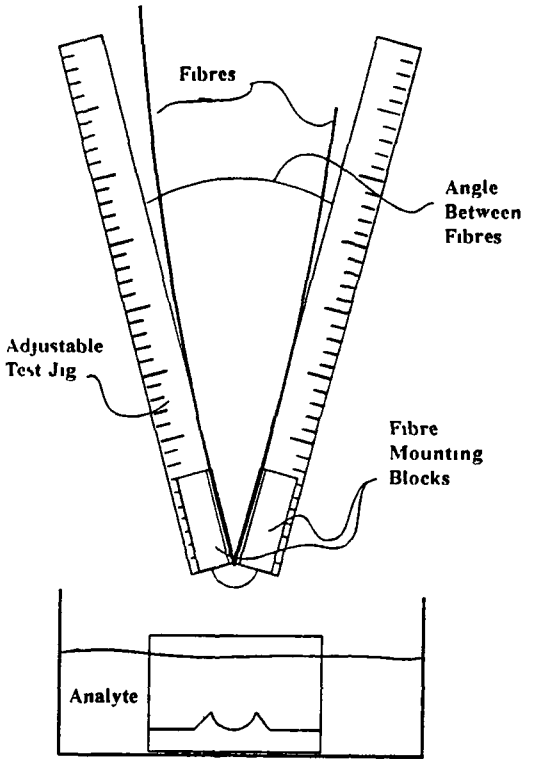

Figure 3.9: Laboratory jig and setup used for probe collection efficiency study.

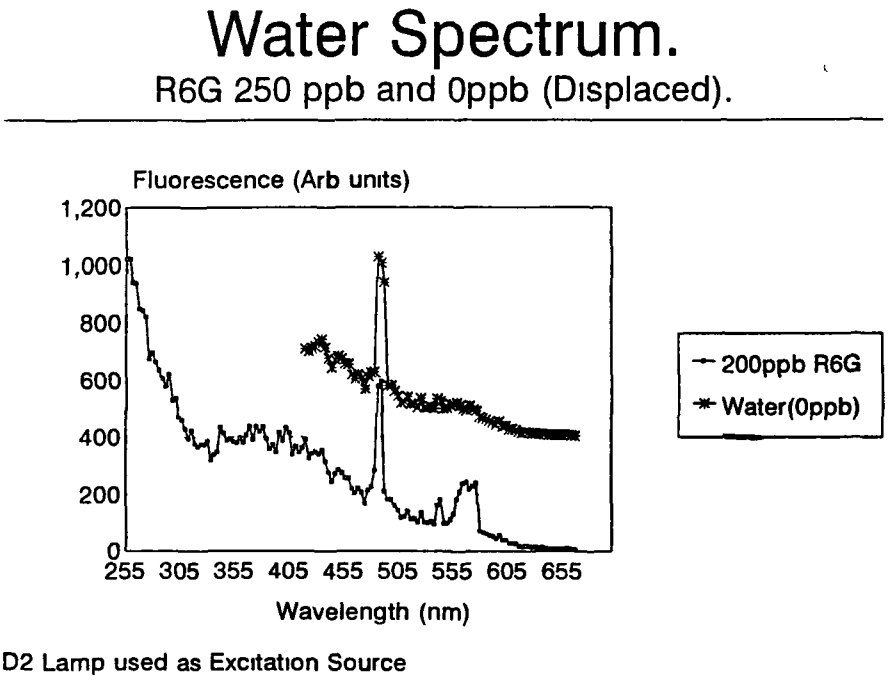

Figure 3.10: Spectral scan of Rhodamine 6G including the discrete D_2 488nm line used to excite the dye.

fluorescence. The fluorescent light collected and guided back along the receiving fibre was coupled to the input slit of the monochromator.

This was achieved via a specially constructed mounting which housed an xy positioner. The fibre was optically matched to an f/2 lens. The subsequent collimated beam was matched to the monochromator via an f/4 lens. A Bentham DM150 Double monochromator fitted with special holographic gratings (1800 lines/mm) was used. The double monochromator reduces the amount of stray light incident on the detector, which is essential for low level fluorescence detection and the 1800 l/mm gratings give the monochromator greater resolution in the UV region for work on Phenol fluorescence detection, described in Chapter 4. The DM150, with focal length of 300mm and f/# of 4.2 was well matched by the input optics described above. The detector system employed a photomultiplier tube in photon counting mode which was interfaced to a personal computer via a Stanford Research SR400 dual channel photon counter[8], described also in Chapter 4.

3.5.2 Results.

Initially a 200ppb solution of Rhodamine 6G was scanned over the region from 450nm to 550nm by stepping the double monochromator through these wavelengths See Fig 3.10. This spectral scan was carried out to determine the wavelength of max fluorescence of the analyte. The system was then set at the angle of max fluorescence and the following approach carried out. The angle between the two fibres, beginning at zero was varied in steps of 2° up to 40° so as to give an idea of the collection efficiency variation with angle. The setup described above using the photon counting method was used with integration times of 100 secs for each angle reading. The readings were firstly taken for increasing angle and then with decreasing angle and the average value for each angle was derived. This showed a definite increase in collection of fluorescent light at an angle of 24°. Further studies using phenol confirmed this was still the case which compared favourably with the theoretically derived values as can be seen in Fig.3.11 (a)and(b).

[8] Photon counting is used to detect very low light levels (Phenol Fluorescence)

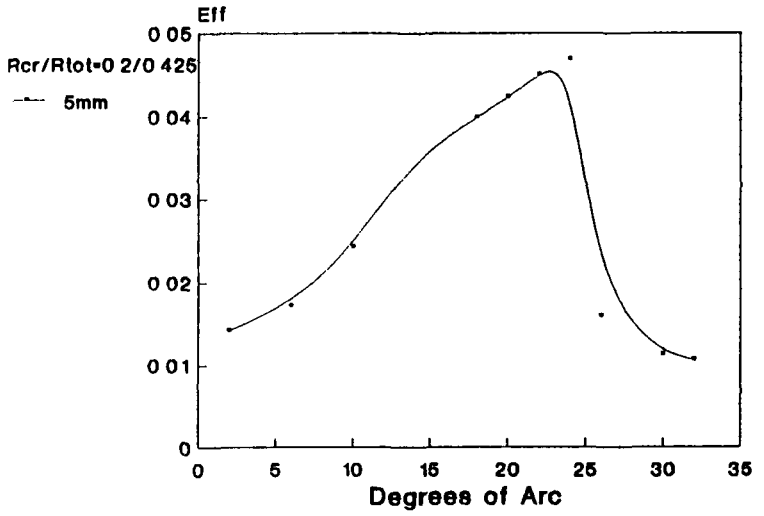

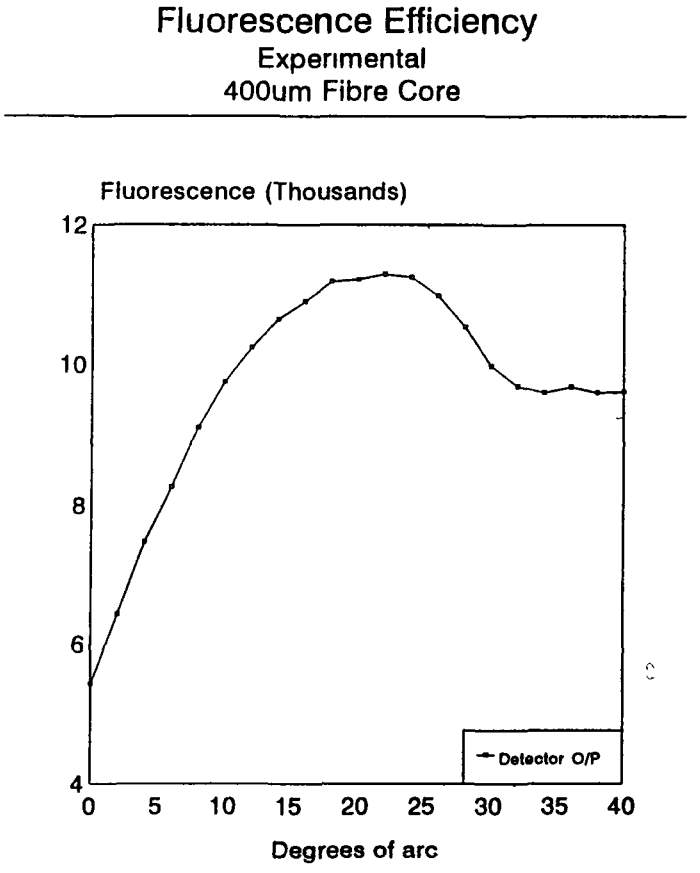

Figure 3.11: (a) Theoretical efficiency and (b) Experimental efficiency.

3.6 Design proposals.

The design for the prototype was driven by a number of considerations. Its planned eventual use would be in boreholes and wells as well as in waterways. It would therefore be required to be rugged and small as well as offering protection to the fibres. The positioning of the fibres with respect to each other is critical so mechanical stability without damage to the fibres was also crucial as well as having the capability of adjusting or replacing fibres if the need arose.

There are a number of important facts to take into account when designing a fibre probe to detect fluorescence. The two most important perhaps are:

(a) Fluorescence generated is proportional to the intensity of the light source used to excite a sample.

(b) In addition, the nature of the fluorescence phenomenon means that the light from a fluorescent event has an equal probability of being emitted in all directions [1].

In order to fulfil (a) a high power, stabilized Deuterium lamp and a pulsed, frequency quadrupled, Nd:Yag laser respectively were used[9]. Where (b) is concerned we know from the above research, (3.5.2) that a PCS 400um fibre probe with a collection fibre at 24° to the excitation fibre gives the maximum fluorescence collection and similarly 16° for 600um fibre. However, if a number of collection fibres are used then the fluorescence collecting power of the probe will be increased [5].

Based on the considerations outlined above the two prototype designs used in this work were developed. The first, for use with the Nd:Yag laser system [Chp 5] is shown in Fig 3.12. A metal jig was machined to hold two 600um core fibres at an angle of 16° to each other.

The second design is slightly more involved. A simple calculation based on Fig 3.13 shows that the maximum number of collection fibres which may surround a single excitation fibre is nine. This is shown in Fig 3.14. This is also more difficult to construct. Both are characterised and described in more detail in Chapters 4 and 5 respectively.

---

[9] See Chapters 4 & 5.

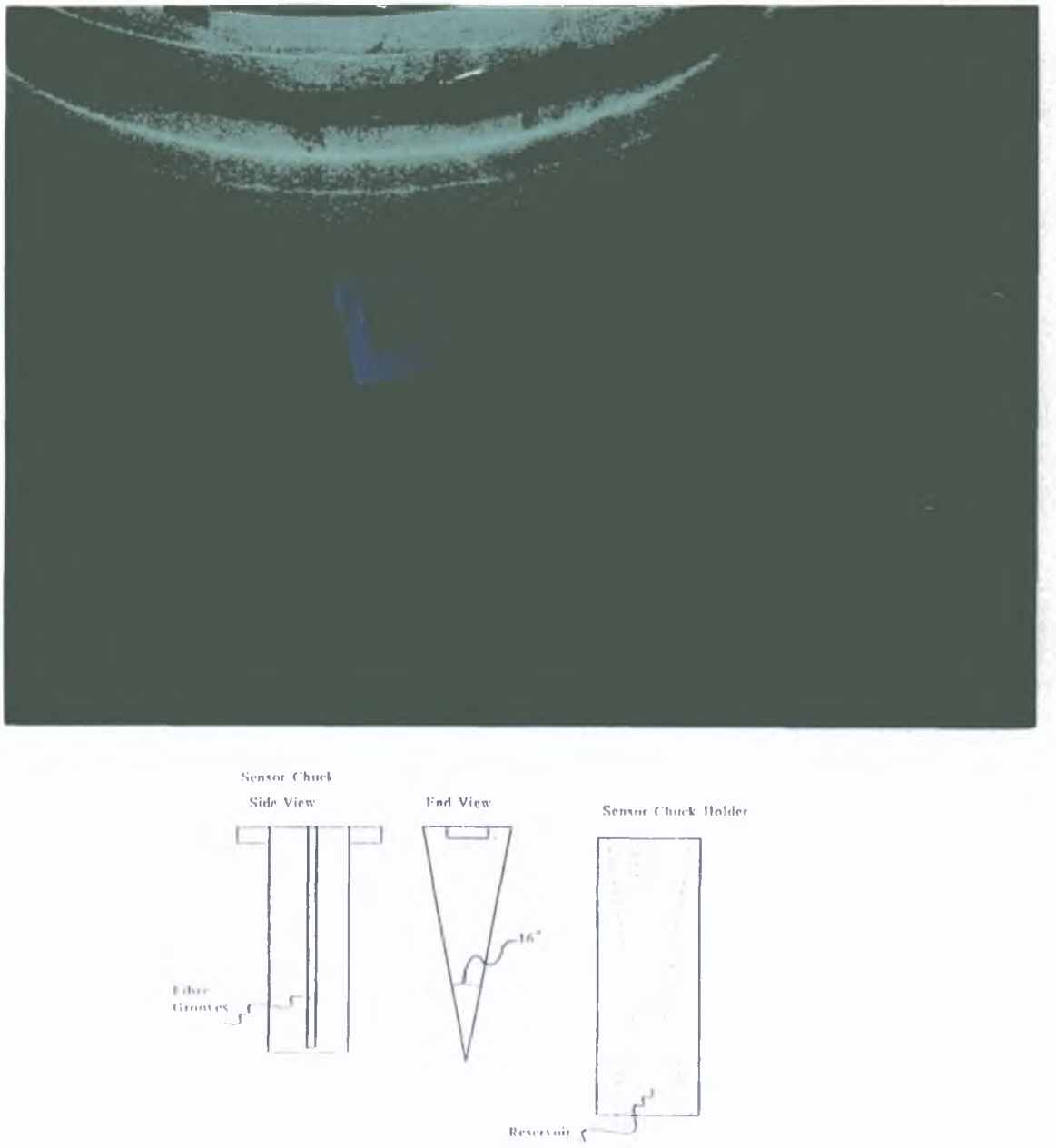

Figure 3.12: Nd:Yag Dual fibre probe

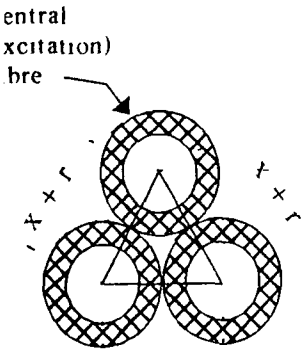

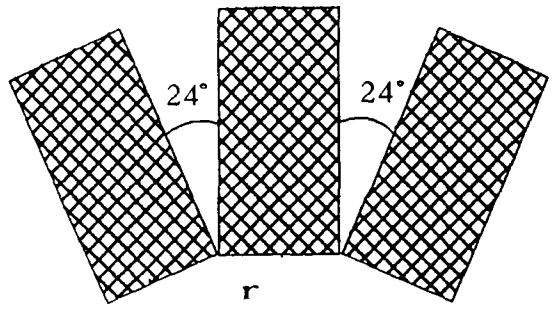

x + r

2r

90 - 24 = 66°

x = rSin 66°

x + r = r(x + Sin 66)

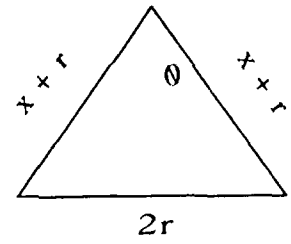

0 = ArcSin [r/(x + r)]

Thus 0 ≃ 35°

And [360°/35] ≃ 10

So, for easy fit· 9 around 1

Figure 3.13: 9 around 1 fibre collection at an angle of 24°.

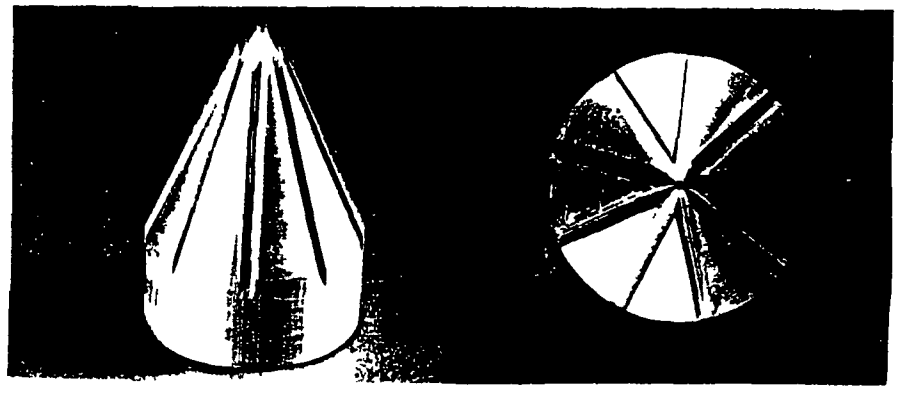

Figure 3 14 Deuterium lamp system fibre probe head (9:1 Design)

3.7 Conclusions.

The aim of the work carried out in this chapter was to characterise the behaviour of a fibre optic fluorescence probe so as to maximise the fluorescence collection efficiency. Previously this type of fibre probe collection efficiency has been theoretically modelled but no publication of experimental verification or disproval of these results could be found and, in any case, it may not have been relevant to the fibre or setup which the work in this thesis covers. For this reason the prototype fluorescence probe was firstly mathematically modelled and then experimentally tested. If the model did not exactly mimic the real setup it did show a close correlation with the experimental results. Perhaps such developments which would take into account additional fluorescence effects as well as skew-ray guiding and cladding modes would improve the validity of the model ie. light guided which would not be included in the simple ray approach to Numerical Aperture. For the 400um core diameter PCS the inter-fibre angle of maximum fluorescence collection was found to be approximately 24° and for the all-silica Superguide 600um core fibre a more shallow angle of 16°. The acceptance angle, in air, for each of the above based on the nominal N.A., is 23.6° +/- 1.5° and 12.7° +/-1.5° which shows a direct correlation between the efficiency of the fibre probe and the numerical aperture of the fibre being used. Further to the above theoretical and experimental tests, two prototype sensor designs were developed and constructed for use with two different sources of excitation light which are to be evaluated as complete systems in chapters 4 and 5 respectively. The maths model achieved all that was required of it for this particular application but perhaps further development of this model supported by the appropriate research could suggest some new designs for sensors not just in fluorescence analysis but also in absorption of liquid media and perhaps also in gaseous media.

References

1. J.N. Miller : **"Standards in Fluorescence Spectrometry-Techniques in Vis and UV Spectrometry"**, Vol.2., p1., Chp, (1981).

2. F.P. Milanovich et al.: **"Remote Detection of Organochlorides with a Fibre Optic Based Sensor"**, Analytical Instrumentation, 15(2), p137-147, (1986).

3. J.F. Louch and J.D.Ingle: **"Experimental Comparison of Single and Double-Fibre Configurations for Remote Fibre-Optic Fluorescence Sensing"**, Analytical Chemistry, Vol 60 ,pp 2540-2542, (1988).

4. P.Plaza, N.Q. Dao et al.: **"Simulation et Optimisation des Capteurs a Fibres Optiques Adjacentes"**, Applied Optics, Vol,No. 19, pp 3448-3454, (1986).

5. C.K. Chong et al.: **"Raman Spectroscopy with a Fibre Optic Probe"**, *Vibrational Spectroscopy.* Vol.3, pp 35-45. (1992).

CHAPTER 4

CHAPTER 4.

EXPERIMENTAL SYSTEM : LAB-BASED.

4.1 Introduction.

In order to test the viability of using optical fibres in-situ for remote sensing of phenols according to the design suggested in chapters 1 and 2 an experimental system was constructed. The system, Fig.4.1(Schematic) is comprised of a Deuterium Light Source, optical fibre (to and from the analyte) and a detection system with a PC utilised as a datalogger.

4.2 The Optical System.

From the initial source to the analyte and finally to the optical detector the system described is based in the ultra-violet region and so its associated problems had to be taken into consideration when designing the system.

The source was a deuterium arc lamp chosen for its high spectral output power in the UV region. Ordinary crown glass absorbs highly below 300nm (See Fig.4.2) whereas UV grade silica transmits well down to 180nm. For this reason the 30W lamp, ORIEL 63163 used in this work had a silica window. The lamp was powered by a low-drift, high reliability "Cathodeon" power supply, , and was mounted in a special lamp housing to prevent personnel exposure to both UV light and the ozone created by D_2 lamps. This particular lamp is classed as a high radiance lamp, with a 0.5 mm arc as opposed to a lamp of the same power with a larger arc and thus higher output irradiance (See Fig.4.3). Earlier research into UV fluorescence of phenols using lamp sources by Joshipura et al.[1], employed high irradiance lamps but the setup involved did not use optical fibres. Because the objective in this work was to focus as much light as possible onto a small area (fibre end-face) the lamp with higher radiance was chosen. Deuterium arc lamps have a broad spectral band peaking around 250nm but also have a number of discrete peaks one of which lies at 488nm and which was used initially in conjunction with a fluorescent Rhodamine 6G solution to align and calibrate the system as a whole and for sensor design tests (Chapter 3). A narrowband filter (AG Electro-Optics G25-

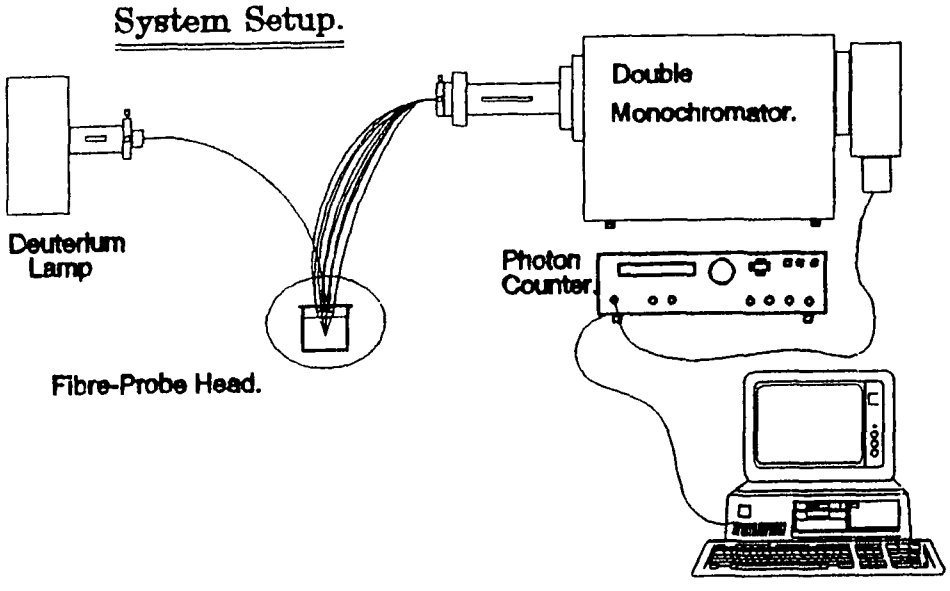

Figure 4 1: Lab-based System (Experimental).

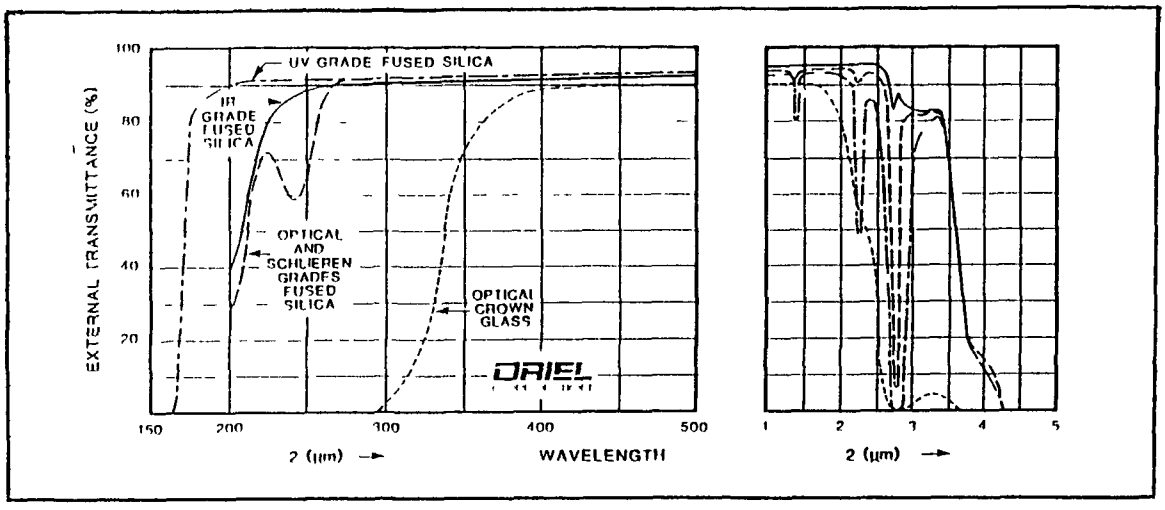

Figure 4 2: UV silica and crown glass absorption.[1]

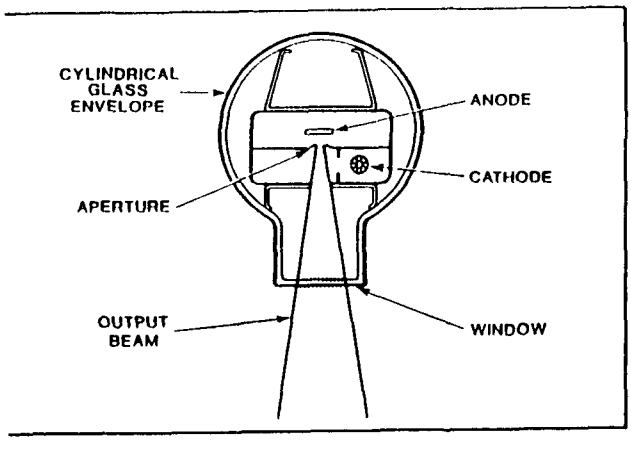

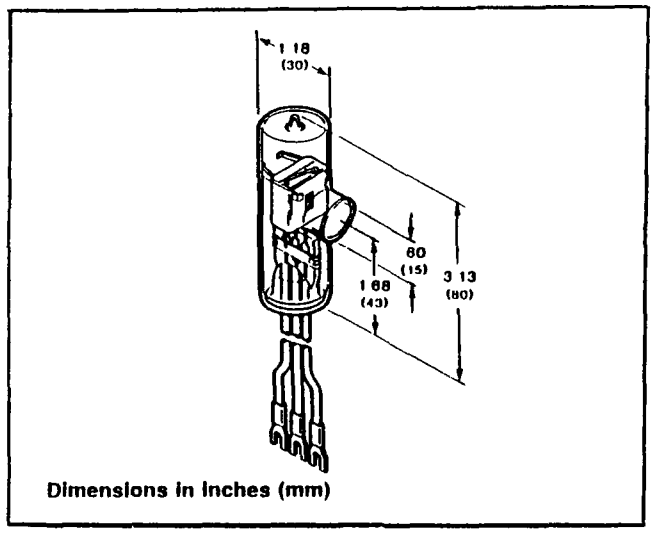

Figure 4 3: Deuterium arc lamp.[2]

[1] Ref #2

[2] Ref #2

254-F), peaking at 254nm with 20nm fwhm, was used to reduce interference due to other optical effects outside the spectral region of interest. The diverging beam of the arc was focused onto the fibre end using an f/2 fused silica lens and an xyz fibre positioner as described in Chapter 3 . Each of the components and the launch assembly as a whole were tested and verified. The entire launch system was held in the aforementioned lamp housing (Fig 4.1) where the lamp, lens, filter and fibre were clamped after alignment.

As mentioned in Chapter 3 the optical fibre used was a specialist Fibreguide Industries Superguide SPC 400B with a 400µm silica core and a black Tefzel outer protective coating. Attenuation was quoted by the manufacturers as being 1dB/m or 80% transmission at λ=250nm, See Fig 4.4. The fibre was quoted as having a numerical aperture of 0.4 in air. For coupling light into fibres the following calculation is considered:

$$\frac{n_c}{n_f} = Cos\theta_t$$

or

$$\frac{n_c}{n_f} = (1-Sin^2\theta_t)^{1/2}$$

Using Snell's Law and rearranging gives:

$$Sin\theta_{max} = \frac{1}{n_o}(n_f^2-n_c^2)^{1/2}$$

The quantity

$$n_o Sin\theta_{max}$$

is the Numerical Aperture, or N A. as defined in Chapter 1 and is dependent to a great deal on the refractive index of the medium, n_o. $(NA)^2$ is a measure of the light gathering power of the system. The term originates in microscopy, where the equivalent expression characterises the corresponding capabilities of the objective lens. The N.A. and f/# of a system are related as follows[3];

$$f/no \approx \frac{1}{2(NA)}$$

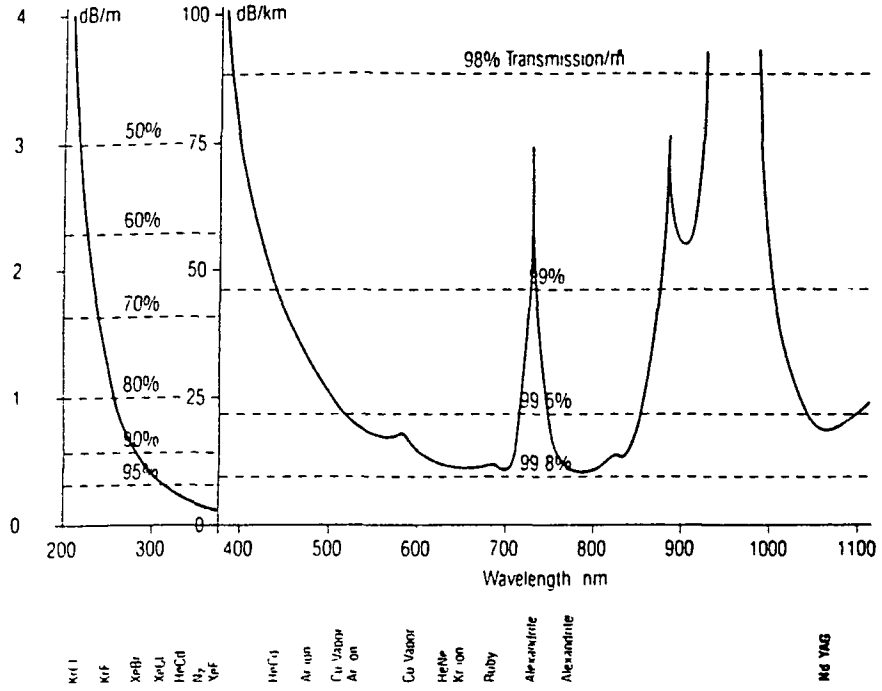

Figure 4.4: UV silica Fibre Transmittance.[3]

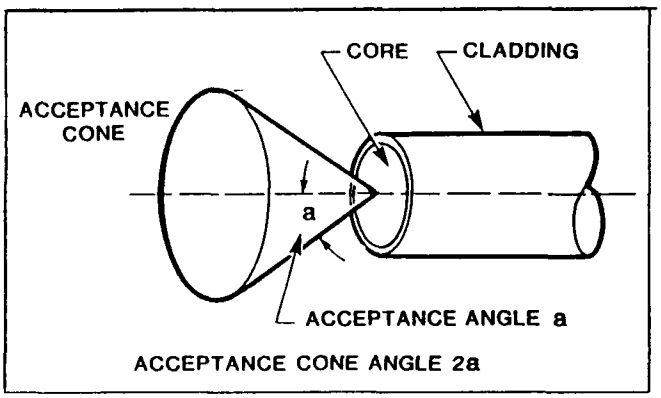

Figure 4.5: Numerical Aperture and its relation to f/#.

[3] Ref #4

In this case the $f/\#_{air} = 1.25$. Fibre end preparation was carried out as described in Chapter 3.

Following the assessment of fibre probe design a "9 around 1" probe head was constructed using an aluminium block with a central axis hole surrounded by 9 grooves at 40° intervals and at an angle of 24° with respect to the axis (See Figure 4.6). Each of the ten 1m length fibres, having been polished and individually checked for transmission was assembled into the probe head and glued in place later to be given increased stability by a fitted Aluminium hood. The fluorescent light collected and guided back along the fibres was then coupled to the input slit of the double monochromator BENTHAM DM150. The input stage of the double monochromator, initially designed to accommodate light from a single fibre , as described in Chapter 3 was adapted to receive 9 fibres. As was outlined also in Chapter 3 the double monochromator offered high resolution with its 1800 lines/mm holographic gratings even with relatively large slit widths See Appendix D. It also considerably reduced the amount of stray light reaching the detector. Coupling of 9 fibre-end images onto the gratings of the monochromator without underfill or overfill required the testing of a number of fibre bundle configurations. A schematic of the most efficient is outlined in Figure 4.7. Again, in this case the fibres were bonded in place into a hollow aluminium cylinder chuck for easy manipulation in the x,y,z planes at the monochromator entrance stage.

4.3 The Optical Detection System.

A variety of optical detectors exist for detection of UV radiation. By far the most sensitive when considering signal to noise ratio and performance at low light levels are photomultiplier tubes. The principal of operation of these detectors can be demonstrated by referring to Fig 4.8. When incident light enters the photocathode of a PMT photoelectrons are emitted from the photocathode. These photoelectrons then travel through the dynode chain where they are multiplied by a factor of typically 10^6 or 10^7. The avalanche electrons are in turn collected by the anode and fed to an external circuit as a current or voltage pulse. If the intensity of incident light is altered then this change is reflected by the change in the output pulses from the PMT. The

Figure 4.6: Fibre Probe (Aluminium Jig).

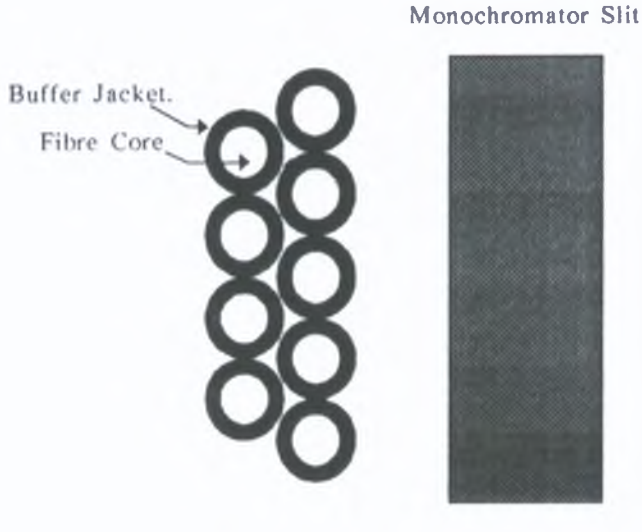

Figure 4.7: Schematic of most efficient coupling setup.

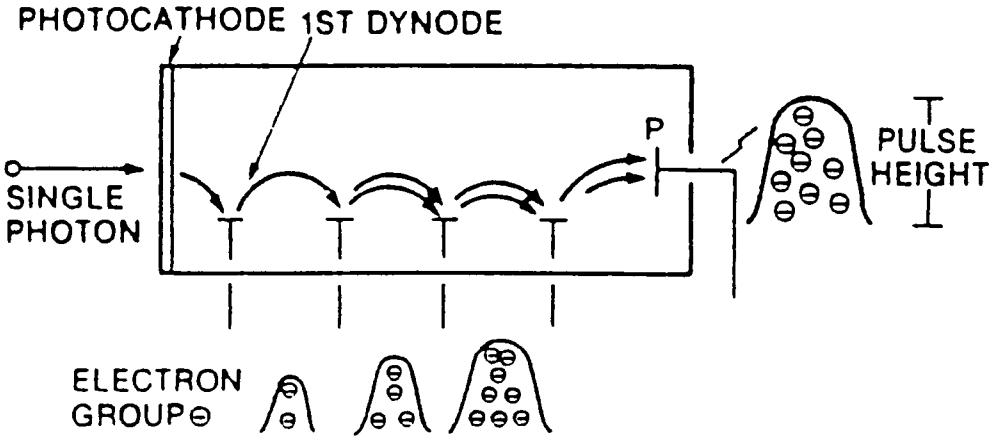

Figure 4.8· Photomultiplier Tube.

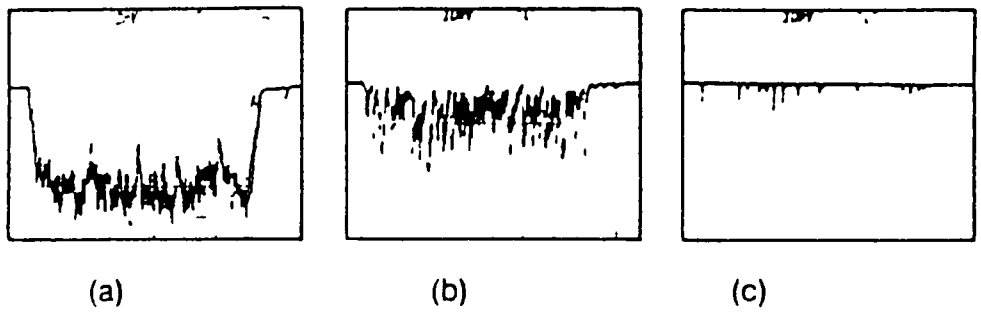

Figure 4 9: (a) Strong,(b) Medium, and (c) Low Light Intensity.

output pulses may appear as shown in Fig 4.9. The output pulses in this trace are superimposed into an analog signal. However as light intensity weakens the individual light photons appear as discrete pulses, Fig 4.9(c). The measurement of these discrete pulses is known as digital mode measurement or photon counting.

In the Fig 4.9(a) analog mode the mean value containing numerous varying signal substances or pulses becomes a DC signal. However, the photon counting mode brings pulses into a binary digit form and counts the pulses of single photoelectron events.

In any case where very low light levels are expected photon counting methods become necessary. Fluorescence of phenol in water in the ppb concentration region, where the fluorescent light to be transmitted over fibre-monochromator link to the detector is just such a case.

4.4 Photon Counting Methods.

Initial studies using a Hamamatsu 1P28 PMT showed large quantities of noise and interference even with strongly fluorescent dyes in the visible region (See Chapter 3). Further study on the effects of various photon counting techniques and methods were necessary. In order to do this the exact nature of the electrical pulses coming from the anode of the PMT must be known.

4.4.1 Pulse Height Distribution.

As was illustrated earlier, (Fig 4.8), a primary electron emitted at the photocathode due to a single photon emission results in a number of secondary emissions from the first dynode and so on until the last electron group finally appears at the anode. The pulses generated at the first dynode with respect to a primary electron are regarded as a Poisson distribution and the mean number of these electrons becomes the current amplification gain "δ" of the PMT in use. This holds true for further multiplication processes from the second dynode to the others giving a total amplitude of δ^n, where n is the number of dynodes. At the anode the pulse heights will vary because of;

1. Statistical probability (variance of δ).
2. Non uniformity of current amplification caused by position of each dynode with respect to where photoelectrons strike photocathode.(Spatial effect)

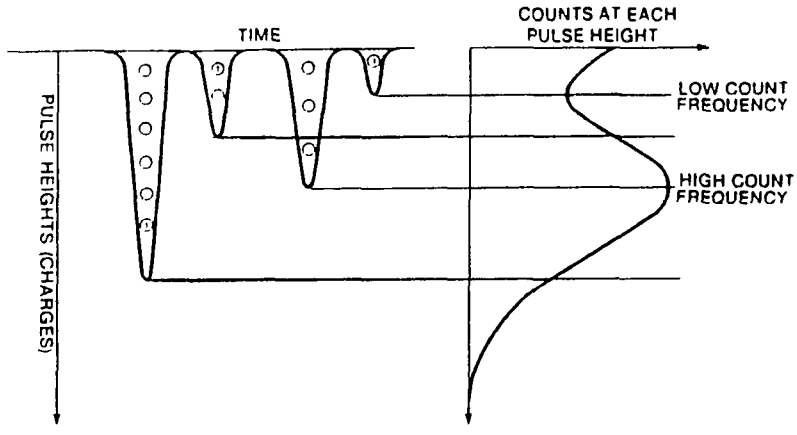

Figure 4 10· PMT Output and various Pulse Heights.[4]

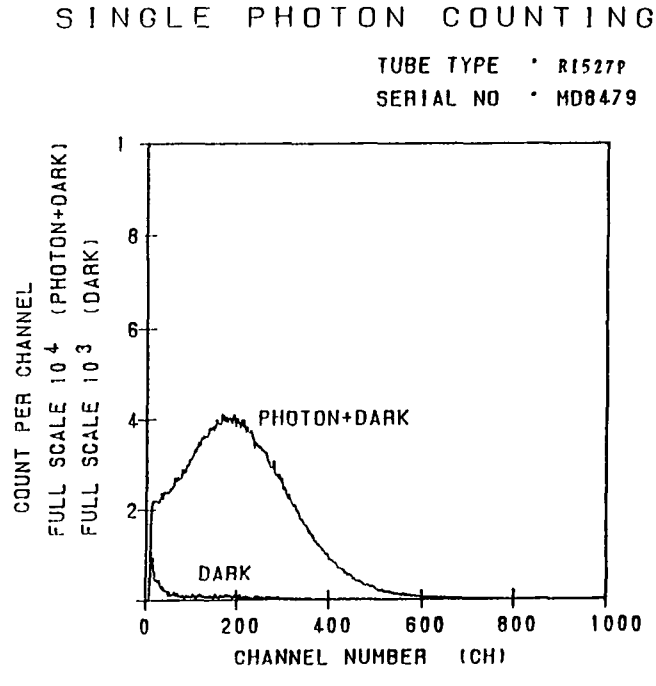

Figure 4 11· Pulse Height Distribution.(PHD)

[4]Ref #5

3. Deviation of electrons from normal multiplication process.

These effects manifest themselves in a pulse height distribution(PHD) as in Fig 4.10 and Fig 4.11 and it is by examining this P.H.D. and by varying the parameters governing PMT operation, that the photon counting system is maximised for a particular application.

4.4.2 Maximising PMT use for Light Detection.

As is evident from Figs. 4.10 and 4.11 there is always a distribution of signal pulse heights from a PMT due to the statistical nature of the secondary emission process. There is another distribution of noise pulse heights from dynode thermionic emission which have a lower mean pulse height than signal pulses. In order to eliminate these pulses from the count and improve the signal to noise ratio, a lower level of discrimination (LLD) is set above most of the noise pulses but below most of the signal pulses. In cases where higher fluxes of light may occasionally appear it may be necessary to set a high level discrimination (HLD) level also to eliminate readings caused by double photon counting. Double photon counting occurs when two photons appear so close together in time at the photocathode that the PMT cannot resolve them and instead of two single photon pulses, one pulse of a much higher level is detected. The HLD may also eliminate counts due to high energy cosmic rays which may impinge on the PMT.

At this point a special photon counting tube and potential divider base were employed; Hamamatsu R1527P and base C956-06. This tube had a UV glass window (higher transmission in the UV) and had a special low noise bi-alkali photocathode. The current amplification was 5 x 10^6, dark current 0.1 nA and a typical risetime of 2.2 ns. The necessity for using the C956-06 photon counting base was that it totally encapsulated the negative high voltage power supply and voltage divider circuit thus reducing EMI/RFI noise signals but also for the following reason. Fig 4.12 shows the collection efficiency observed when changing the voltage of the photocathode to first dynode of a typical R268 PMT in photon counting mode. Thus it is obvious that in order to stabilize collection efficiency it is necessary to apply kilovolts to the photocathode and first

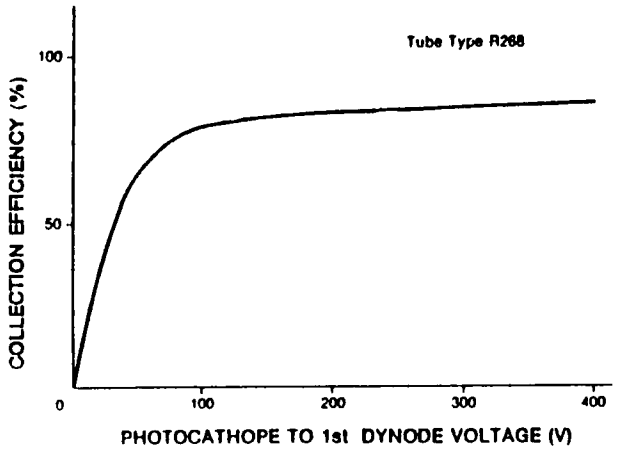

Figure 4.12: Collection Efficiency vs Potential at Ist Dynode.

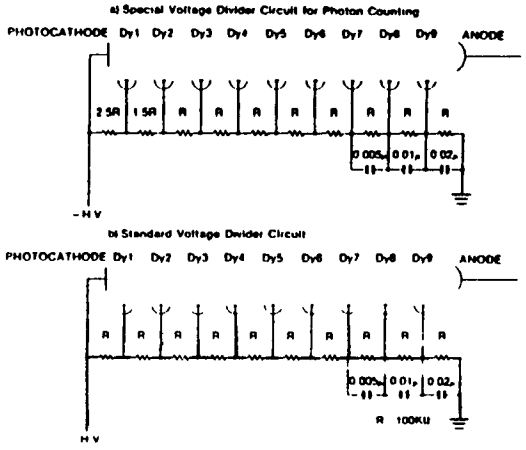

Figure 4.13: a) Standard Dividing Base and b) Special Photon-counting Divider.

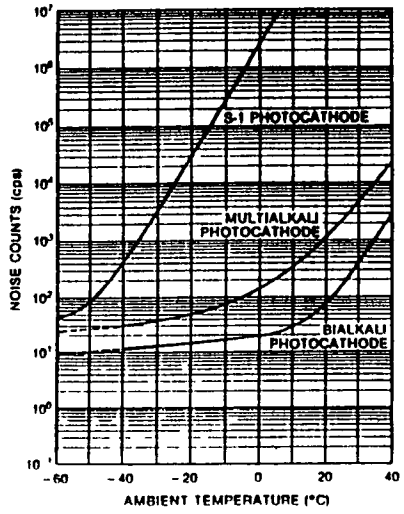

Figure 4 14· Thei mal Noise Performance.[5]

[5]Ref #5

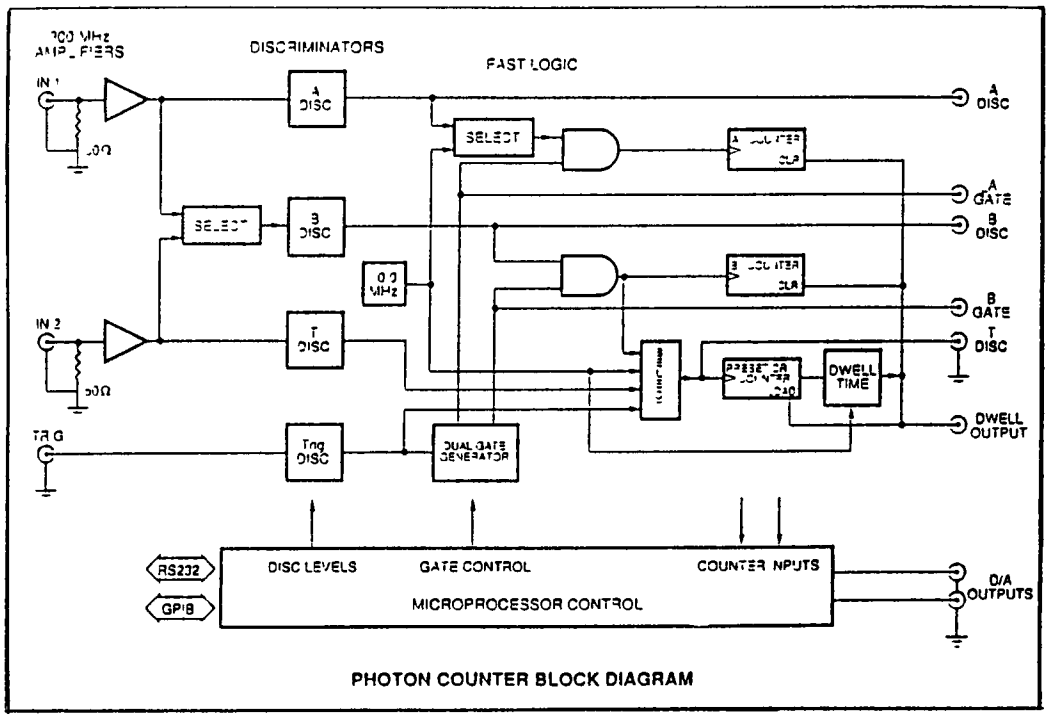

Figure 4 15. Photon Counter (Schematic).[6]

[6] Ref #6

dynode. Photon counting divider circuits enhance the collection efficiency and secondary emission amplification by applying more voltage than in the normal case across the first and second dynodes See Fig 4.13. This type of voltage divider has a slightly lower current amplification than the standard bleeder circuit but enhances the PHD characteristic curve making it easier to determine the best LLD.

Noise in PMT's may also occur by thermionic emissions from the photocathode and glass scintillations but as these were not noted as being of significance initially they were included in background noise and were referenced out in most measurements carried out in this work. This may have been due to the superior thermal noise performance of the bi-alkali photocathode (Fig 4.14). It was further noted that leaving the PMT in total darkness to stabilize (Slits closed) for an hour before use reduced PMT noise to insignificant levels.

4.4.3 The Photon Counter.

The final step in signal conditioning before datalogging is converting the analog pulses from the PMT to a digital signal for counting. The Stanford Research Systems SR400 Dual-channel Gated Photon Counter [6] was used for this purpose. This unit contained all of the individual modules needed for photon counting in one microprocessor-controlled unit. Included in this are three 200MHz counters which can be configured in a number of different counting modes. Each counter has an associated fast bipolar discriminator to allow window discrimination of pulses. The fast input amplifiers are sensitive to 10mV and dual gate generators can provide count gates from 5nsec to 1sec (See Fig 4.15). This module was accessible via RS232 interface and was interfaced to an AT personal computer. The SR400 front panel was accessed via the pc and the necessary setups were programmed in the pc to help automate the data acquisition process

4.5 Sample Preparation and Testing.

The samples used in order to investigate the variation of fluorescence of phenol with wavelength and with concentration were made up from a serial solutions of a 100ppm stock solution. This was further diluted into solutions varying from 1ppm down to 1ppb in steps of (1,2,5) per decade. The procedure for both

wavelength and concentration studies involving regular reference to a pure water solution is outlined in Appendix E. This procedure for low concentration samples followed rigorously the guidelines set out by the EPA [7][8].

4.6 Results.

4.6.1 Spectral Dependence of Phenol Fluorescence.

After the DM150 monochromator was calibrated using a HeNe laser 622.8nm a scan of the light backscattered from a pure water solution was taken from 250nm to 330nm using a customised setup on the SR400. This procedure was then repeated using 0ppb and 800ppb solutions. The monochromator step increment was 1nm/sec and the spectrum consisted of the number of counts at each wavelength. The count rate at each wavelength represents not just the phenol fluorescence but also the response due to lamp output, reflections, filter responses, lens aberations, fibre spectral attenuation and detector response. However, if it can be proved that these factors do not vary in the short term then dividing the phenol solution fluorescence spectrum by the pure water spectrum will cancel out the overall system response. Figs 4.16(a) and 4.16(b) show that even before this has been carried out that a fluorescence effect peaking in the 290-298nm region is evident. Fig 4.17 is a graphical display of Fig 4.16(a)/Fig4.16(b) giving a pure phenol fluorescence spectrum from 280-310nm and finally, Fig 4.18 shows the temporal response of the system in the region of interest over a 24hr period for pure water. This is a fibreoptic version of the rarely-used approach outlined in Chapter 2 section 2.3.4 and could easily be used to establish a phenol calibration curve.

4.6.2 Concentration Dependence of Phenol Fluorescence.

The concentration variation of the phenol solutions tested is illustrated in Figs. 4.19 and 4.20. Each of these plots represents a 100 second integration time at 294nm. The y axis on each represents the number of photons counted in this 100sec integration time and as illustrated in Fig 4.21 this is linear with concentration within statistical $\sqrt{N}$ error bars. Note that these plots show the fluorescence effects due to concentration change and that the effect is marked even at low ppb concentrations. Fig 4.22 shows a number of similar plots taken

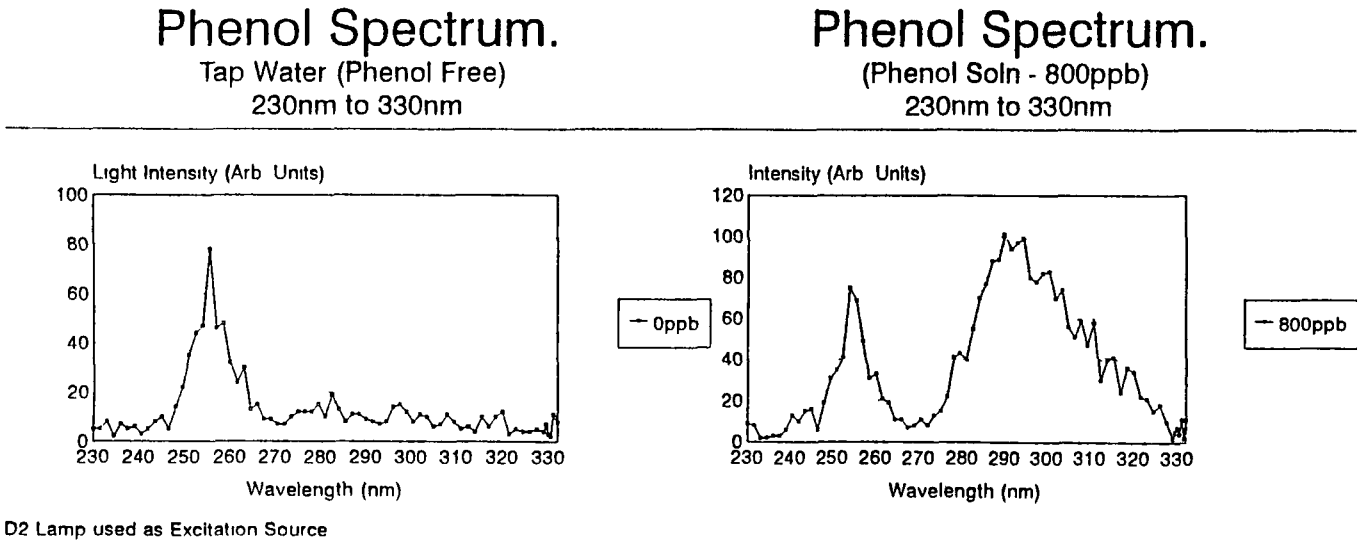

Figure 4 16 (a) 250nm to 350nm (800ppb phenol),(b) (0ppb).

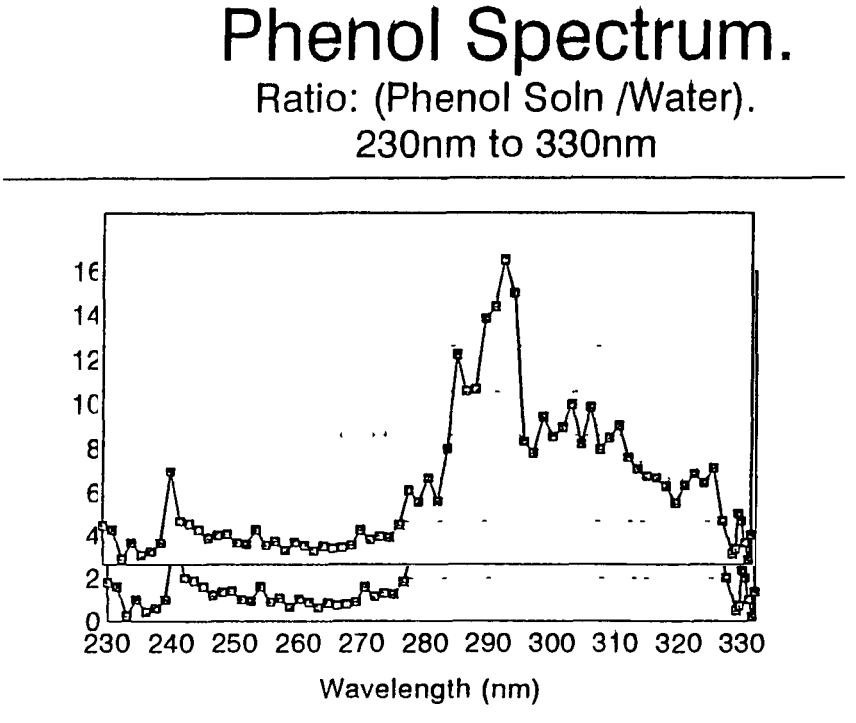

Figure 4 17: System response + phenol/System response.

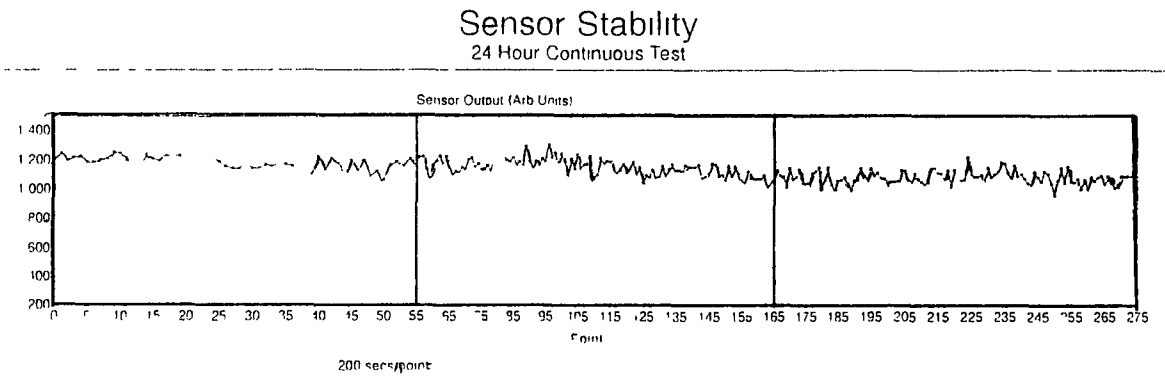

Figure 4 18 Temporal Response of System (24hr)

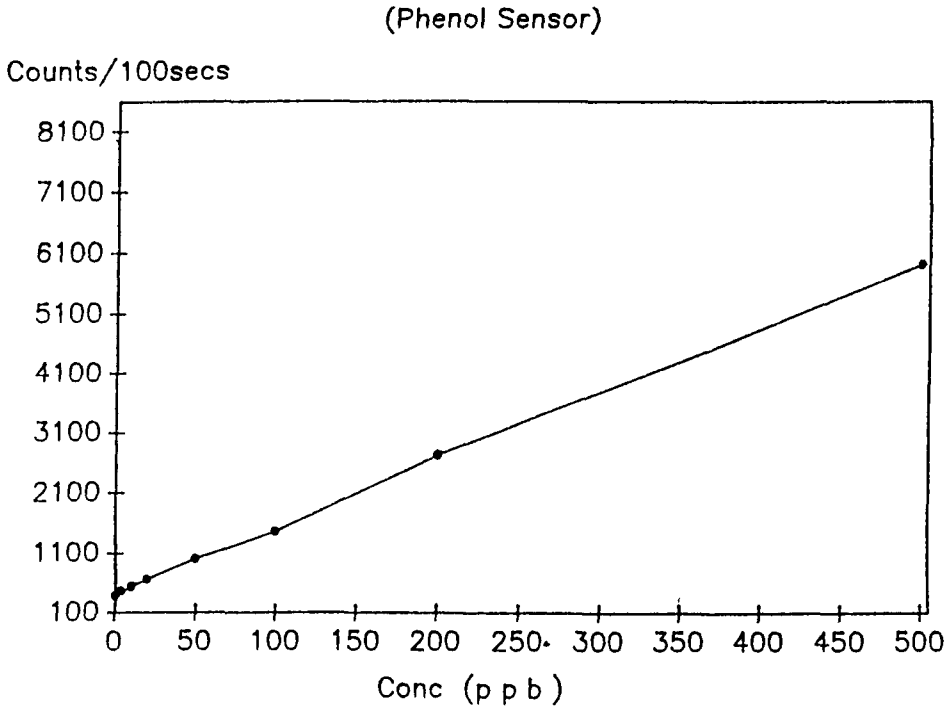

Figure 4 19· Phenol Fluorescence vs. Concentration.(1000ppb Range)

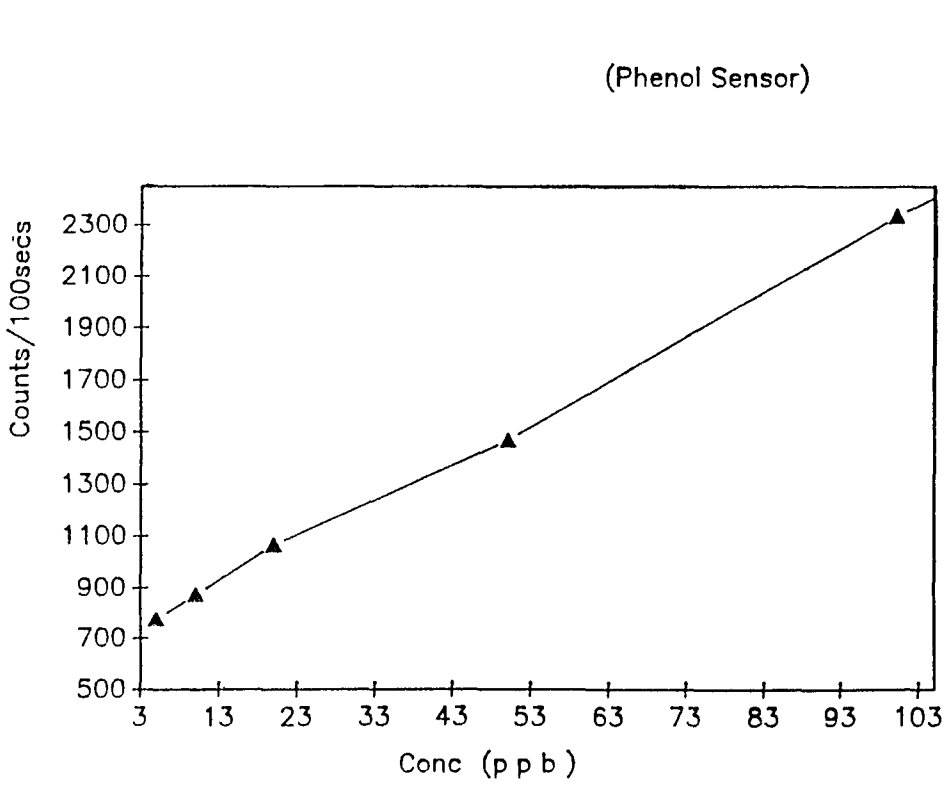

Figure 4.20 Phenol fluorescence vs Conc (0-100ppb Range)

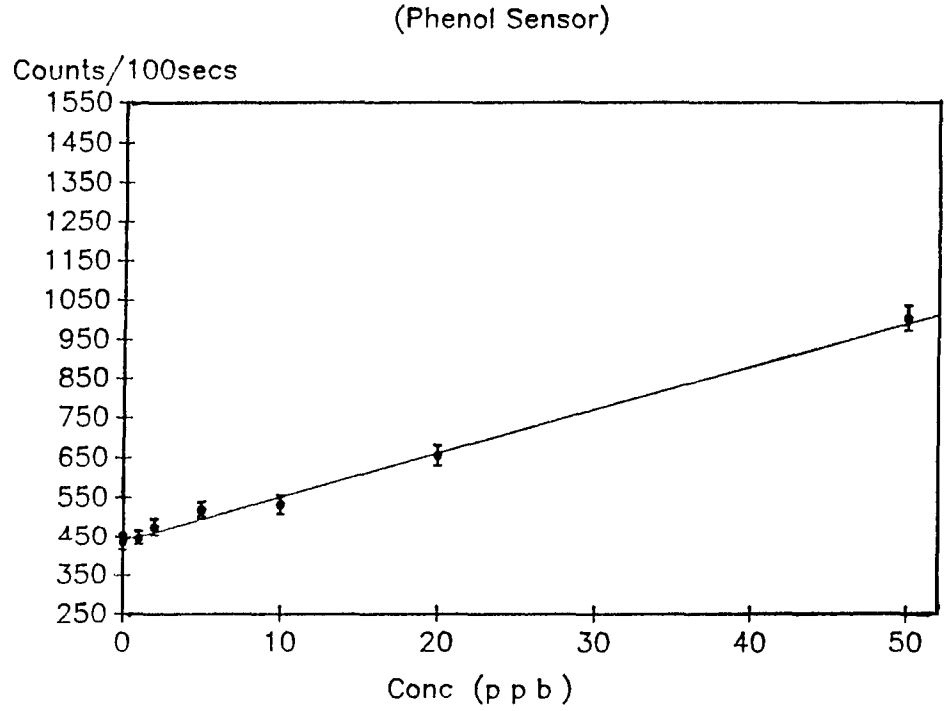

Figure 4.21 Statistical Errors $\sqrt{N}$

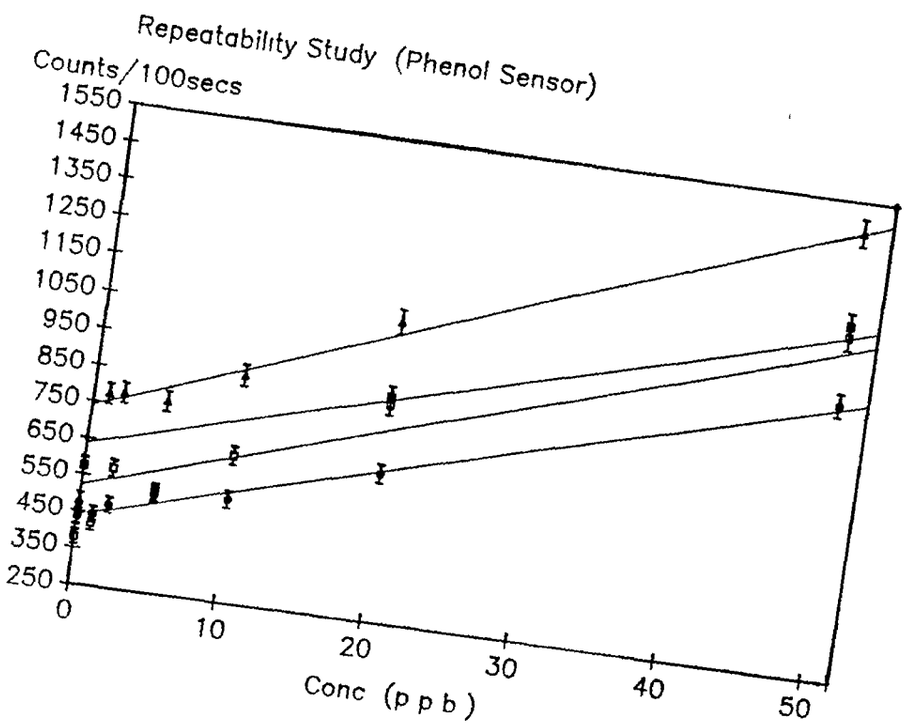

Figure 4 22 Repeated Phenol Fluorescence Scans.

on different days and with different batch solutions and it may be noted that the slope is always similar. The daily variations and the apparently large difference between individual sample results is due to degradation of the sample used. Phenol is very volatile and degrades very quickly in daylight and at room temperatures. The system demonstrated that the slope of the degrading sample was always the same. It should also be noted however that the system was in no way maximised ie no source compensation, ageing effects referencing etc. These plots are simply raw fluorescence readings.

4.7 Conclusion.

The work in this chapter was carried out to estimate the use of the fluorescence of phenol in water as a diagnostic tool for contaminant concentration determination. This work was also used as a baseline for the development of a fibre based transportable field instrument for real-time assessment of phenol contamination in water. Furthermore it verified previous work [7] which claimed a fluorescence peak for phenol exists between 280 and 310nm and also showed a degree of sensitivity with concentration. Although it was not developed further this "9 around 1" fibre probe design with appropriate hardware and system compensation could show promise as a field instrument in its own right. This may happen if an alternative high power light source was identified other than the cumbersome Deuterium lamp and power supply and if a filter approach was used instead of the monochromator. Alternatively further development of the present system could lead to a resolution of sub ppb level and thus find use as a lab-based instrument. As it is it provided an excellent step in the direction of the laser based system discussed in Chapter 5.

References

1. J.E. Fountaine, P.B Joshipura et al.: "**New Ultraviolet Ratio Spectrophotometric System for the Determination of trace amounts of Phenolic Compounds**", Analytical Chemistry, Vol. 46, pp. 62-66,(1974).

2. ORIEL Corporation: "**Light Sources : Technical Specifications and Reference Data for Deuterium Lamp Sources**", pp 70-75, Vol.2, (1992).

3. Hecht: "**OPTICS**", 2nd Edition, Addison Wesley, Chp. 3, pp. 170-172, (1987).

4. Fibreguide Industries "**Fibreguide Industries Superguide SPC 400B", Information/Specification** Sheet, (1990).

5. HAMAMATSU: "**How to Perform Photon Counting using Photomultiplier Tubes" Technical Information Publication No. ET-06** ",.(Feb 1990).

6. Stanford Research Systems: "SR400 Dual Channel Gated Photon Counter Manual"

7. Mary S. Quinby-Hunt: "**Instrumentation for Environmental Monitoring: Lawrence Berkley Lab. Environmental Instrumentation Study**", pp 497-538, Chp.12, Vol.2 (Water), J. Wiley and Sons (1986).

8. American Public Health Assoc. et al.: "**Standard Methods for the Examination of Water and Wastewater**", 15th ed., American Public Health Assoc., Washington DC. (1981).

9. W. A. Chudyk et al.: **"Remote Detection of Groundwater Contaminants Using Far-Ultraviolet Laser Induced Fluorescence"**, Analytical Chemistry, *57, pp1237-1242, (1985)* .

10. F. Bosch, G. Font and J Manes: **"Ultraviolet Spectrophotometric Determination of Phenols in Natural and Waste Waters with Iodine Monobromide"**, *Analyst*, Vol. 112, pp 1335-1337, (1987).

11. J.N. Miller : **"Standards in Fluorescence Spectrometry: Techniques in VIS and UV Spectrometry"**,Vol.2.,Chapmann and Hall, Chp1, p1, (1981).

CHAPTER 5

CHAPTER 5.

DUAL FIBRE PROBE: FIELD SYSTEM.

5.1 Introduction.

The following chapter is a detailed description of the portable sensor prototype which was built, based on the work previously carried out and discussed in Chapter 4. The main features of this system are the change in the source used (a lightweight compact Nd:Yag laser), the fibre used and also the analog detection mode used to quantify the fluorescence generated by the phenol. Also incorporated into the prototype is a detector which compensates for variations in the source intensity. A detailed account of the software developed to run the sensor in detecting both pure phenol as well as a combination of phenols is analysed and the results presented.

5.2 The UV Laser System: Laser, Probe and Optical Configuration.

A decision was taken to further develop the sensor conceived in Chapter 3. As discussed in 3.6 there were two main designs in which the sensor could take form. The first, constructed and tested and comprehensively detailed in Chapter 4 is a 1m long probe with a multi-fibre collection configuration. The second, which is discussed here, and illustrated in Fig 5.1 is a 15m dual-fibre probe. This length was chosen as it is the maximum useful distance to which a well or borehole would need to be probed in order to find pollutants and was the initial impetus for the project. It was decided to use one transmission and one collection fibre but a fibre with higher transmission characteristics than previously used. This is an extension of the approach used by Chudyk et al.[1]. A stronger source of UV excitation radiation was also used. Ostensibly, there is no material which can provide laser light in the 250-260nm region of the UV spectrum. However, if the 1064nm emission line of the Nd:Yag laser is frequency quadrupled using the second harmonic generation properties of a non-linear crystal (BBO) a laser output centred at 266nm is produced.

The laser used was a "New Wave Research" Minisystem 266 and works on the following principle. The YAG rod is pulsed by a Xenon lamp to excite the

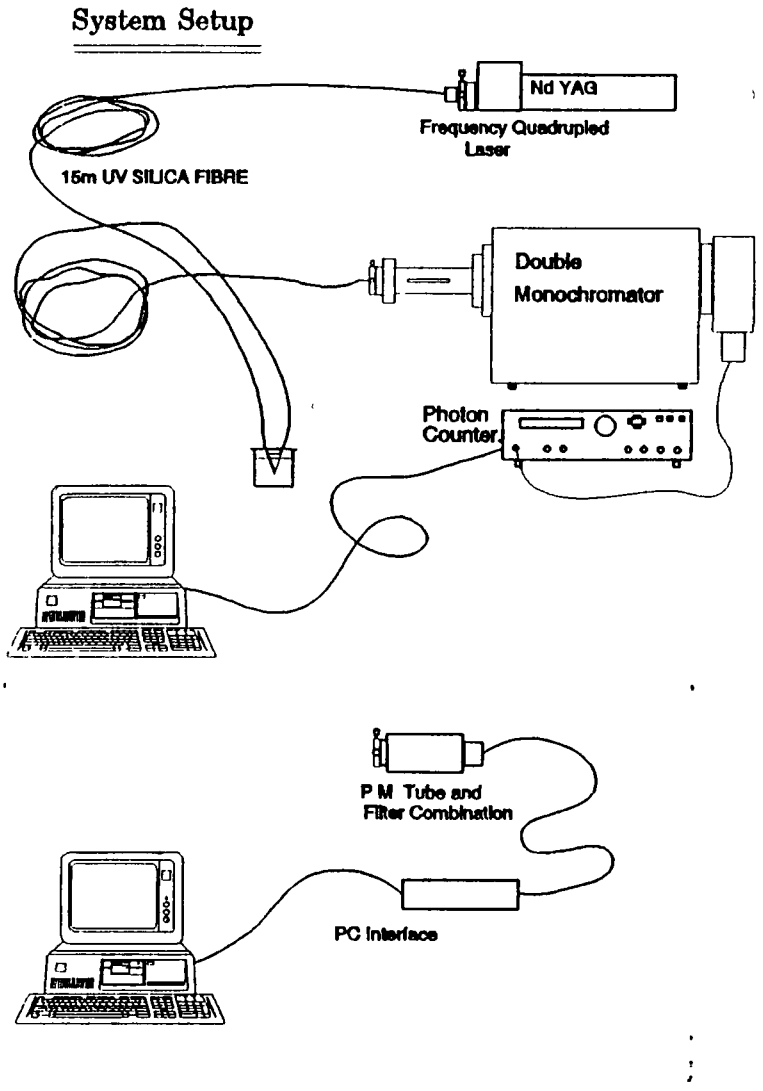

Figure 5.1: Prototype System (Experimental).

neodymium into a higher energy state. A Q-switch is created by applying varying voltage to an electro-optic device made of a KDP crystal. 3.5 kV is applied to the crystal to give the quarter wave voltage for KDP at 1064nm (the laser's wavelength). In conjunction with the KDP a quarter waveplate and polariser comprise the Q-switch. The beam then enters the BBO crystal where the beam frequency is quadrupled (See Fig 5.2(a)). The non-linear optical effect enables the laser's fundamental frequency to be increased at the harmonics by simple doubling tripling and quadrupling. BBO has a high figure of merit for frequency conversion, has high transmittance in the UV, Visible and Infra-Red and can withstand high peak intensity laser beams without damage. The wavelength-quartered light (266nm) exiting the crystal is then twice reflected at an angle of 45° so as to coincide with the path of a laser diode pointer incorporated into the system. The laser diode is necessary for alignment purposes. The final stage of the laser system is an attenuator. The attenuator is comprised of a halfwave plate (266nm) and a calcite polariser, where the half-wave voltage is adjusted by using a 1000 stage potentiometer. When the 1000 stage potentiometer is set to 000 the polarisation is rotated 90° and the calcite polariser rejects the maximum amount of UV light. At its max, the Q-switch delivers a pulse of approximately 0.3 mW [2]. Although this laser was compact (See dimensions on diagram) and had a number of notable features some modifications were carried out to customise it for use in the phenol sensor prototype. The spotsize was greater than the diameter of the fibre being used and so an f/2 silica lens of 12mm diameter (Howard Smith Precision Optics) was mounted in the path of the 266nm beam between the mirror and the attenuator within the laser housing(See Fig 5.2(a)). A special jig was constructed so that the fibre could be positioned precisely at the new focus of the output beam using an x-y positioner (See Fig 5.2(b)). The laser was then rigorously tested. Firstly, the spectral distribution of the pulse was examined and was found to have two distinct major peaks at approx. 265 and 267nm as shown in Fig 5.3. Traces verifying the temporal stability and the attenuator accuracy are given in Appendix F.

The fibre used in this two fibre probe was superior to one used in the multiple fibre probe system in that it had both a silica core and cladding and also had

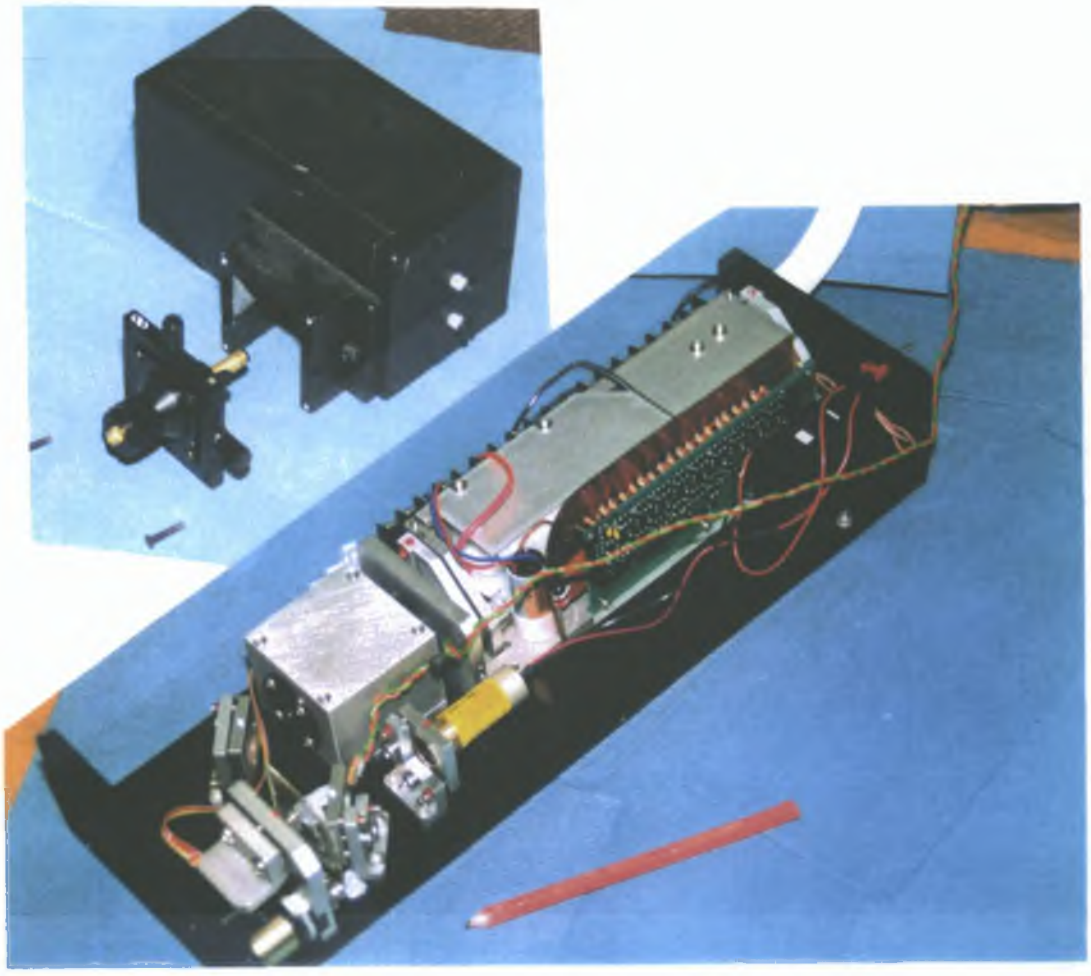

Figure 5.2: (a)Laser Head Layout. (b)X-Y Positioner for Laser Head.

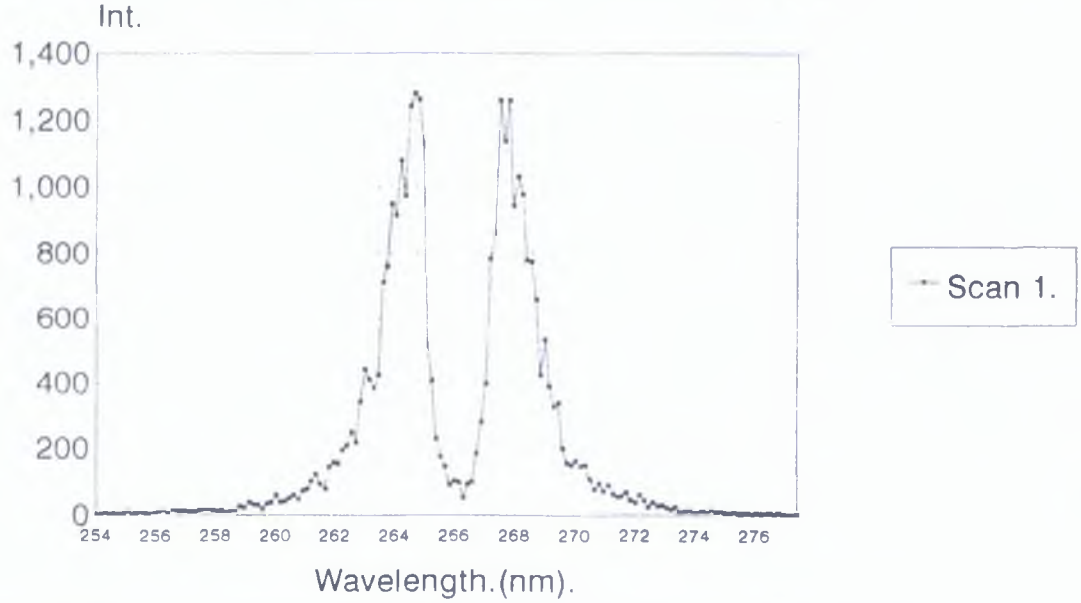

Figure 5.3: Frequency-Quadrupled Nd:YAG Laser Spectral Distribution Note;(0.5nm Resolution System).

double the core diameter. This was necessary in order to transmit the laser power and collect the fluorescence over the 30m round trip. As was previously discussed in Chapter 3 the excitation and collection fibres were mounted on a jig at an angle of 16° with respect to each other, the angle being dependent on the fibre characteristics.

5.3 The Detection System.

The detection system is analog in nature, as opposed to the photon counting system employed in the lab-based system. The detector used was the same as was used in Chapter 4; a HAMAMATSU R1527P side-on photomultiplier tube. In its entirety the system consists of a photomultiplier tube used to detect the low fluorescent light levels, a compensation circuit to reference peak power of each laser pulse to its corresponding fluorescence pulse and an A/D convertor "BYTRONIC MPIBM3" multifunction I/O card and pc software to co-ordinate delays and data collection and manipulation. The remainder of this chapter deals with description of the various facets of the system, the tests carried out using the system and the results of these tests.

5.3.1 Analog Detection System.

The collection fibre is fed into an x-y positioner which was initially mounted on the BENTHAM DM150 monochromator for spectral studies with the Hamamatsu R1527P mounted at the exit end of the monochromator. The final prototype design however implemented an X-Y fibre chuck positioner mounted to a screw-in fitting which in turn screws into the PMT mount (See Fig 5.4). The screw-in fitting was designed to hold a filter (OCA Microcoatings MC-297) 294.2nm centre wavelength, 32.4nm fwhm, which takes the place of the monochromator. The entire stage was light-tight using a custom designed O-Ring system and low mechanical torque to ensure stability and reduce background light to a minimum. No collection lens was used as the fibre endface was sufficiently close to the window of the PMT to avoid overfill of the detection area. The pulse created due to the fluorescence (negative polarity) is fed through an inverting amplifier and a pulse broadener and into channel 1

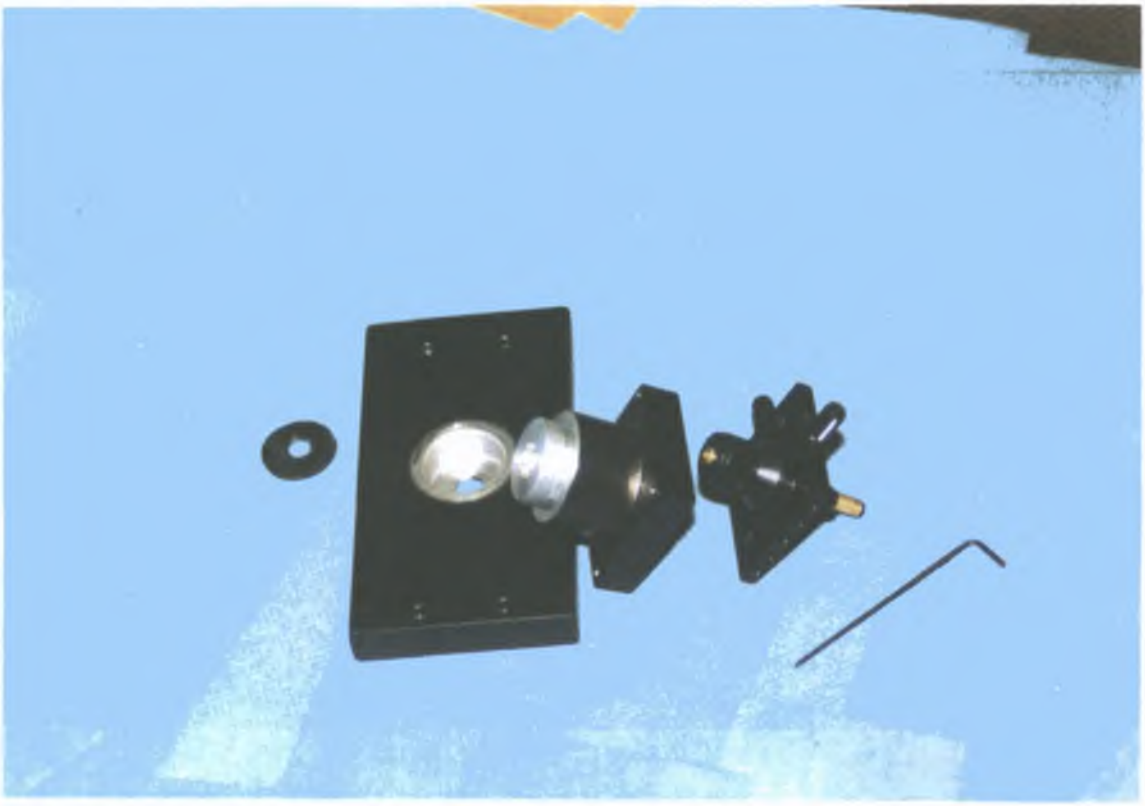

Figure 5.4: Prototype Sensor Housing (Most Recent Design).

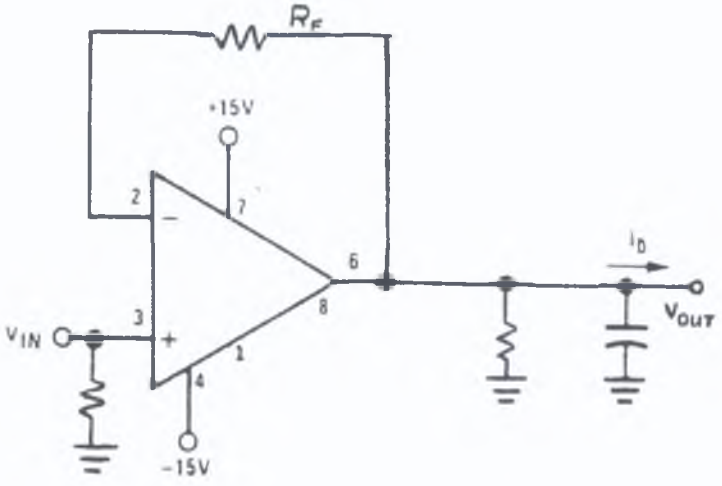

Figure 5.5: Phenol Fluorescence Detection Circuit.

of the analog to digital controller card. The reason for broadening the pulse is to take as many samples of each pulse as possible in order to best represent the fluorescence intensity. The circuit shown in Fig 5.5 is a schematic of the fluorescence detection circuit. The light is detected by the PMT and is converted to a current pulse of negative polarity. The pulse is then broadened and amplified using an RC circuit and an amplifier. The fluorescence pulse is then picked up by the A/D convertor through Channel A and is saved to a file for further analysis. The timing and co-ordination of the system is outlined in section 5.4.

5.3.2 Source Compensation.

The source compensation circuit is a regular photodiode BPX-65 with the protective transparent filter removed followed by an amplifier and a pulse height detection (peak-hold) circuit; Fig 5.6. The filter on the photodiode was removed to enable it to detect light below 350nm. The photodiode is mounted off-axis within the laser and the signal is fed via the green-red wire pair to the amplifier. The amplifier signal, in turn, is fed to the pulse height detector where the maximum height of the pulse is stored on the Capacitor which is prevented from discharging by the diode. If the input voltage of the amp1 is greater than the output of amp2 the output of amp1 will go positive charging the capacitor until the output and input voltages are equal. This voltage value is read into the A/D convertor along channel B and stored in the computer for further evaluation (See Section 5.4).

5.4 System Control and Software Development.

The timing within the system, as a whole, is governed by the speed of acquisition of data points after a trigger pulse and thus on the clock within the computer/datalogger. The system control and controlling software can best be described by examining Fig 5.7. The computer program called "Tes.c" is written in Turbo C for speed as this is the closest computer language to machine code and thus is also the fastest. When "Tes.c" is run, it opens three data files, one for fluorescence values, one for source power values and one for source compensated fluorescence values. It also enables both channels A and B of the

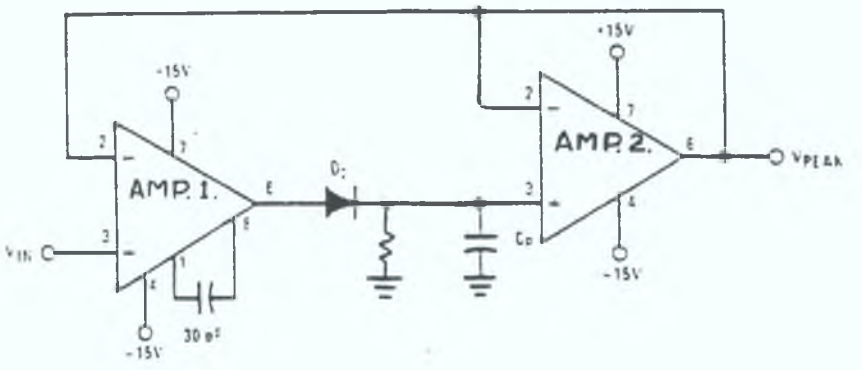

Figure 5.6: Pulse Height (Peak-Hold) Circuit.

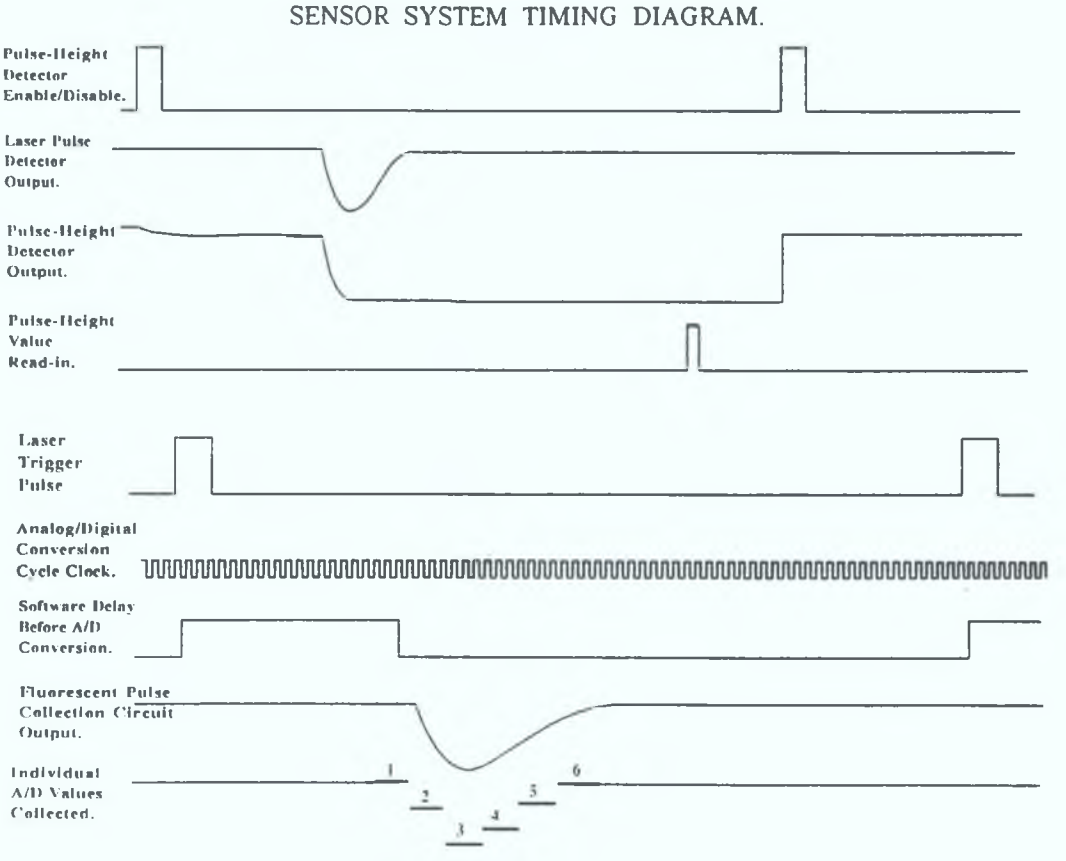

Figure 5.7: Prototype System Timing Diagram.

Analog to Digital convertor card and awaits a trigger from the laser. This trigger coincides with the initial flashlamp pulse used to pump the laser. The trigger was the pivot of the timing sequence within the system. In Fig 5.7 it is the first event displayed at the top of the timing diagram. All other events (laser pulse, fluorescence and analog to digital conversion) take place at a fixed time later and with respect to this pulse. An earlier software program "Pulsfind.c" utilised variable software delays to find the position in time of the other events displayed in Fig 5.7. This also allowed the fluorescence pulse characteristic to be studied. "Tes.c" waits for this initial pulse and then counts out a fixed delay before data from the fluorescence pulse is collected and stored.

On the row labelled "A/D conversion cycle clock" the duration of the high state is the time it takes to carry out one A/D conversion (typically 22μs) [3]. During the low state the value is labelled and then the cycle is repeated. When the software delay mentioned above expires the program begins to take in sample values (six in all) which represent the intensity of the fluorescence pulse as can be seen from Fig 5.7. These values are taken in on Channel A of the A/D Convertor.

Because of the close proximity of the laser pulse and the fluorescence pulse in time and the limited resolution of the system the laser power value is fed to a pulse height storage circuit as described in 5.3.2 above. This circuit is enabled by a "Tes.c" generated signal from the computer. The A/D control card used had only two channels (Channel A: Fluorescence)(Channel B: Laser Pulse) so the pulse-height storage circuit was enabled/disabled via the printer port. When the fluorescence values have been stored the analog value is read in on Channel B of the A/D convertor then digitized and stored. The pulse detection circuit is then disabled (Storage capacitor discharged) via the printer port. Thus the characteristic shape of each fluorescent pulse and its corresponding laser power pulse is recorded. "Tes.c" then calculates the ratio of one to the other and flashes this value to the screen as well as storing it on file before the next trigger pulse occurs. A number of other software programs written to calculate statistics from this data for presentation as completed results are described in detail in Appendix G. "Tes.c" and "Pulsfind.c" are also included.

5.5 Results.

5.5.1 Spectral Study and Fluorescence Effects.

As in chapter 4 the spectral dependence of Phenol was studied bearing in mind that this was duplication as a new source and detection system were being used. The solutions were again prepared according to EPA guidelines as in Chapter 4. The result can be seen in Fig 5.8. In addition, the same setup was used to analyze a combined phenols solution ie. 60% Phenol: 15% O-Cresol: 15% M-Cresol: 10% P-Cresol (Ref) Fig 5.9. It was on the basis of these results that the filter mentioned in 5.3.1 (OCA Microcoatings) with wavelength centred at 294.2nm and fwhm of 32.4nm was chosen for the final prototype. There has long been a recognised effect on fluorescence with variation in pH so a brief study of this effect was also carried out the result of which can be seen in Fig 5.10. The combined phenols solution was used with a buffer solution. This buffer solution consisted of 0.4 molar Phosphoric acid, 0.4 molar Boric acid and 0.4 molar Acetic acid. The pH was then adjusted by using HCl solution to decrease the pH level and NaOH to increase it. Fig 5.10 shows the variation between identical concentrations with different pH level demonstrating that alkalinity quenches fluorescence. Previous work by Kullbom et al. [5] has shown that fibre fluorescence has been a major source of interference in optical fibre fluorescence studies of chemical analytes. For this reason the system was tested both with and without the fibre in situ and a region of fluorescence was found approximately 100nm wide and centred approximately at 400nm was found (Fig 5.11). As the work involving phenol fluorescence is concerned with wavelengths not greater than 330nm this fibre fluorescence was not a concern. Acting on this investigative information the prototype was developed into its final stage for use as a tool to determine concentration of phenol/phenols in groundwater.

5.5.2 Phenol Concentration Study.

As before solutions were prepared from stock solutions and serial dilutions gave the various concentrations desired. The first concentration study was carried out on pure Phenol to examine the resolution of the system. Pure water

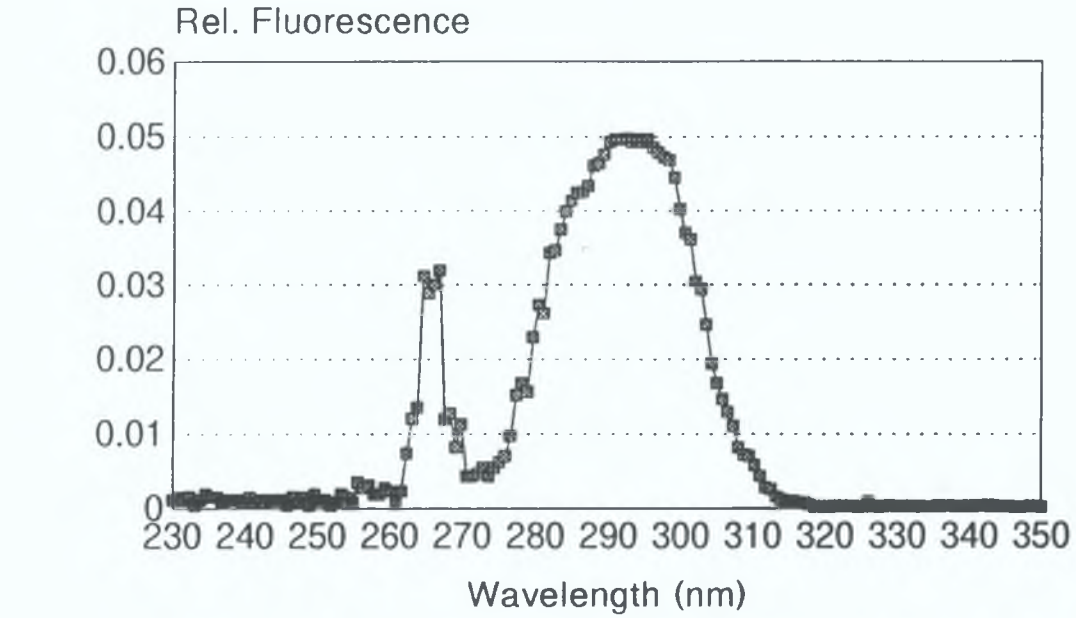

Figure 5.8: Phenol Spectral Study (15m Prototype Sensor).

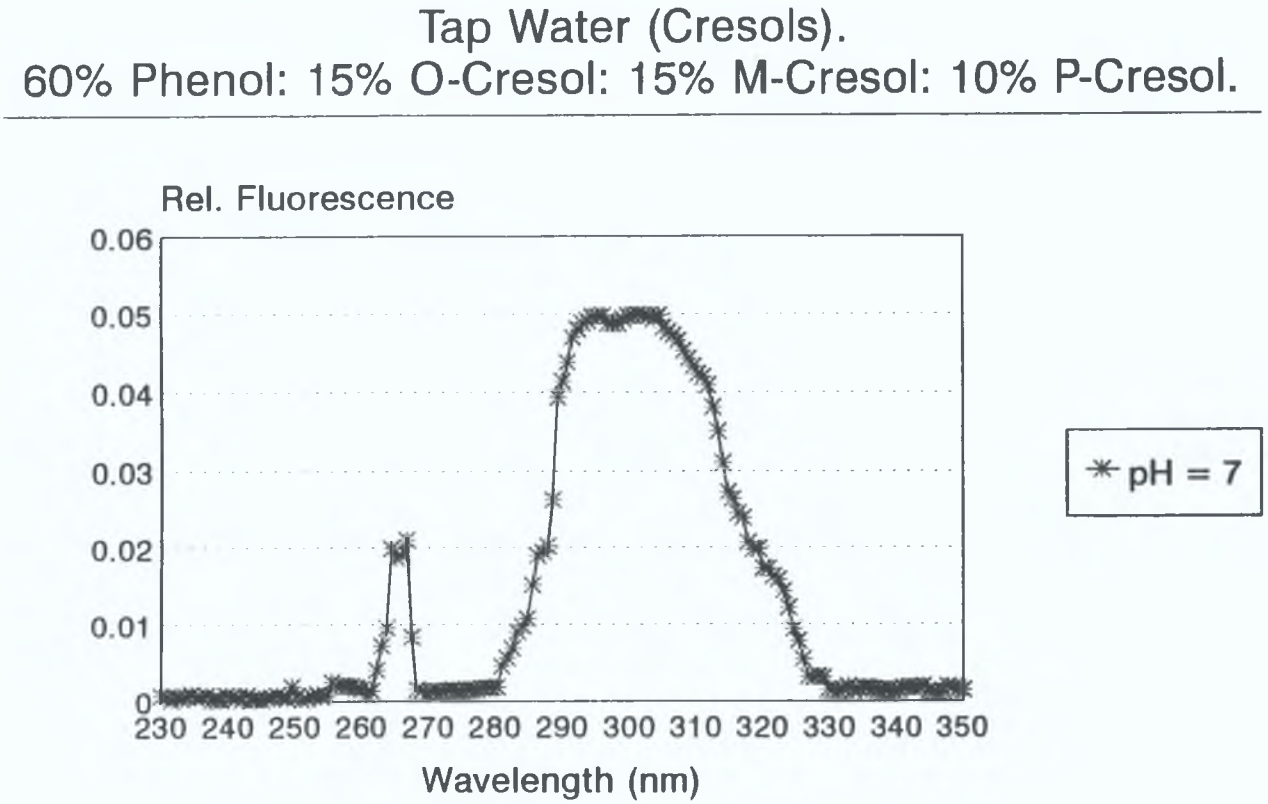

Figure 5.9: Phenol/Cresols Spectral Study.

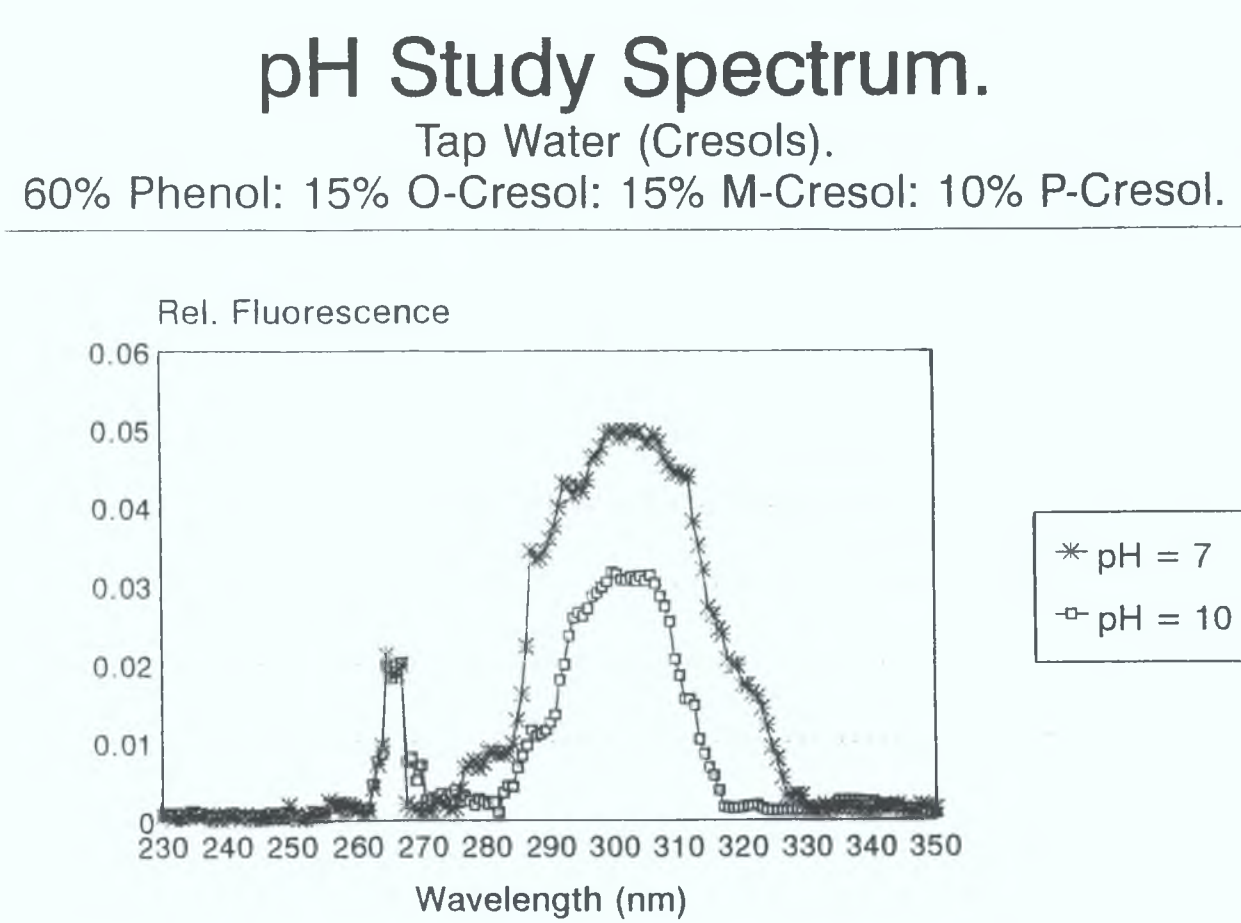

Figure 5.10: Spectral Analysis of pH Study (Phenol combination).

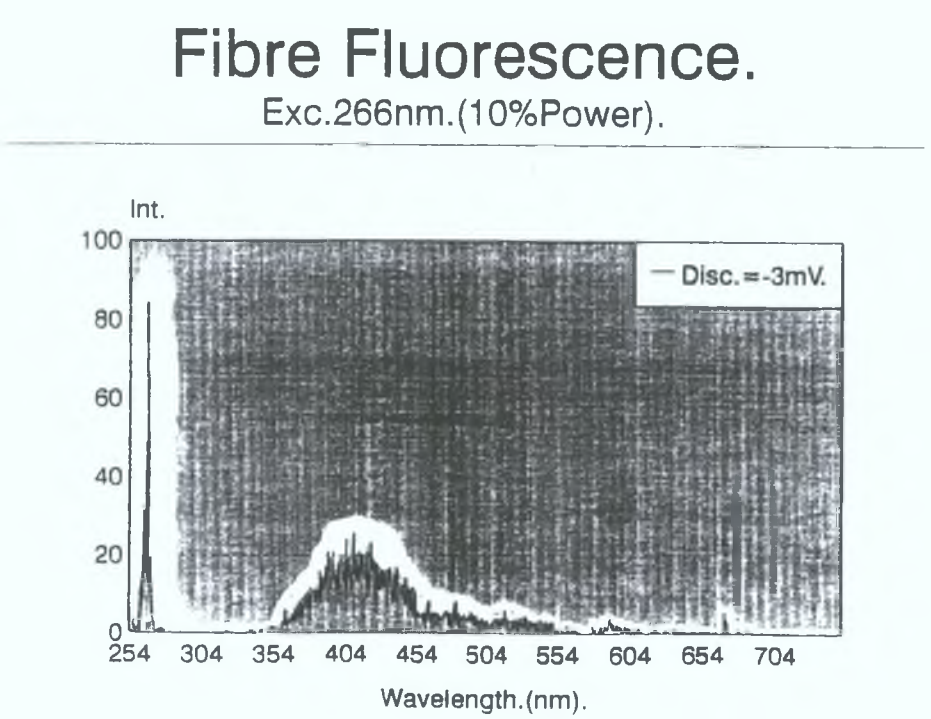

Figure 5.11: Fibre Fluorescence (Excitation Wavelength: 266nm).

was first examined to assess the signal returned and to give a base value. The system was then tested from 1ppb to 500ppb and the resultant calibration data recorded. To test the system for hysteresis the procedure was repeated from 500ppb to 0ppb. The data taken was tabulated and assessed and a number of interesting effects noted. The only difference in the data presented for Figs. 5.8 to 5.11 is the points from the fluorescence pulse which were used to outline the concentration performance of the sensor. If the points can be labelled 1 to 6 as in Fig 5.7 then in Fig 5.12(a) points 3 and 4 were added and referenced to the corresponding laser power. In Fig. 5.12(b), however all six points were totalled and referenced. Thus we see a marked difference in both linearity and resolution of the system by interpreting the results differently.

Fig 5.12(b) shows linearity over the full range but the resolution based on a Signal/Noise ratio of 2 is approximately 20 ppb although this is discussed in more detail in 5.5.3 below. Fig 5.12(a), while displaying excellent S/N ratio at 1ppb (~2) has a region of non linearity between 1ppb and 75ppb which can possibly be attributed to fluorescence saturation or bleaching which is not uncommon at low concentrations. The calibration curve for both methods is shown in Table 5.1 below and could be incorporated in later prototypes as a programmable hardware reference (EPROM).

TABLE 5.1			
CALIBRATION CURVE DATA			
Method	**Conc (ppb)**	**Relative Fluorescence**	**Standard Error:($\sigma/\sqrt{200}$)**
3-4 Method	0	0.0252052	0.0001468
	1	0.0272933	0.0001265
	2	0.0293106	0.0001034
	5	0.0294511	0.0000954
	10	0.0294580	0.0000745
	16	0.0298492	0.0000330
	20	0.0301960	0.0000362
	30	0.0303541	0.0000341
	40	0.0307550	0.0000292
	50	0.0310192	0.0000316
	75	0.0314227	0.0000327
1-6 Method	50	0.0440872	0.0000488
	75	0.0445704	0.0000492
	100	0.0456822	0.0000750
	200	0.0499173	0.0000946
	300	0.0546487	0.0001041
	400	0.0600987	0.0001620
	500	0.0645674	0.0001673

5.5.3 Commissioning of Prototype Sensor.

From the above analysis, it is assumed that the sensor will be treated as a device with three linear regions; The 0 to 5ppb region and 5ppb to 75ppb which uses the "3-4" calibration curve as outlined above and the 75ppb to 500ppb region which makes use of the "1-6" calibration curve. The data outlined in Fig 5.8 to Fig 5.12 is simply the sum of a number of source-compensated raw fluorescence points (200). This is perhaps made more clear by Fig.13 where the 200 readings taken at each of three concentrations as well as a zero level is displayed. The average of the 200 readings for each respective concentration is displayed by a least squares regression best-fit line. Each point in Figures 5.8 to 5.12 is an average value and is thus equivalent to one of these lines. While this gives a description of the process taking place and an approximation

of the effectiveness of the prototype system it was necessary to specify the range and resolution and a number of other parameters in a more definite manner with an estimation of the standard error involved. These parameters are described as follows:

(i) *Range*: This is the number of measurand values over which the sensor gives an unambiguous signal. The range of this sensor for the two regions outlined above is 0 to 500ppb.

(ii) The *sensitivity* is the measure of the incremental change in signal with change in concentration. For this sensor this value varies due to the non-linear region at lower concentrations. For this sensor the sensitivity in the range (a) 0ppb to 5ppb is ≈5% of full scale/ppb, (b) 5ppb to 75ppb is ≈0.2% f.s/ppb, and (c) 75ppb to 500ppb is ≈0.1% f.s/ppb.

(iii) *Resolution* is the ability of a sensor to distinguish between closely adjacent values of concentration. The best resolution can be calculated as two standard errors from the indicated value. For the three ranges mentioned above the resolution is (a) < 1ppb, (b) 2ppb and (c) 3ppb.

(iv) *Repeatability* is the measure of the agreement between a number of consecutive measurements of a chosen value, in this case the concentration of phenol in water. Repeatability is expressed in terms of another parameter known as the confidence interval. The confidence interval is a range within which one may reasonably assume that the true value of concentration will be found. The 95% confidence interval is given by the equation:

$$\mu = x +/- t(s.e.)$$

where μ is the true value, x is the average value, t is a constant obtained from statistical tables and s.e. is the standard error [6], (See Appendix H). The value of t compensates for the uncertainty introduced by using a sample size less than infinity. A 95% confidence level is a recognised standard worldwide for instrumentation as most calibration is based on this level.

(v) The *detection limit* is the concentration of phenol at which the signal is equal to the blank signal plus three standard errors of the blank. Using this approach the limit of detection for this sensor is *less than 1ppb.*

(vi) *Response Time* is the time taken for the sensor to record a change in phenol concentration. Although a reading is logged once every second (the

interval between laser Q-switches) and this interval is displayed on-screen the an average of 200 points is taken due to the low concentrations being measured. This, in effect is the response time of the sensor.

A summary of the above parameters for this sensor is provided in Table 5.2.

TABLE 5.2	
PROTOTYPE SENSOR 15m	
Range	0 to 500ppb
Sensitivity (3 Ranges)	7%, 0.2% and 0.1% of Full Scale
Resolution	< 1ppb, ≈2ppb and ≈3ppb
Detection Limit	< 1ppb
Response Time	~ 200 secs

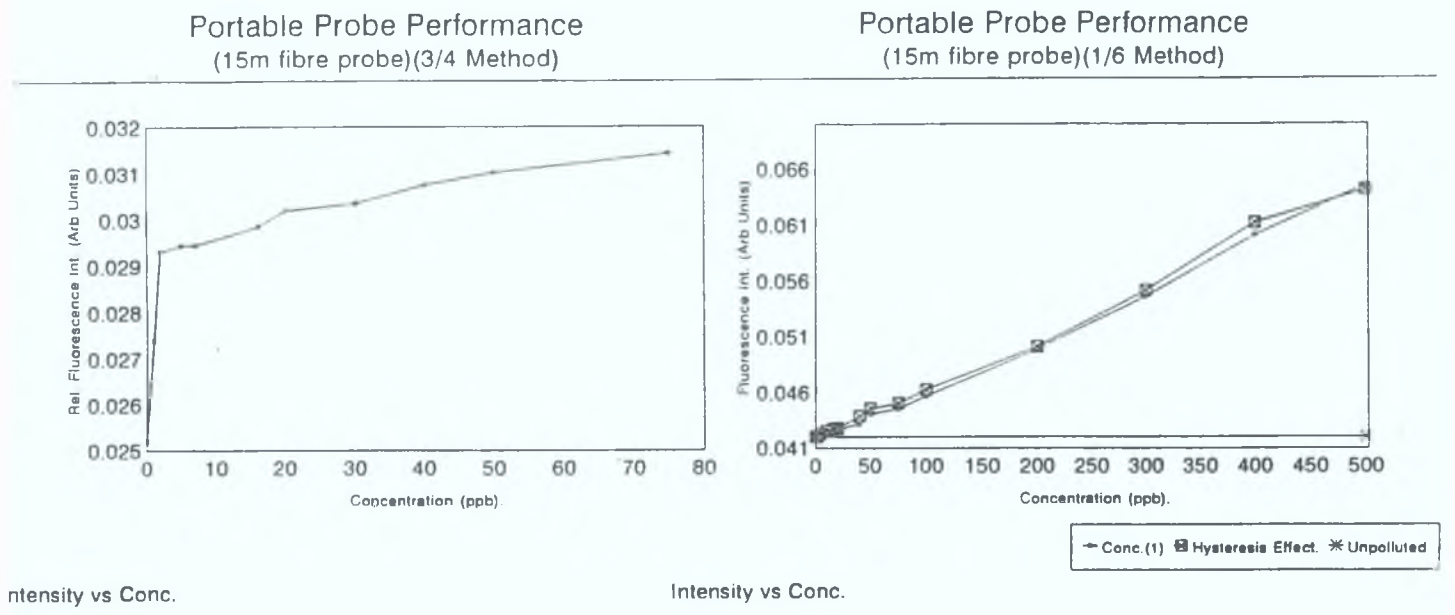

Figure 5.12: (a)"3-4" Fluorescence. (b)"1-6" Fluorescence.

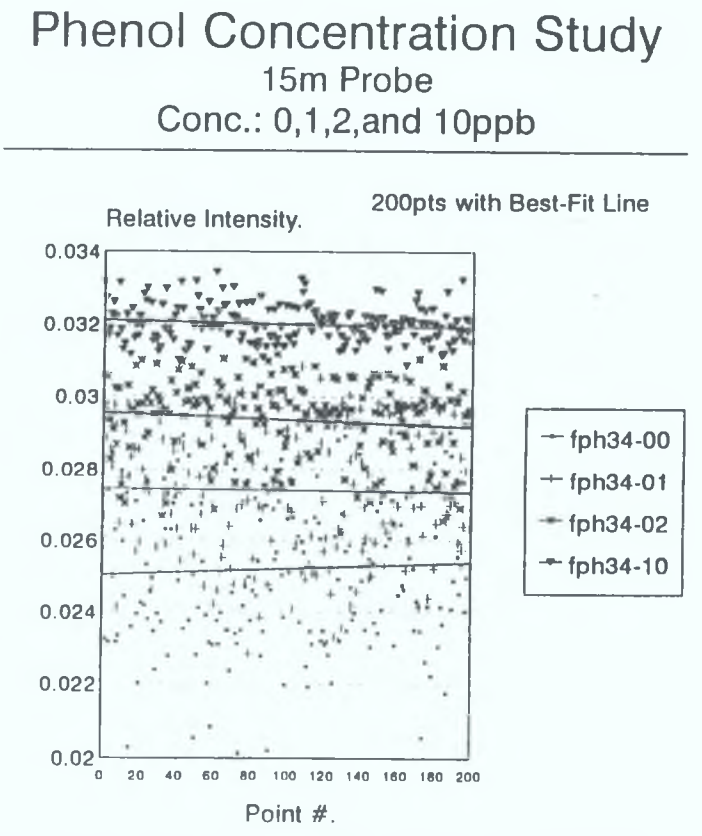

Figure 5.13: "3-4" Fluorescence over 200pts (0,1,2 and 10ppb)

5.6 Conclusion.

The work outlined in this chapter was carried out to estimate the efficacy of a particular design of pulsed laser-induced phenol fluorescence sensor. The sensor incorporated a novel sensor-head design developed in chapter 3 and also a special high transmission UV grade silica optical fibre. The sensor worked in analog mode using simple circuitry for both fluorescence detection and source compensation and a number of software manipulations were used to analyse the data. The sensor was built and tested on both pure phenols and also on phenol combinations and possible interference effects were also examined. The sensor was shown to be able to detect phenols at low concentrations effectively. Added development could further develop its effectiveness especially with respect to parameters such as response time, detection limit and resolution. These improvements could be made through using a continuous frequency quadrupled Nd:YAG source, using a faster A/D convertor and by further developing the analytical software. The latter is perhaps the most important as the 0 to 10 ppb range is the limit of detection for almost all currently available phenol concentration methods (See Chp. 2). It is unfortunate that the sensor was not tested by comparison with other phenol detection methods using the same sample solution. This was not possible because firstly there is no commercially available portable phenol sensor and secondly it was not possible to access any lab-based system with comparable accuracy to those described in Chapter 2. However, the sensor, as it stands, is very useful as the performance it has displayed is over a 30m round trip and this, coupled with the head design make it very useful on-site in-situ analysis of phenol concentration in boreholes and reservoirs. This is particularly important as even daylight can effect concentration readings of phenol solutions. The sensor is in its entirety, transportable and indeed portable and is already suitable with present software for datalogging over long periods. If incorporated with a lookup calibration curve on an EPROM as discussed in 5.3.2, it could be very useful as a high accuracy on-site tool for detecting in water these most-volatile of any chemical substances; phenols.

References

1. W. A. Chudyk et al.: **"Remote Detection of Groundwater Contaminants Using Far-Ultraviolet Laser Induced Fluorescence"**, Analytical Chemistry, 57, pp1237-1242, (1985).

2. New Wave Research Inc.: **"Minisystem 266-Special UV Laser With Laser Pointer"**, Operators Manual, 1992.

3. Bytronic : **"MPIBM3 Multifunction I/O Card"**, Instruction Manual.

4. American Public Health Assoc. et al.: **"Standard Methods for the Examination of Water and Wastewater"**, 15th ed., American Public Health Assoc., Washington DC. (1981).

5. S.D. Kullbom, H.F. Smith and P.S. Flandeau: **"Fluorescence Spectroscopy in the Study and Control of Water Pollution"**, Paper no. 288, Presented at the Pittsburgh Conference on Analytical Chemistry and Applied Spectroscopy, Perkin-Elmer Corporation, (1970).

6. Fluke/Philips Training: **"Metrology, Chp. 14: Error, Uncertainty of Measurement and Confidence Level",(1987).**

CHAPTER 6

CHAPTER 6.

OVERALL CONCLUSION AND FUTURE DEVELOPMENTS.

Overall Conclusion.

The body of this work has demonstrated the need for a portable sensor to detect the presence of phenols at ppb levels in groundwater, on-site, at boreholes and well sites. The characteristic properties of phenols and the problems associated with accurately detecting the concentration of these volatiles in solution were outlined. Following on this, the current methods/systems for determination of phenol concentration were discussed, and assessed in detail. It was established that there is no commercial sensor currently available which can measure phenol levels, in-situ in borehole type applications.

The principle of induced fluorescence of this species and how it can be used with optical fibres to estimate species concentration was then discussed. Due to the low yield of this method an extensive study was carried out on maximizing the efficiency of the sensor resulting in two main design types. Both of these designs were constructed and rigorously tested, one as a lab-based system and the other as an on-site system. The results collected were comparable with currently available commercial systems while working on a much simpler principle and needing no chemical support, and no sample preparation as many of the current lab based systems do. In addition, the portable dual-fibre probe offered on-site capability and better than average performance for a phenol sensor especially at lower concentrations.

Future Developments.

There are a number of possible developments which could be made on the equipment. If it were possible to get a non-pulsed laser which was as compact as the Nd:YAG in the present laser system then both stability and response time could be improved. The replacement of the present data-logging system with a faster A/D card would also improve stability as well as improving the

resolution.

For the lab based system (9 around 1) a reduction in source size without reduction in power may make this system a more viable option as an on-site tool. This system was noted to be very stable and reliable. A source with a high output (discrete or broadband) in the 250 to 270 region would be ideal.

A combination of both of the above, with a laser and lamp source, which would be packaged in the one box may offer the best type of sensor. This type of arrangement has been achieved previously for an another sensor [1]. Indeed, the future of environmental sensing lies in the ability of one unit to be able to measure a number of parameters as mentioned above. Just such a unit is outlined in Appendix I. However an optical fibre based version of this sensor could offer more durability, access a larger number of locations, and parameters, and offer a much more serviceable unit (one sensor head).

References

1. T. Vo-Dinh, G.D. Griffin and K.R. Ambrose: **"A Portable Fibreoptic Monitor for Fluorimetric Bioassays"**, Applied Spectroscopy, *Vol 40, No. 5, pp696-700, (1986).*

APPENDIX A

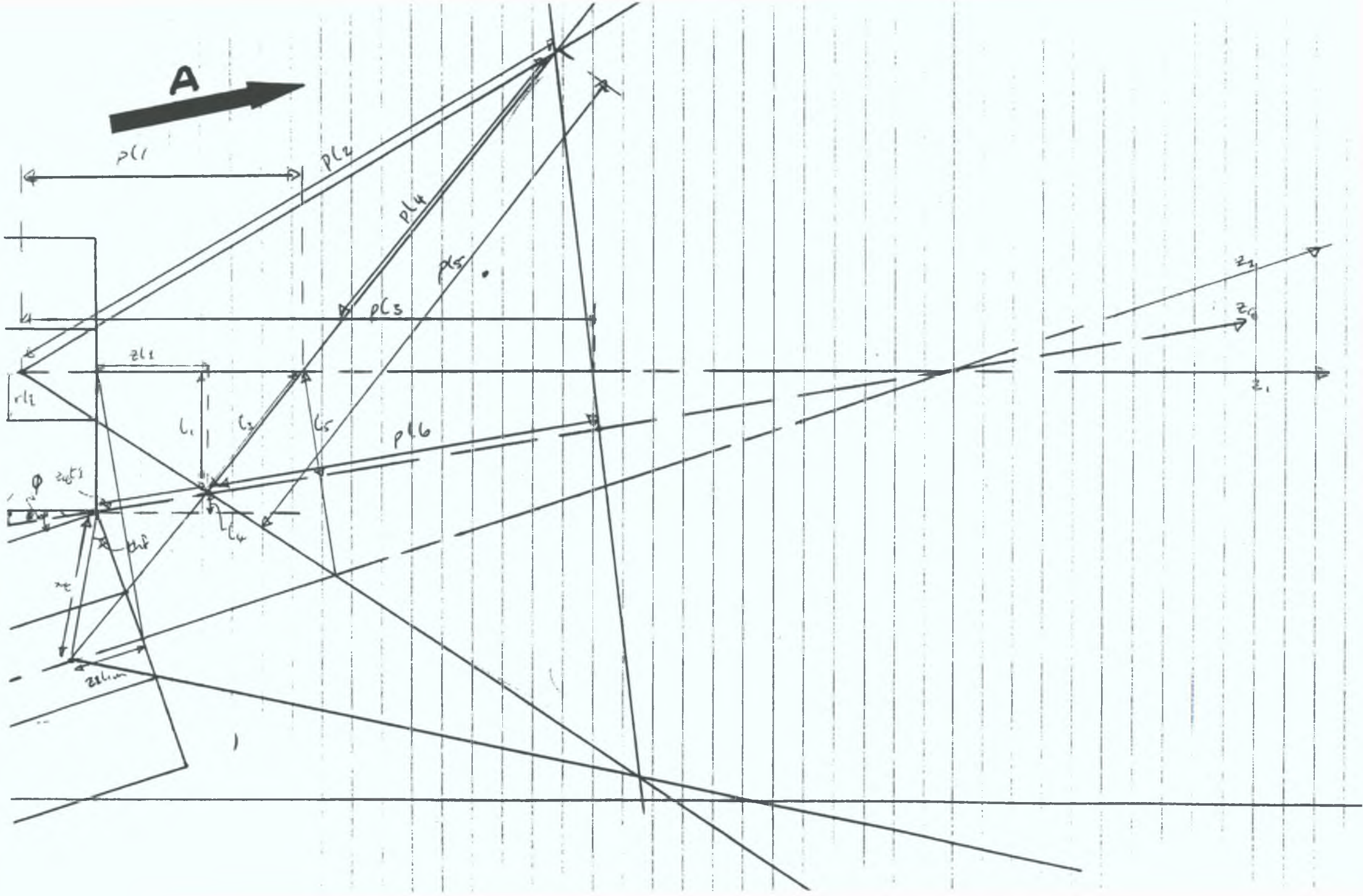
A
p(1
p(2
p(4
p(5
p(3
p(6
z1
z2
z3
z4
z5
z6
l1
l2
l5
l4
φ

APPENDIX A.

FLUORESCENCE PROBE: MATHEMATICAL MODEL.

The Raman Intensity dI_R given in (Watts /sr) provided by the element of volume $\delta x,\delta y,\delta z$ incident on a point x,y,z is given by;

$$dI_R = \frac{P_o \beta N dx, dy, dz}{s}$$

where B is the coefficient describing the quantum yield of fluorescence, and N is the density of diffusing centres in (molecules/cm^3)

Diagram 1 shows the Basis $\mathbf{R}_1$ describing the ideal cone of emission of light from the excitation fibre which is identical, in form, to that of the cone of collection $\mathbf{R}_2$. Thus any point in either Basis in the common medium outside the fibre face can be described in Carthesian Co-ordinates as follows:

Cone$_1$:Emitter

$$x_1^2+y_1^2 \le z_1^2 \tan\alpha_1 \qquad x_1 = r_1 \cos\theta_1$$

$$y_1 = r_1 \sin\theta_1$$

$$z_{1_{lim}} \le z_1 \qquad 0 \le \theta_1 \le 2\pi \qquad \underline{3.4.1}$$

with;

$$z_1 lim = r_1 \tan\alpha_1 \qquad z_1 lim \le z_1 \le z_1 max$$

Cone$_2$:Collector

$$x_2^2+y_2^2 \le z_2^2 \tan^2\alpha_2 \qquad x_2 = r_2 Cos\theta_2$$

$$y_2 = r_2 Sin\theta_2$$

$$z_2 lim \le z_2 \le z_2 max \qquad 0 \le \theta_2 \le 2\pi \qquad \underline{3.4.2}$$

with;

$$z_2 \ge z_2 lim = r_2/\tan\alpha_2 \qquad 0 \le r_2 \le z_2 \tan\alpha_2$$

In the case of multimode fibre and especially with large core diameters the inhomogenity of the beam emitted from the fibre face must be taken into account Ref FHD. Thus it is assumed that all of the points of the end face of the fibre are as point sources illuminating a core of max half-angle α_1. The

irradiance due to each of these sources , of co-ordinates ($rCos\theta, rSin\theta, z_{1lim}$) in the coordinate system $\mathbb{R}_1$ with surface r,dr,dθ is;

$$dI_o = \frac{P_o}{\pi r_1^2} \frac{r dr d\theta}{2\pi [1-Cos\alpha_1]\rho_1^2}$$

$$with \quad \rho^2{}_1 = (x_1 - rCos\theta)^2 + (y - rSin\theta)^2 + (z_1 - z_1 lim)^2 \quad [1] \qquad 3.4.3$$

Thus, at the point $M(x_1,y_1,z_1)\mathbb{R}_1$ (Exit face of illuminating fibre core) the total irradiance is given by;

$$I_o = \oint_{FibreFace_1} dI_o \qquad 3.4.4$$

Obviously the integration must only be made over that part of the fibre endface which may illuminate the point $M(x_1,y_1,z_1)\mathbb{R}_1$ i.e.($Core_1$). Thus for ease of programming

$$I_o = \int_{r=0}^{r_1} \int_{\theta=0}^{2\pi} Test_1(r,\theta)\, dI_o \qquad 3.4.5$$

where $Test_1$ is the condition that the slope between the point on the fibre face and the point $M(x_1,y_1,z_1)\mathbb{R}_1$ is less than or equal to the tan of the N.A. α_1

$$\alpha_1 = Tan^{-1}\left[\frac{y_{11} - y_{10}}{x_{11} - x_{10}}\right] \qquad 3.4.6$$

($Test_1$ is either 0 or 1)

Similarly for the collection of the fluorescent light the Raman Intensity dI_R (W/sr) given by an element of volume dx_1,dy_1,dz_1) centered on the point $M(x_1,y_1,z_1)\mathbb{R}_1$ is given by

$$P_c = \iiint_{Intersection\ of\ NA\ Cones} dI_o \quad \Omega(M) \qquad 3.4.7$$

where Ω(M) is the divergent solid angle given by the point $M(x_2,y_2,z_2)\mathbb{R}_2$ and arriving on the surface of the collecting fibre;

$$\Omega(M) = \int_{r=0}^{r_2} \int_{\theta=0}^{2\pi} Test_2(r,\theta)\, \frac{Cos\psi}{\rho_2^2}\, r dr d\theta \qquad 3.4.8$$

[1] See Appendix B

with

$$\rho_2^2 = (x_2 - r_2 Cos\Theta_2)^2 + (y_2 - r_2 Sin\Theta_2)^2 + (z_2\text{lim} - z_2)^2 \qquad 3.4.9$$

$$Cos\psi = (z_2 - z_2\text{lim}) / \rho$$

The method used to estimate the collection efficiency of the fibre probe is firstly to estimate P_c for the overlap volume defined by "Test$_0$"[2] and then to estimate $P_{c\ max}$ for the case where all points within the Numerical Aperture of the collection fibre are assumed to be illuminated i.e.(as though the excitation and collection cones were one).

$$P_{Cmax} = \iiint_{\substack{Frustum\,of\,Emission \\ NA\,Cone}} dI_o \quad \Omega(M) \qquad 3.4.10$$

The ratio of the P_c to $P_{c\ max}$ is an estimate of the collection efficiency.

[2] See Appendix B.

APPENDIX B

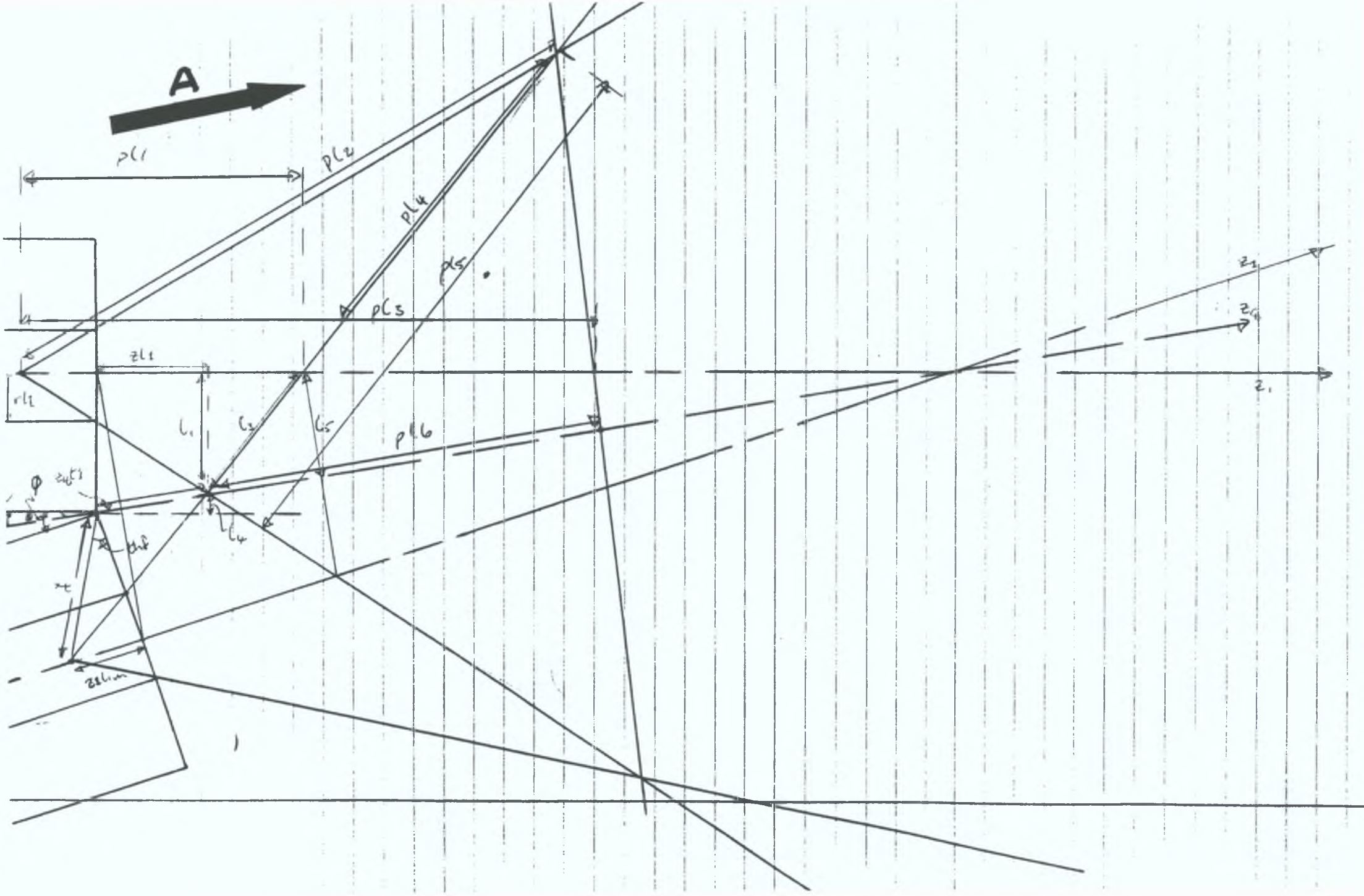
A
pC1
pL2
pL4
pC5
pC3
pL6
z1
z4
z5

APPENDIX B.

FLUORESCENCE PROBE: Cone Overlap Volume.

"$TEST_0$": Model governing angular dependance of this volume and the related software.

From the diagram opposite the illustrated parameters are worked out by simple trigonometry as is outlined below. From this the volume of the intersection of the two cones can be worked out and a set of carthesian co-ordinates for the elements of this volume can be generated to calculate the efficiency. Note that the number of points generated is only dependant on the interval of r and θ set in the software. The key to the software variables as well as their origin is outlined below:

alp = α; fi = ϕ; fi2 = $\phi/2$

alfi2 =($\theta + \phi/2$); almfi2 = ($\theta - \phi/2$); alfi =($\theta + \phi$);

tfi2 = tan($\phi/2$); talp = tan(θ); talfi2 = tan($\theta + \phi/2$); talmfi2 = tan($\theta - \phi/2$);

cfi2 = cos($\phi/2$); calfi2 = cos($\theta + \phi/2$);

salp = sin(θ); sfi = sin(ϕ); sfi2 = sin($\phi/2$);

hy = (l1/sin(θ)); l2 = (l1 x tan($\pi/2$-($\theta - \phi$)));

l5 = (l3 x sin($\theta + \phi/2$));

pl2 = ((pl1 x sin(π -($\theta + \phi$)))/ sin((ϕ)));

pl3 = ((pl2*(sin(π-($\theta - \phi/2$))))/(sin($\pi/2 - \phi/2$)));

/* Calculating further variables. */

$z1_{lim}$ = (rl1/tan α); thf= ($\tan^{-1}$(z1lim/Rl1));

xt =(Rl1/(cos(thf)));

$z1_{int}$ = (Rl1/tan($\phi/2$));

zq_{int} = (Rl1/sin($\phi/2$));

/* cos($\phi/2$)= zq_{int}/ zq_{tot} and zq_{tot} = zq_{int} + zq_{t2} */

zqt1 = ((z1int/cos($\phi/2$))-zqint);

$zl1 = ((Rl1-rl1)/(\tan \alpha + \tan(\phi/2)));$

$l1 = ((zl1 \times \tan \alpha)+rl1);$

$l3 = (l1/(\cos (\pi - (\alpha+\phi))));$

$l4 = (zl1*\tan(\phi/2));$

$pl1 = (l3/\sin \alpha);$

$pl4 = ((pl1 \times \sin \alpha)/ \sin \phi);$

$pl5 = (pl4+l3);$

$pl6 = (pl5 \times \cos(\alpha+ \phi/2));$

$pl7 = ((z1_{int} + z1_{lim}) \times \sin(\phi/2));$

$z_{lq1} = (l4/\sin(\phi/2));$ $z_{lq2} = (z_{lq1} + (l3 \times \cos(\alpha+\phi/2)));$

$z_{lq3} = (z_{lq1} + pl6);$

These values allow a swift calculation of the limits of the volume with respect to radius from the z_q axis in the $\mathbb{R}_q$ basis.

```
/*

        " TEST0.c "
   Point-finder for intersection of both fluorescence
          and collection cone frustums.(Volume).
   Hig.  Feb. '92                                  */

#include <stdio.h>
#include <conio.h>
#include <math.h>
#define RADIAN(X) (double)((M_PI/180)*X)

char ch;
void main(void)
{

  FILE *fb1;
  FILE *fb2;

 /* Initialising variables.      */

  long int i,j,k,jj,kk;
  double an,fii,rl1,Rl1;
  double alp,fi,fi2,alfi,alfi2,almfi2;
  double talp,tfi2,talfi2,talmfi2,cfi2,calfi2,salp,sfi,sfi2;
  double z1lim,thf,xt,zqt1,zl1,z1int,zqint,l1,l3,l4,pl1,pl4,pl5,pl6,pl7;
  double zlq1,zlq2,zlq3;
  double zq,zqi,zqma,delzq;
  double rq,rqmi,rqma,delrq,thq,thqmi,thqma,delthq;
  double rqi,rqi1,rqi2,rqimi,rqima,delrqi,rqi1ma,delrqi1,rqi2ma,delrqi2;
  double thqi,thqimi,thqima,delthqi;
  double xq1,yq1,zq1,x11,y11,z11,x21,y21,z21;
  double xq2,yq2,zq2,x12,y12,z12,x22,y22,z22;
  double xq3,yq3,zq3,x13,y13,z13,x23,y23,z23;
  double xq4,yq4,zq4,x14,y14,z14,x24,y24,z24;
  double zqsfi2;




/* ( Setting variables= 0 )   */

  i =0; j=0; k=0; jj=0; kk=0;
  rl1 = 0; Rl1 = 0;
  an   = 0; fii   = 0; alp   =0; fi    =0; fi2   =0; alfi2 =0; alfi  =0;
  almfi2   =0;
  talp  =0; tfi2=0; talfi2=0; talmfi2=0;
  cfi2  =0; calfi2=0;
```

```
salp  =0; sfi   =0; sfi2  =0;

zl1=0; z1lim=0; thf=0; xt=0; zqt1=0; z1int=0; zqint=0;
l1=0; l3=0; l4=0;
pl1=0; pl4=0; pl5=0; pl6=0; pl7=0;
zlq1=0; zlq2=0; zlq3=0;

zq=0; zqi=0; zqma=0; delzq=0;
rqmi=0; rqma=0; delrq=0; thqmi=0; thqma=0; delthq=0;
rqimi=0; rqima=0; delrqi=0; rqi1=0; delrqi1=0; rqi2ma=0; delrqi2=0;
thqimi=0; thqima=0; delthqi=0;
zqsfi2=0;

/* Data input Stage. */

printf("\nEnter N.A.angle in deg.: ");
 scanf("%lf", &an);
printf("Enter 0(fi.angle between fibres) in deg.: ");
 scanf("%lf", &fii);
printf("Enter core radius in mm.: ");
 scanf("%lf",&rl1);
printf("Enter outer radius of fibre in mm.: ");
 scanf("%lf",&Rl1);


fb1 = fopen("102b1.dat","w");
fb2 = fopen("102b2.dat","w");

alp   =RADIAN(an);                    /* This portion converts     */
                                          /* degrees of arc to radians  */
fi    =RADIAN(fii);
fi2   =fi/2;
alfi2 =(alp+(fi2)); almfi2=(alp-(fi2)); alfi  =(alp+fi);
tfi2 = tan(fi2); talp = tan(alp); talfi2 = tan(alfi2); talmfi2 = tan(almfi2);
cfi2 = cos(fi2); calfi2 = cos(alfi2);
salp = sin(alp); sfi = sin(fi); sfi2 = sin(fi2);


/* printf("Thus Alpha in radians is %.12f",alp);

     hy = (l1/salp);  l2 = ( l1*tan(M_PI_2-(alp-fi)) );
     l5 = ( l3*salfi2 );
     pl2 = ( (pl1*sin(M_PI-alfi))/ sfi );
     pl3 = ( (pl2*(sin(M_PI_2-(alp-fi2))))/(sin(M_PI_2-fi2)) );

          */
                                   /* Calculating further variables. */
```

```
  z1lim = (rl1/talp);       thf= ( atan(z1lim/Rl1) );
  xt =( Rl1/(cos(thf)) );
  z1int = (Rl1/tfi2);
  zqint = (Rl1/sfi2);
/* cos(fi/2)= z1int/zqtot  :  zqtot= zqint+zqt2 */
  zqt1 = ( (z1int/cfi2)-zqint );

  zl1 = ( (Rl1-rl1)/(talp+tfi2) );
  l1 = ( (zl1*talp)+rl1 );
  l3 = ( l1/(cos (M_PI_2 - alfi)) );
  l4 = (zl1*tfi2);

  pl1 = ( l3/salp );
  pl4 = ( (pl1*salp)/sfi);
  pl5 = ( pl4+l3 );
  pl6 = ( pl5*calfi2 );
  pl7 = ( (z1int+z1lim)*sfi2 );

     zlq1 = ( l4/sfi2 );     /* NOTE: This is the depth where the
                                    two fibres come into contact.*/
     zlq2 = ( zlq1+(l3*calfi2) );
     zlq3 = (zlq1+pl6);

printf("\nz1int is %.18f(mm)", z1int);

printf("\nzlq1 is %.18f(mm)", zlq1);
printf("\nzlq2 is %.18f(mm)", zlq2);
printf("\nzlq3 is %.18f(mm)", zlq3);

    printf("\nEnter depth of penetration of fibre probe beam in mm.: ");
    scanf("%lf",&zqma);

       delzq = zqma/20;

    zq = 0;
       for(i=0 ; i<21; i++)
      {
       while(zq<zlq1)              /* Until intersection pt. is reached */
       zq+=delzq,i+=1;              /* continue to increase penetration */
                                    /* depth without calculating co-ords.*/

       zqsfi2=(zq*sfi2);
       if(zq<zlq3)              /* From intersection pt. of cones to z_q limit*/
       {
          rq=0;
          rqmi  = ((zlq1+zqt1)*talfi2);
              rqma  = ((zq+zqt1)*talfi2);
              delrq = ((rqma-rqmi)/10);
              rq=rqma;
```

```
        for(j=1; j<=10; j++)
    {
        thq=0;
        thqmi = ( asin(rqmi/rq) );
        thqma = (M_PI_2);
        delthq= ((thqma-thqmi)/20);
        thq=thqmi;

        for(k=0; k<=19 ; k++)
                {
        if((rq*sin(thq)) < rqmi)
        {
        thq+=delthq;
        }
        else
        {
        xq1=0; yq1=0; zq1=0; x11=0; y11=0; z11=0; x21=0; y21=0; z21=0;
        xq2=0; yq2=0; zq2=0; x12=0; y12=0; z12=0; x22=0; y22=0; z22=0;
        xq3=0; yq3=0; zq3=0; x13=0; y13=0; z13=0; x23=0; y23=0; z23=0;
        xq4=0; yq4=0; zq4=0; x14=0; y14=0; z14=0; x24=0; y24=0; z24=0;


/*1st. Quadrant. */
        xq1 =( rq*cos(thq) );
        yq1 =( (rq*sin(thq))-(rqmi) );
        zq1 =( zq );


        xq2 = (xq1*(-1));   yq2 = yq1;          zq2 = zq1;
        xq3 = (xq1*(-1));   yq3 = (yq1*(-1));   zq3 = zq1;
        xq4 = xq1;          yq4 = (yq1*(-1));   zq4 = zq1;

                if(zq>=zqint)
                {
                x11 = xq1; y11 =(yq1-((zq-zqint)*sfi2)); z11 =(zq1*cfi2);
                x12 = xq2; y12 =(yq2-((zq-zqint)*sfi2)); z12 =(zq2*cfi2);
                x13 = xq3; y13 =(yq3-((zq-zqint)*sfi2)); z13 =(zq3*cfi2);
                x14 = xq4; y14 =(yq4-((zq-zqint)*sfi2)); z14 =(zq4*cfi2);

                x21 = xq1; y21 =(yq1+((zq-zqint)*sfi2)); z21 =(zq1*cfi2);
                x22 = xq2; y22 =(yq2+((zq-zqint)*sfi2)); z22 =(zq2*cfi2);
                x23 = xq3; y23 =(yq3+((zq-zqint)*sfi2)); z23 =(zq3*cfi2);
                x24 = xq4; y24 =(yq4+((zq-zqint)*sfi2)); z24 =(zq4*cfi2);

                }
                else
                {
                x11 = xq1; y11 =(yq1-(Rl1-(zqsfi2))); z11 =(zq1*cfi2);
```

```
                x12 = xq2; y12 =(yq2-(Rl1-(zqsfi2))); z12 =(zq2*cfi2);
                x13 = xq3; y13 =(yq3-(Rl1-(zqsfi2))); z13 =(zq3*cfi2);
                x14 = xq4; y14 =(yq4-(Rl1-(zqsfi2))); z14 =(zq4*cfi2);

                x21 = xq1; y21 =(yq1+(Rl1-(zqsfi2))); z21 =(zq1*cfi2);
                x22 = xq2; y22 =(yq2+(Rl1-(zqsfi2))); z22 =(zq2*cfi2);
                x23 = xq3; y23 =(yq3+(Rl1-(zqsfi2))); z23 =(zq3*cfi2);
                x24 = xq4; y24 =(yq4+(Rl1-(zqsfi2))); z24 =(zq4*cfi2);
                }


        /*
          fprintf(fb1,"%f\t%f\t%f\n",xq1,yq1,zq1);
          fprintf(fb1,"%f\t%f\t%f\n",xq2,yq2,zq2);
          fprintf(fb1,"%f\t%f\t%f\n",xq3,yq3,zq3);
          fprintf(fb1,"%f\t%f\t%f\n",xq4,yq4,zq4);
        */



          fprintf(fb1,"%f\t%f\t%f\n",x11,y11,z11);
          fprintf(fb1,"%f\t%f\t%f\n",x12,y12,z12);
          fprintf(fb1,"%f\t%f\t%f\n",x13,y13,z13);
          fprintf(fb1,"%f\t%f\t%f\n",x14,y14,z14);
          fprintf(fb2,"%f\t%f\t%f\n",x21,y21,z21);
          fprintf(fb2,"%f\t%f\t%f\n",x22,y22,z22);
          fprintf(fb2,"%f\t%f\t%f\n",x23,y23,z23);
          fprintf(fb2,"%f\t%f\t%f\n",x24,y24,z24);

        thq+=delthq;


        }

        }
      rq+=delrq;
     }
}
else          /*  i.e. for zq>= zlq3  */
{
    zqi+=delzq;
  {

        rqimi  = ( ((zlq1+(zqt1))*talfi2) );
        rqi1ma  =   ( ((zq+zqt1)*talfi2) );
        rqi2ma  = ( ((zlq3-zqt1)*talfi2)+(zqi*talmfi2) );
        delrqi1 = ((rqi1ma-rqimi)/10);
        delrqi2 = ((rqi2ma-rqimi)/10);
```

```
        rqi1=rqi1ma;
        rqi2=rqi2ma;

        for(jj=1; jj<=10; jj++)
    {
       thqi=0;

        thqimi = ( asin(rqimi/rqi1) );
        thqima = (M_PI_2);
        delthqi= ((thqima-thqimi)/20);
       thqi=thqimi;

       for(kk=0; kk<=19; kk++)
       {
         if((rqi2*sin(thqi)) < rqimi)
         {
           thqi+=delthqi;
         }
         else
         {
         xq1=0; yq1=0; zq1=0; x11=0; y11=0; z11=0; x21=0; y21=0; z21=0;
         xq2=0; yq2=0; zq2=0; x12=0; y12=0; z12=0; x22=0; y22=0; z22=0;
         xq3=0; yq3=0; zq3=0; x13=0; y13=0; z13=0; x23=0; y23=0; z23=0;
         xq4=0; yq4=0; zq4=0; x14=0; y14=0; z14=0; x24=0; y24=0; z24=0;



         xq1 =( rqi2*cos(thqi) );
         yq1 =( (rqi2*sin(thqi))-(rqimi) );
         zq1 =( zq );


         xq2 = (xq1*(-1));   yq2 = yq1;          zq2 = zq1;
         xq3 = (xq1*(-1));   yq3 = (yq1*(-1));   zq3 = zq1;
         xq4 = xq1;          yq4 = (yq1*(-1));   zq4 = zq1;


if(zq>=zqint)
              {
              x11 = xq1; y11 =(yq1-((zq-zqint)*sfi2)); z11 =(zq1*cfi2);
              x12 = xq2; y12 =(yq2-((zq-zqint)*sfi2)); z12 =(zq2*cfi2);
              x13 = xq3; y13 =(yq3-((zq-zqint)*sfi2)); z13 =(zq3*cfi2);
              x14 = xq4; y14 =(yq4-((zq-zqint)*sfi2)); z14 =(zq4*cfi2);

              x21 = xq1; y21 =(yq1+((zq-zqint)*sfi2)); z21 =(zq1*cfi2);
              x22 = xq2; y22 =(yq2+((zq-zqint)*sfi2)); z22 =(zq2*cfi2);
              x23 = xq3; y23 =(yq3+((zq-zqint)*sfi2)); z23 =(zq3*cfi2);
              x24 = xq4; y24 =(yq4+((zq-zqint)*sfi2)); z24 =(zq4*cfi2);
```

```
                    }
                    else
                    {
                    x11 = xq1; y11 =(yq1-(Rl1-(zqsfi2))); z11 =(zq1*cfi2);
                    x12 = xq2; y12 =(yq2-(Rl1-(zqsfi2))); z12 =(zq2*cfi2);
                    x13 = xq3; y13 =(yq3-(Rl1-(zqsfi2))); z13 =(zq3*cfi2);
                    x14 = xq4; y14 =(yq4-(Rl1-(zqsfi2))); z14 =(zq4*cfi2);

                    x21 = xq1; y21 =(yq1+(Rl1-(zqsfi2))); z21 =(zq1*cfi2);
                    x22 = xq2; y22 =(yq2+(Rl1-(zqsfi2))); z22 =(zq2*cfi2);
                    x23 = xq3; y23 =(yq3+(Rl1-(zqsfi2))); z23 =(zq3*cfi2);
                    x24 = xq4; y24 =(yq4+(Rl1-(zqsfi2))); z24 =(zq4*cfi2);
                    }
      /*
              fprintf(fb1,"%f\t%f\t%f\n",xq1,yq1,zq1);
              fprintf(fb1,"%f\t%f\t%f\n",xq2,yq2,zq2);
              fprintf(fb1,"%f\t%f\t%f\n",xq3,yq3,zq3);
              fprintf(fb1,"%f\t%f\t%f\n",xq4,yq4,zq4);
       */


              fprintf(fb1,"%f\t%f\t%f\n",x11,y11,z11);
              fprintf(fb1,"%f\t%f\t%f\n",x12,y12,z12);
              fprintf(fb1,"%f\t%f\t%f\n",x13,y13,z13);
              fprintf(fb1,"%f\t%f\t%f\n",x14,y14,z14);
              fprintf(fb2,"%f\t%f\t%f\n",x21,y21,z21);
              fprintf(fb2,"%f\t%f\t%f\n",x22,y22,z22);
              fprintf(fb2,"%f\t%f\t%f\n",x23,y23,z23);
              fprintf(fb2,"%f\t%f\t%f\n",x24,y24,z24);


          zqsfi2=0;
          thqi+=delthqi;

           }
           }
            rqi1+=delrqi1;
            rqi2+=delrqi2;
            }

       }
       }
      zqsfi2=0;

      zq+=delzq;
      printf("   zq1=:%f",zq1);
      }
fclose(fb1);
fclose(fb2);
```

```
printf("\nzlq1 is %.18f(mm)", zlq1);
printf("\nzlq2 is %.18f(mm)", zlq2);
printf("\nzlq3 is %.18f(mm)", zlq3);

ch=getch();


}
```

APPENDIX C

APPENDIX C.

COLLECTION EFFICIENCY OF FIBRE PROBE.

"EFF.c": Model and related software governing collection efficiency of fibre probe.

From App. B the overlap volume of the collection and emmision cones can be determined and the points within this volume recorded. The program below estimates the efficiency of a dual fibre configuration. The program is divided into two parts. The first part calculates the relative light intensity incident on a point in space with respect to the fibre core face of the excitation fibre. The second part estimates the ammount of fluorescent light which will be guided into the collection fibre which is dependent on a number of factors, not least of which is the first part of "EFF.c". "EFF.c" systematically takes each point within the test volume and the total efficiency is recorded for that volume before examining the test volume for a different angle. "EFF.c" in co-operation with "TESTo.C" can be used to determine the efficiency of fibre probes for a number of configurations of fibre probe ie. varying angle between fibres, core diameter, total fibre diameter, and numerical aperture.

```
/* Collection of Efficiency of Raman Fluorescence by Fibre Probe. */
/* hig.                */
/* Feb 24, 1992.       */


#include <conio.h>
#include <stdio.h>
#include <math.h>

int i,j,ii,jj;
double z1lim,talp;

double r2,r2ma,delr2;
double th2,delth2,delr2th2;
double ro2,ro22;
double x2,y2,z2,z2lim,alp,gam;
double xr2cth2,yr2sth2,zz2lim;
```

```
double col,col1,colt;
double eff,ef1,ef;

double r1,r1ma,delr1;
double th1,delth1,delr1th1;
double x1,y1,z1,zz1lim,xr1cth1,yr1sth1;
double fl,fl1,flt,flu,c1;

double t1,t2,t3;

char ch;

void main(void)
{


   FILE *fptr1;
   FILE *fptr2;
   z1lim=.635784751;
   talp=.314569782;
   r1ma=.2;

   ef=0; ef1=0, eff=0;
   r2=0;  r2ma=0.2;
   ro2=0; ro22=0; col1=0; colt=0; flt=0;
   col=0; z2lim=z1lim;
   alp=0.304769394;          /*17.462 deg in radians*/
   gam=0;

   t1=0; t2=0; t3=0;

/* Flux at a pt. excited by a fibre.  */
/* hig.                */
/* Oct 21, 1991                        */



        r1=0; x1=0; y1=0; z1=0;
             x2=0; y2=0; z2=0;
        xr2cth2=0;yr2sth2=0;
        c1=0; xr1cth1=0; yr1sth1=0; zz1lim=0;
        fl1=0;fl=0;

        r1ma = 0.2;
        delr1= (r1ma/10);
        delth1 = ((2*(M_PI))/10);
        delr1th1 = (delr1*delth1);
       th1 = delth1;
```

```
r1=delr1;
 c1 =( 1/((2*(M_PI*M_PI))*(r1ma*r1ma)*(1-cos(alp))) );


 fptr1= fopen("102b1.dat","r");
 fptr2= fopen("102b2.dat","r");


  fscanf(fptr1," %lf %lf %lf",&x1,&y1,&z1);

do{



 for(ii=1; ii<=10 ;ii++)
   {


        for(jj=1; jj<10 ;jj++)
         {


           xr1cth1 = (x1-(r1*(cos(th1))));
           yr1sth1 = (y1-(r1*(sin(th1))));
           zz1lim   = (z1);

         if( ((fabs(y1-yr1sth1)) /z1 ) >talp)
              {
              fl1=0;
              }
         else
              {
              fl1 =( 1/( (xr1cth1*xr1cth1) +
                         (yr1sth1*yr1sth1) +
                         (zz1lim*zz1lim) ) );

              }
             fl  += fl1;
           fl1=0;
           xr1cth1=0;
           yr1sth1=0;
           zz1lim  =0;

           th1 += delth1;


         }
```

```
      r1 +=delr1;
      }



/*Collection efficiency, */
/*for the fiber probe. */



 delr2 = (r2ma/10);
 delth2 = ((2*(M_PI))/10);
 delr2th2 = (delr2*delth2);



  fscanf(fptr2," %lf %lf %lf",&x2,&y2,&z2);

    r2=delr2;
    for(i=1; i<=10 ;i++)
      {
       th2 = delth2;

           for(j=1; j<=10  ;j++)
             {
              xr2cth2 = (x2-(r2*(cos(th2))));
              yr2sth2 = (y2-(r2*(sin(th2))));
              zz2lim   = (z2);

              ro22  =      (  (xr2cth2*xr2cth2) +
                              (yr2sth2*yr2sth2) +
                              (zz2lim*zz2lim)  ) ;

              ro2  =     pow( (  (xr2cth2*xr2cth2) +
                              (yr2sth2*yr2sth2) +
                              (zz2lim*zz2lim)  ) ,0.5 );

              gam  = acos(z2/ro2);

              if(gam>alp)
                   {
                   col1 = 0;
                   }
              else
```

```
                    {
                    col1 =( (zz2lim)/((ro22)*ro2) );
                    }

                  col += col1;
                  col1=0;

                 th2 += delth2;
                 zz2lim=0;
                 xr2cth2=0;
                 yr2sth2=0;
                 ro2=0;
                 ro22=0;
               }

     r2 +=delr2;

    }




    flt+=fl;
    colt+=col;
    ef1 =(fl*col);
    ef+= ef1;
    col=0;
    fl=0;
    ef1=0;
    x1=0;y1=0;z1=0;
    x2=0;y2=0;z2=0;

    /*printf("!");*/



    }
    while(fscanf(fptr1," %lf %lf %lf",&x1,&y1,&z1)!=EOF);
    fclose(fptr1);
    fclose(fptr2);


flu=(flt*c1);
eff=(ef*c1);

printf("\nFlux per mm.sr.(flu) is%.16f\n",flu);
printf("\nFlux per mm.sr.(flt) is%.16f\n",flt);
```

```
    printf("\nCollection per mm.sr. is%.16f\n",colt);


    printf("\n Efficiency(eff) is%.16f\n",eff );
     printf("\n Efficiency(ef) is%.16f\n",ef );


ch= getch();
}
```

APPENDIX D

APPENDIX D.

SPECIFICATIONS AND GRAPHICAL PROOF OF "BENTHAM DM150" DOUBLE MONOCHROMATOR PERFORMANCE.

2. SPECIFICATION

OPTICAL CONFIGURATION: Symmetical Czesney-Turner with alternative slit positions and extensive baffling.

FOCAL LENGTH: 300mm.

APERTURE RATIO: f/4.2

STRAY LIGHT:

1.5	bandwidths	from	laser	line	.18%
3.0	"	"	"	"	.025%
10.0	"	"	"	"	.004%

Measurements were made with an 1800 L/mm holographic grating at FULL APERTURE with a 1mm bandwidth.

GRATINGS: 69mm x 69mm plain diffraction gratings, kinematically mounted.

WAVELENGTH RANGE:

1800L/mm	- zero order to	950nm
1200L/mm	"	1.4μ
900L/mm	"	1.9μ
600L/mm	"	2.9μ
300L/mm	"	5.7μ
150L/mm	"	11.4μ

The above figures refer to the theoretical range of the instrument with each grating. In practice the usable range will depend on the blaze or peak efficiency wavelength of the grating. As a general guide, the useful range of a blazed grating is .6 to 1.5 times the blaze wavelength.

SLITS: The instrument is fitted with continuously variable, bilateral slits or with interchangeable fixed slits. Slits height is 20mm.

Continuously variable slit width is adjustable between 10 μ and 5mm.

WAVELENGTH SCANNING: Most models are fitted with a stepping motor for wavelength scanning. The motor is fitted below the floor inside the Monochromator and is coupled directly to the lead screw in the E version and via a 5.1 reduction gear in the HR version.

Limit switches at both ends of the lead screw prevent overscanning. Connection to the stepping motor is made via a multiway connector mounted on the outside of the Monochromator.

WEIGHT: Complete with grating 12.4kg.

ACCESSORIES: A range of accessories is available for use with the M300. The range includes:Photomultiplier and photodiode detection systems with housings and electronics: Automatic and manual order sorting filter inserters: Arc and filament lamp light sources: Telescopic, microscopic and fibre-optic entrance optics: Hardware and software for computer control.

THE FOLLOWING SPECIFICATIONS REFER TO THE INSTRUMENT FITTED WITH 1800 LINES/MM GRATING AND USED IN FIRST ORDER. UNLESS OTHERWISE SPECIFIED, MULTIPLY BY 1800/(ruling density) FOR OTHER GRATINGS.

DISPERSION: 1.8nm/mm. This figure, when multiplied by the slits width (equal for both slits) gives the approximate full width at half height of the instrument bandpass function (bandwidth) provided that the bandwidth being demanded does not approach the instrument limiting resolution.

With the above proviso, the instrument bandpass function is approximately triangular.

Bandwidth varies slightly with wavelenght, see figure.

LIMITING RESOLUTION: M300HR .05nm, M300E, .5nm.
The maximum obtainable resolution in any monochromator is limited by misfocus. In the HR version, one of the collimating mirrors is mounted on a translation stage allowing fine positioning by the user. In the E version all the mirrors are jig set in manufacture. All instruments are set up to achieve the specified resolution before delivery.

LIGHT GATHERING CAPABILITY: .63
= slit height / (f number^2 x*dispersion nm/mm).

WAVELENGTH READOUT: 4 digit display reading directly in nm with readability of .02nm

WAVELENGTH STEP: Each step of the stepping motor results in a wavelength change of .01nm for the HR version and .05nm for the E version.

MAXIMUM SCAN SPEED: HR 4.5nm/s E 22.5nm/s.

WAVELENGTH ACCURACY: $\pm$ .2nm of true throughout range.

*Multiply by (ruling density) / 1800

(1) FWHH (nm), 1mm SLIT WIDTH, 1200 L/mm RULED GRATING, DIVIDED BY THREE

(2) FULL WIDTH AT HALF HEIGHT WITH 2mm SLIT WIDTH, DIVIDED BY TWO (nm)
1800 L/mm HOLOGRAPHIC GRATING

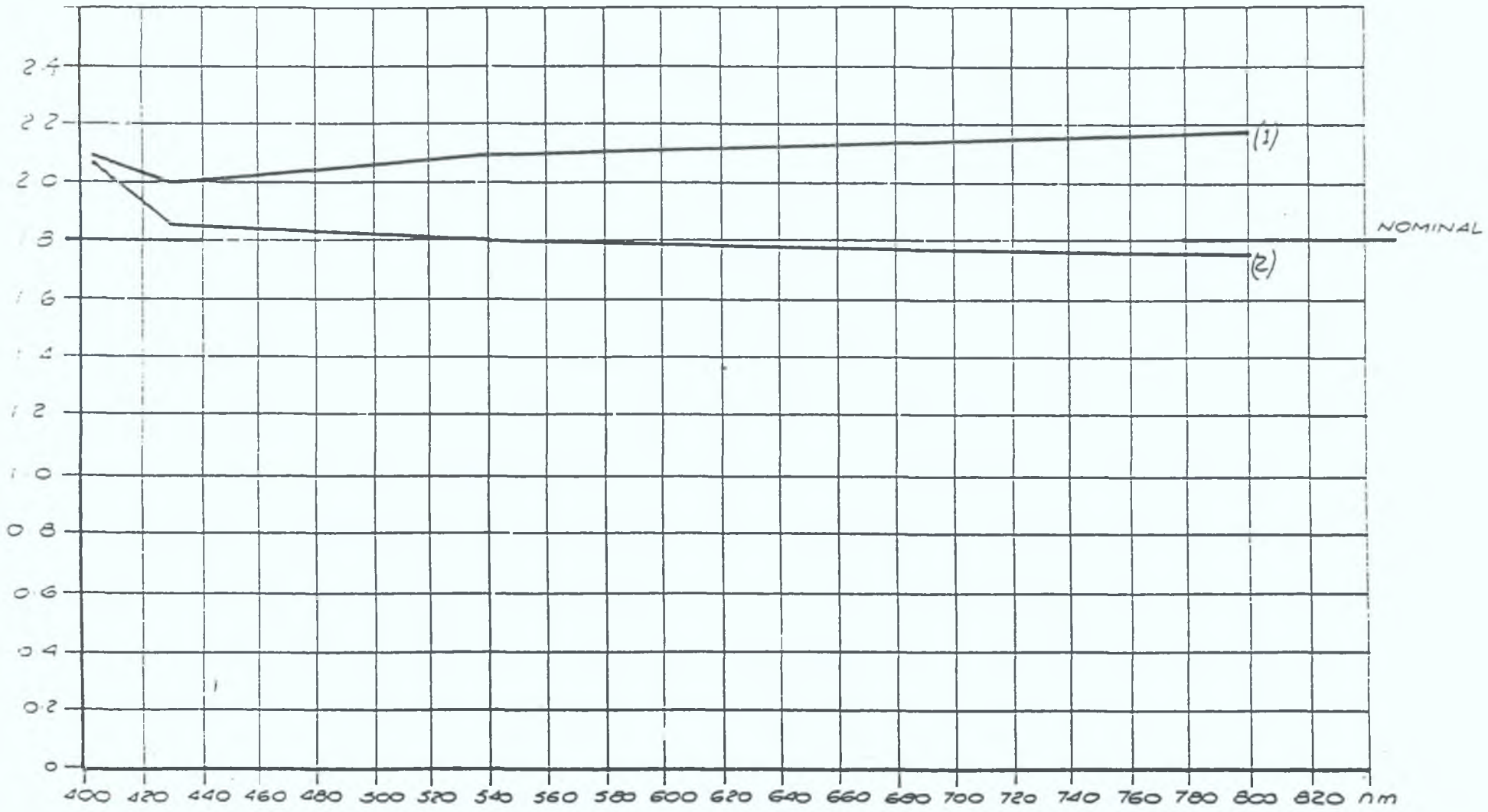

APPENDIX E

APPENDIX E.

PREPARATION OF PHENOL SAMPLE SOLUTIONS IN THE RANGE 0 TO 500ppb ACCORDING TO EPA GUIDELINES.

SAMPLE PREPARATION.

1) All glassware soaked in "RGB" sterilizing solution to neutralize any bacteria or chemical traces, and subsequently heat-dried.

2) 3 x 1 litre flasks of 100ppm.(i.e. 0.1g of 99.9% pure crystalline phenol in water).
3 standard solutions for cross referencing.

3) All standard solutions and serial solutions kept in darkness to prevent oxidation.

4) At concentrations usually found in drinking water; <1mg/litre (1ppb), phenols are suceptible to oxidative degradation by biological organisms or chemicals. Analysis can not be delayed for more than four hours. Otherwise solutions must be artificially preserved. All samples tested in this work were tested within 3 hours of being generated unless otherwise stated.

APPENDIX F

APPENDIX F.

SPECIFICATIONS AND GRAPHICAL PROOF OF "NEW WAVE RESEARCH: MINISYS 266" LASER PERFORMANCE.

RESEARCH
1286 HAMMERWOOD AVE., SUNNYVALE, CA 94089 • TEL: 408/734-8128 • FAX: 408/734-9273

MINISYS 106, 532, 355, 266

MINIATURE LASER SYSTEMS FOR SCIENCE AND INDUSTRY

The Minisystems from New Wave Research are based on the reliable ACL-1 Air Cooled Laser. They are designed with end users in mind who desire a completely packaged laser source consisting of the laser, frequency converters, dichroics and attenuator. These are single frequency units that have been optimized to serve specific applications requiring complete control of the output beam amplitude.

Beam attenuation is controlled remotely from the power supply front panel. The attenuator consists of a rotating half wave plate and a polarizer both of which are selected for the wavelength of interest. An optional RS232 interface allows computer control of all the important laser functions as well as the attenuator level.

MINISYS 106	LASER AND ATTENUATOR FOR 1064 nm
MINISYS 532	LASER, DOUBLER, DICHROICS AND ATTENUATOR FOR 532 nm
MINISYS 355	LASER, TRIPLER, DICHROICS AND ATTENUATOR FOR 355 nm
MINISYS 266	LASER, QUADRUPLER, DICHROICS AND ATTENUATOR FOR 266 nm
SCI-1	SERIAL COMPUTER INTERFACE

TYPICAL PERFORMANCE	MINISYS 106	MINISYS 532	MINISYS 355	MINISYS 266
MAX ENERGY (mJ)	30	5	1	1
ATTEN RANGE (mJ)	.1–30	.02–5	.003–1	.003–1
PULSEWIDTH (ns)	6	5	4	3
BEAM DIA. (mm)	2	1.5	1	.75
BEAM DIV. (mrad)	<2	<1	<1	<1
STABILITY (% p-p)	7	15	20	25

mJ
nS

Specifications subject to change without notice.

NEW WAVE RESEARCH INC.

ACL-1
AIR-COOLED LASER

The ACL-1 is a compact air cooled Q-switched Nd:YAG laser designed for medical and industrial uses. The laser head and power supply are an ideal size for semiconductor cutting stations, ophthalmic medical systems and other applications having similar size, power and cost requirements.

The output energy at 1064 nm is greater than 30 millijoules at one Hertz. Optional second and fourth harmonic crystals offer energies exceeding 5 millijoules and 1 millijoule respectively.

The ACL-1 is invar stabilized and its mirror mounts are secured at the factory to ensure trouble-free operation under normal operating conditions. The flashlamp and power supply are air cooled. The power requirement is standard 110 Volt service.

A control panel switch can select laser operation at 1 Hz, manual firing of the laser, or firing by external pulses. The laser can also be remotely controlled via an interface connector in the power supply.

The ACL-1 is a product of over twenty years of solid state laser design experience and incorporates the appropriate technology to deliver a reliable cost effective solution for equipment manufacturers. All in all, the ACL-1 is unique among alternative laser sources when the need for energy, size and cost are mandatory.

Specifications (@ 1 Hz):

- **Optical Characteristics:**
  - Pulse Energy @ 1064 nm: >30mJ
  - Pulse Energy @ 532 nm: >5 mj
  - Pulse Energy @ 266 nm: >1 mj
  - Pulse width @ 1064 nm: 6 nsec (nominal)
  - Spatial Mode: TEM_{00}
  - Beam Diameter @ 1064 nm: 2.5 nm (nominal)
  - Beam Divergence @ 1064 nm: 3 mrad
  - Polarization @ 1064 nm: Vertical
- **Repetition Rate:** 1 Hz continuous; 2 Hz for up to 8 pulses followed by 4 sec. off time
- **Stability:** Pulse-to-pulse
  - Energy @ 1064 nm: 10%
- **Power Supply Characteristics:**
  - Electrical Service: 110 or 230 VAC, 5A, 50/60 Hz
  - Internal fusing: 1 amp, Slo-Blo
  - Cooling: Air Cooled
- **Dimensions:** (see drawing)
  - Laser Head: 3 X 2 X 8.31"
  - Power Supply: 7.88 x 4.06 x 11.75"
  - Umbilical Length: 1 Meter
- **Weight:**
  - Laser Head: 3.5 lbs.
  - Power Supply: 11.5 lbs.

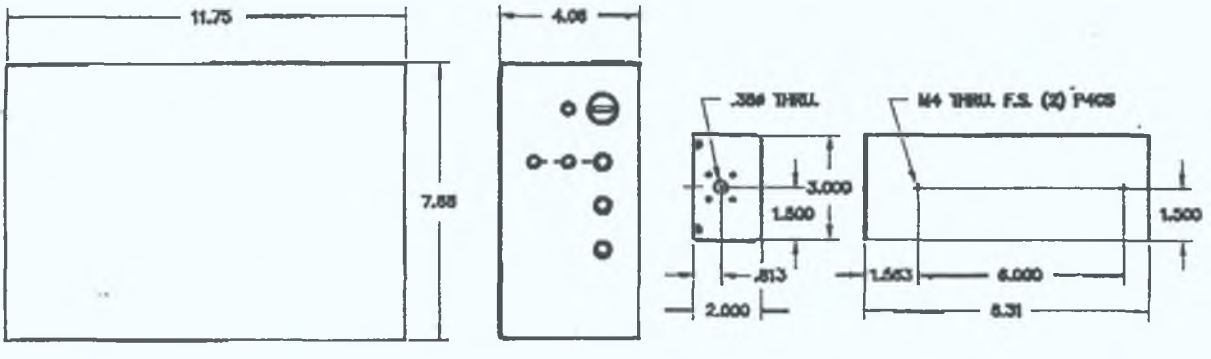

(Specifications subject to change without notice)

NEW WAVE RESEARCH INC. • 3476 Ramstad St., San Jose, CA 95127 • (408) 729-9409 • FAX (408) 258-9910

NEW WAVE RESEARCH INC.

ACL-1
AIR-COOLED LASER

The ACL-1 is a compact air cooled Q-switched Nd:YAG laser designed for medical and industrial uses. The laser head and power supply are an ideal size for semiconductor cutting stations, ophthalmic medical systems and other applications having similar size, power and cost requirements.

The output energy at 1064 nm is greater than 30 millijoules at one Hertz. Optional second and fourth harmonic crystals offer energies exceeding 5 millijoules and 1 millijoule respectively.

The ACL-1 is invar stabilized and its mirror mounts are secured at the factory to ensure trouble-free operation under normal operating conditions. The flashlamp and power supply are air cooled. The power requirement is standard 110 Volt service.

A control panel switch can select laser operation at 1 Hz, manual firing of the laser, or firing by external pulses. The laser can also be remotely controlled via an interface connector in the power supply.

The ACL-1 is a product of over twenty years of solid state laser design experience and incorporates the appropriate technology to deliver a reliable cost effective solution for equipment manufacturers. All in all, the ACL-1 is unique among alternative laser sources when the need for energy, size and cost are mandatory.

Specifications (@ 1 Hz):

- Optical Characteristics:
  - Pulse Energy @ 1064 nm: >30mJ
  - Pulse Energy @ 532 nm: >5 mj
  - Pulse Energy @ 266 nm: >1 mj
  - Pulse width @ 1064 nm: 6 nsec (nominal)
  - Spatial Mode: TEM_{00}
  - Beam Diameter @ 1064 nm: 2.5 nm (nominal)
  - Beam Divergence @ 1064 nm: 3 mrad
  - Polarization @ 1064 nm: Vertical
- Repetition Rate: 1 Hz continuous; 2 Hz for up to 8 pulses followed by 4 sec. off time
- Stability: Pulse-to-pulse
  - Energy @ 1064 nm: 10%
- Power Supply Characteristics:
  - Electrical Service: 110 or 230 VAC, 5A, 50/60 Hz
  - Internal fusing: 1 amp, Slo-Blo
  - Cooling: Air Cooled
- Dimensions: (see drawing)
  - Laser Head: 3 X 2 X 8.31"
  - Power Supply: 7.88 x 4.06 x 11.75"
  - Umbilical Length: 1 Meter
- Weight:
  - Laser Head: 3.5 lbs.
  - Power Supply: 11.5 lbs.

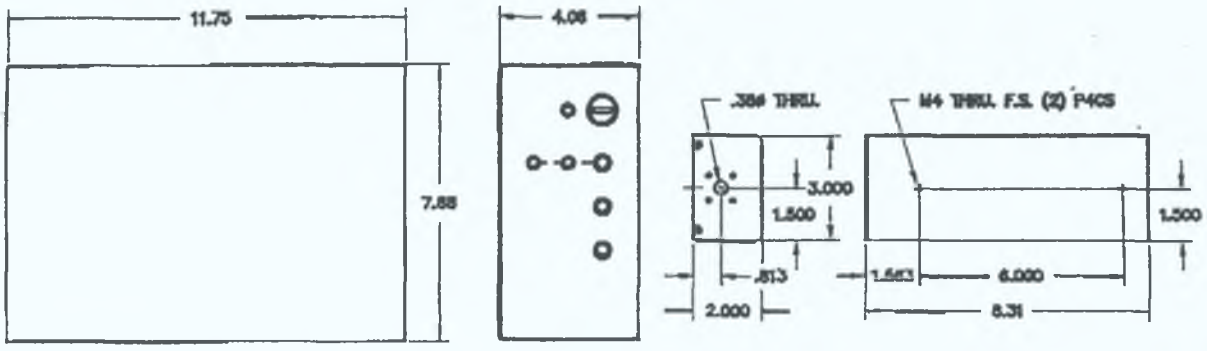

(Specifications subject to change without notice)

NEW WAVE RESEARCH INC. • 3476 Ramstad St., San Jose, CA 95127 • (408) 729-9409 • FAX (408) 258-9910

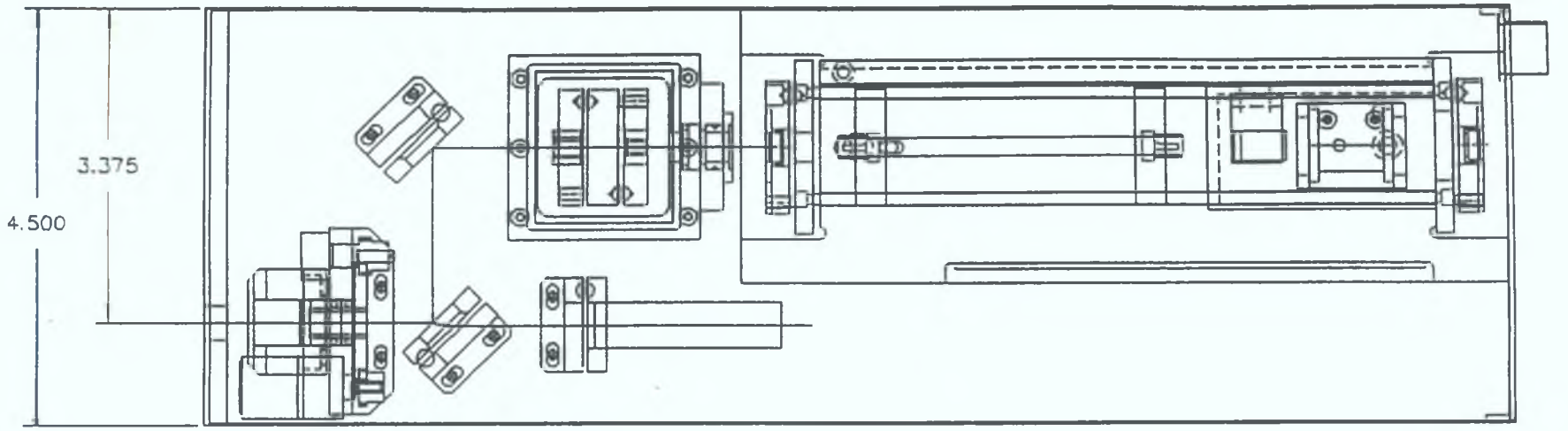

TOP VIEW

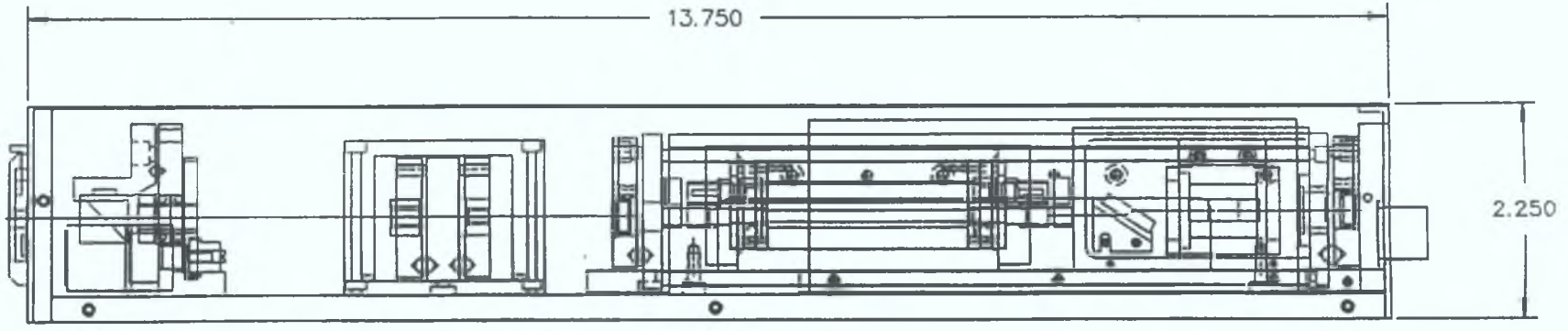

FIG. 5

SIDE VIEW

NW\BDF532A

01 10 02

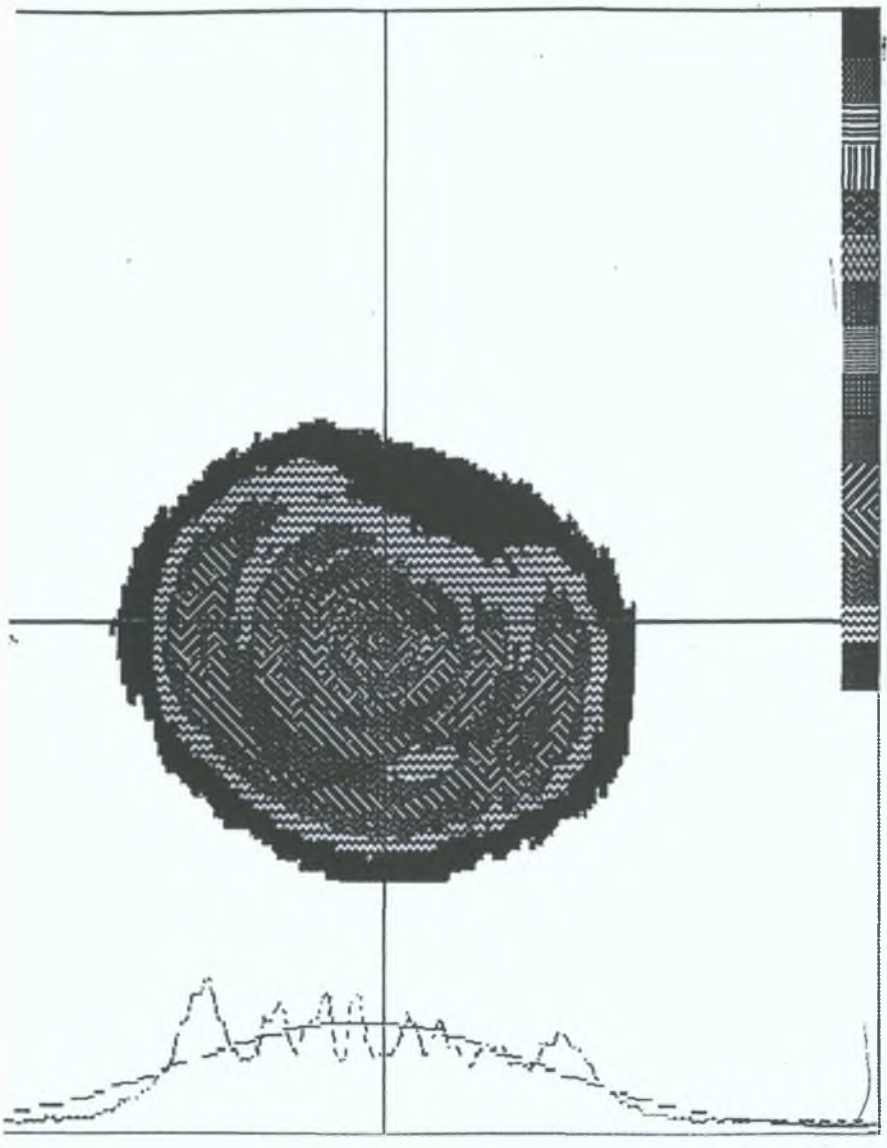

Pk(x,y,%)=(153,153, 45.5)	
Centroid (x,y)	(117,130)
Power [mW]	4.000
Beam Dia [mm]	2.778
Eff Area [mm²]	4.110
Pk Dnsty [W/cm²]	0.097
——Gauss Fits: Horz,Vert-	
Coeff =	0.89, 0.94
Centroid=	110, 144
Peak =	71, 72
Dia [mm]=	4.16, 3.28

CSR (x,y,I):(117,130, 55)		
SRC:CW	CAP:Cont	BG:Off
CPU:Idle	MODE:Stop	S#: 1
GPIB:L	ZOOM:1	

FIG 4

FIG. 3-1

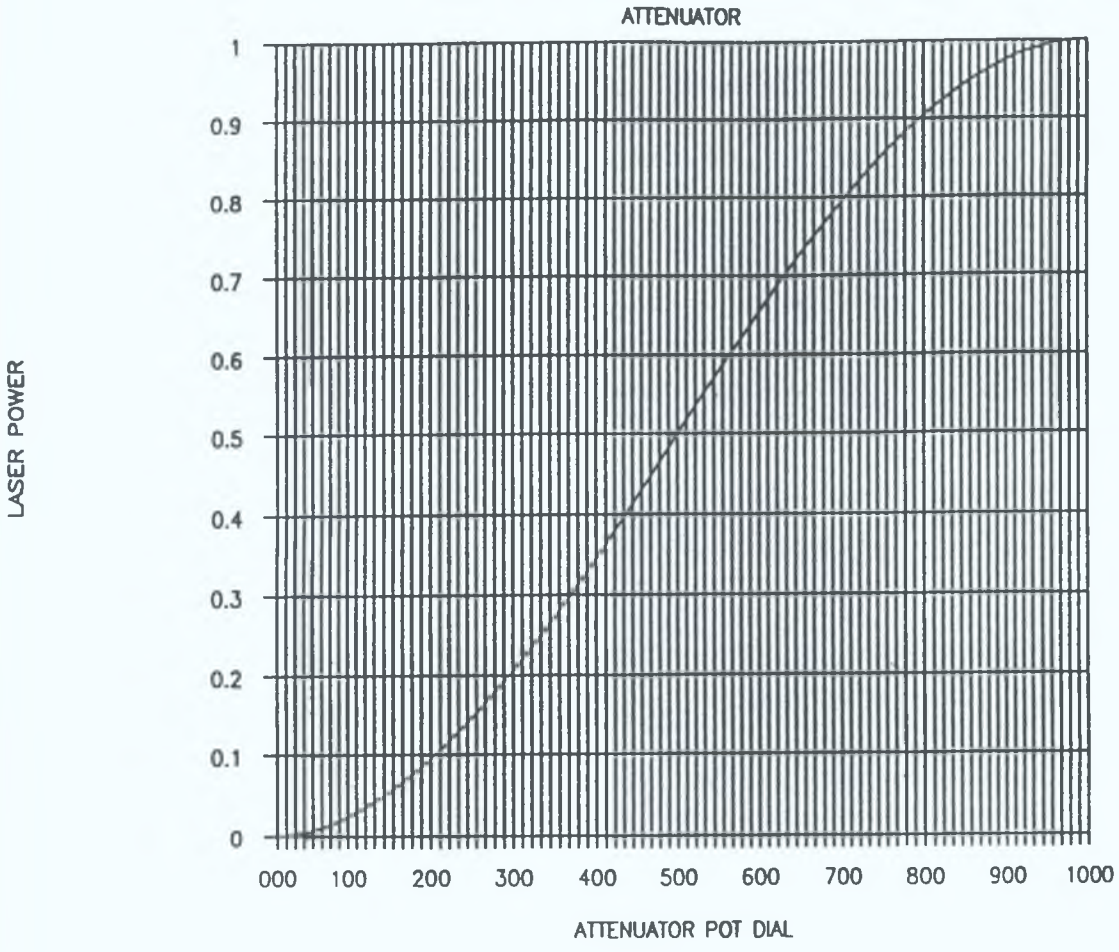
ATTENUATOR
LASER POWER
1
0.9
0.8
0.7
0.6
0.5
0.4
0.3
0.2
0.1
0
000
100
200
300
400
500
600
700
800
900
1000
ATTENUATOR POT DIAL

Made in Germany
Made in Germany

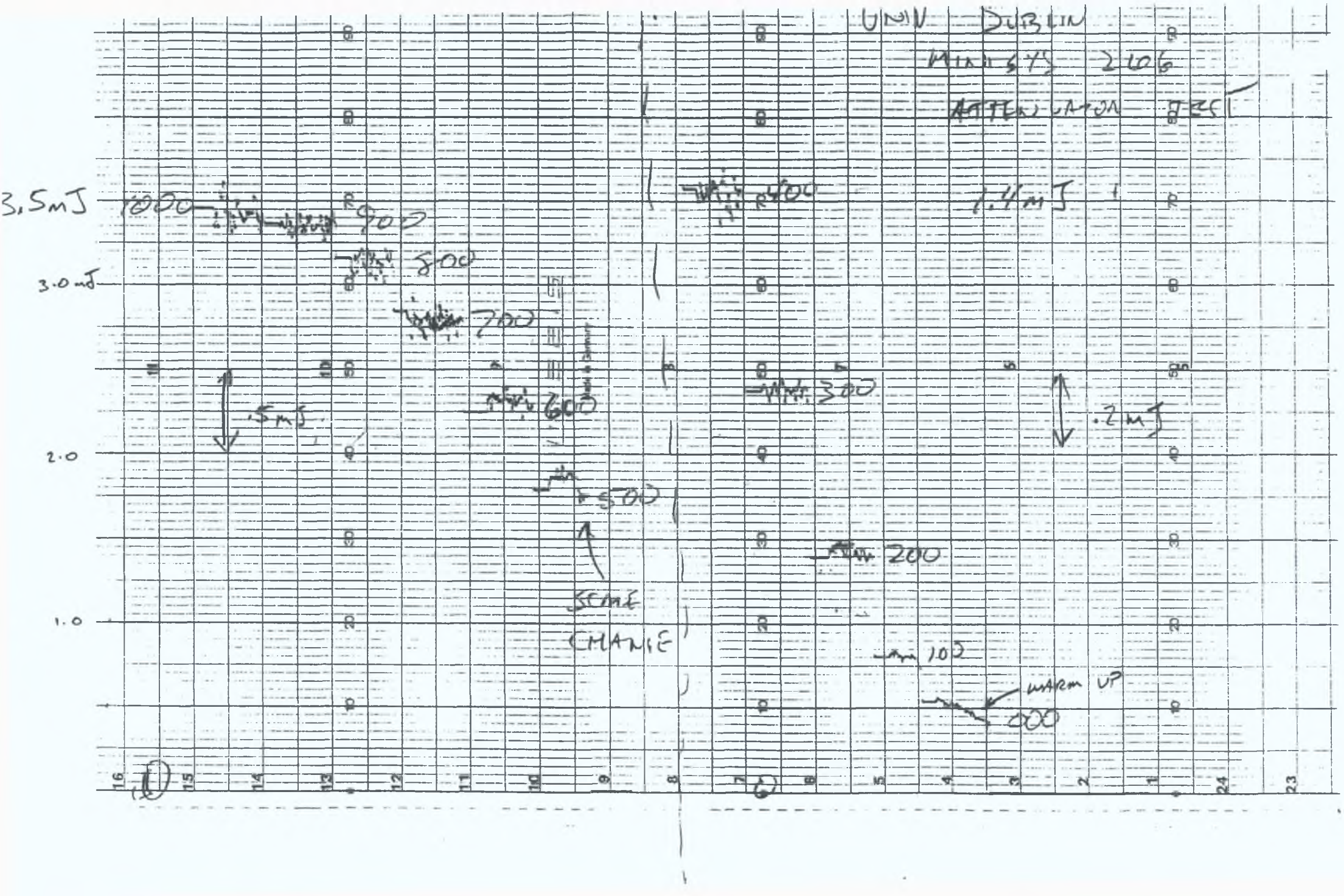
UNIV DUBLIN
MINISTS 2406
AFTER CALIBRATION
1.4 mJ
3.5mJ
3.0 mJ
2.0
1.0
1000
900
800
700
600
500
400
300
200
100
.5mJ
.2mJ
SLOW CHANGE
WARM UP

APPENDIX G

APPENDIX G.

COLLECTION AND EFFICIENCY CALCULATION OF CONCENTRATION FROM FLUORESCENCE DATA.

"TES.c":

The total control of the phenol fluorescence prototype system and collection and logging of data for concentration assesment.

Collection of data and system control in this program is based on the system sequence timing diagram Fig 3.7 which is also shown below.

```
/* Tes.c
 "Control of prototype sensor and collection of fluorescence data."

 #include <stdio.h>
 #include <dos.h>
 #include <math.h>
 #include <conio.h>
 #include <time.h>
 #define BASE      640
 FILE  *fptr1;
 FILE  *fptr2;

 void main(void)
         {
              long   l,m,num,l1,l2,l3,l4,l5,l6,l7,l8,m1,m2,m3,m4,m5,m6,m7,m8;
              long valf,val1,val2,val3,val4,val5,val6,val7,val8;
              long valt,val1a,val2a,val3a,val4a,val5a,val6a,val7a,val8a;
              long i,j;
              double valta;
              i=0;  num=0; valt=0; valta=0;  valf=0;
              fptr1=fopen ("flur50dd.dat","w");

              clrscr();
              outportb(BASE + 7,146);              /* set up ports a and     */
```

```
                printf("ready Hig !");
                getch();


        for (j=0;j<100;j++)
          {
          /*        while (inportb(BASE+4)&1); */        /*check A0 lo */


            while (!(inportb(BASE+4) & 1));  /*If A0 is HI proceed*/


            for (i=0;i<77;i++)
             {
             }

                    outportb(BASE +16,0);           /*start a to d, channel 0 */
                    while (!(inportb(BASE + 20)&1) );     /*eoc check
*/                  m1 = inportb(BASE+18);           /*msb read in          */
                    l1 = inportb(BASE+19);           /*4lsb read in         */

                    outportb(BASE +16,0);           /*start a to d, channel 0 */
                    while (!(inportb(BASE + 20)&1) );     /*eoc check
*/                  m2 = inportb(BASE+18);           /*msb read in          */
                    l2 = inportb(BASE+19);           /*4lsb read in         */

                    outportb(BASE +16,0);           /*start a to d, channel 0 */
                    while (!(inportb(BASE + 20)&1) );     /*eoc check
*/                  m3 = inportb(BASE+18);           /*msb read in          */
                    l3 = inportb(BASE+19);           /*4lsb read in         */

                    outportb(BASE +16,0);           /*start a to d, channel 0 */
                    while (!(inportb(BASE + 20)&1) );     /*eoc check
*/                  m4 = inportb(BASE+18);           /*msb read in          */
                    l4 = inportb(BASE+19);           /*4lsb read in         */

                    outportb(BASE +16,0);           /*start a to d, channel 0 */
                    while (!(inportb(BASE + 20)&1) );     /*eoc check
*/                  m5 = inportb(BASE+18);           /*msb read in          */
                    l5 = inportb(BASE+19);           /*4lsb read in         */


                    outportb(BASE +16,0);           /*start a to d, channel 0 */
                    while (!(inportb(BASE + 20)&1) );     /*eoc check
*/                  m6 = inportb(BASE+18);           /*msb read in          */
                    l6 = inportb(BASE+19);           /*4lsb read in         */

                    outportb(BASE +16,0);           /*start a to d, channel 0 */
                    while (!(inportb(BASE + 20)&1) );     /*eoc check
```

```
*/                  m7 = inportb(BASE+18);          /*msb read in          */
                    l7 = inportb(BASE+19);          /*4lsb read in         */

                    outportb(BASE +16,0);           /*start a to d, channel 0 */
                    while (!(inportb(BASE + 20)&1) );    /*eoc check
*/                  m8 = inportb(BASE+18);          /*msb read in          */
                    l8 = inportb(BASE+19);          /*4lsb read in         */



                    val1a= ( ((m1*16)+(l1/16))-780) ;
                    if (val1a<0)
                     {  val1=((val1a)*(-1));
                     }
                    else
                     {  val1=val1a;
                     }
                    val2a= ( ((m2*16)+(l2/16))-780) ;
                    if (val2a<0)
                     {  val2=((val2a)*(-1));
                     }
                    else
                     {  val2=val2a;
                     }
                    val3a= ( ((m3*16)+(l3/16))-780) ;
                    if (val3a<0)
                     {  val3=((val3a)*(-1));
                     }
                    else
                     {  val3=val3a;
                     }
                    val4a= ( ((m4*16)+(l4/16))-780) ;
                    if (val4a<0)
                     {  val4=((val4a)*(-1));
                     }
                    else
                     {  val4=val4a;
                     }
                    val5a= ( ((m5*16)+(l5/16))-780) ;
                    if (val5a<0)
                     {  val5=((val5a)*(-1));
                     }
                    else
                     {  val5=val5a;
                     }
                    val6a= ( ((m6*16)+(l6/16))-780) ;
                    if (val6a<0)
                     {  val6=((val6a)*(-1));
                     }
```

```
        else
         {  val6=val6a;
         }
        val7a= ( ((m7*16)+(l7/16))-780) ;
        if (val7a<0)
         {  val7=((val7a)*(-1));
         }
        else
         {  val7=val7a;
         }
        val8a= ( ((m8*16)+(l8/16))-780) ;
        if (val8a<0)
         {  val8=((val8a)*(-1));
         }
        else
         {  val8=val8a;
         }



      /*        printf("%d\t",val1);
        printf("%d\t",val2);
        printf("%d\t",val3);
        printf("%d\t",val4);
        printf("%d\t",val5);
        printf("%d\t",val6);
        printf("%d\t",val7);
        printf("%d\n",val8);    */


    valf = (val1+val2+val3+val4+val5+val6+val7+val8);

      valt+=valf;
        printf("%d\n",valf);


        fprintf(fptr1,"%d\n",valf);

}
        fclose(fptr1);

        valta=(valt/100);
        printf("\n%lf\n",valta);
        printf("Done Hig !");


        getch();

}
```

"PULSFIND.c"

This program finds a periodical pulse by incrementing a time window and recording the related signal for each window.

```
/* "Pulsfind.c"

   Higgy, Aug 1992  */

#include <stdio.h>
#include <dos.h>
#include <math.h>
#include <conio.h>
#include <time.h>
#define BASE      640
FILE  *fptr1;
FILE  *fptr2;

void main(void)
        {
            long l,m,l1,m1,num;
            long i,j,k;
            long val;
            i=0;  num=0; val=0;
            fptr1=fopen ("puls.dat","w");
            clrscr();
            outportb(BASE + 7,146);              /* set up ports a and     */

            num=1;

          for(k=0;k<100;k++)
            {
            while (inportb(BASE+4)&1);          /*check A0 lo */

            while (!(inportb(BASE+4) & 1));  /*If A0 is HI proceed*/

            for (i=0;i<num;i++)
             {
             }


            outportb(BASE +16,0);            /*start a to d, channel 0 */
```

```
                while (!(inportb(BASE + 20)&1) );     /*eoc check
*/

                m = inportb(BASE+18);            /*msb read in          */
                l = inportb(BASE+19);           /*4lsb read in          */
            /*    m1 = inportb(BASE+18);  /*          /*msb read in
*/           /*    l1 = inportb(BASE+19);  /*         /*4lsb read in

              /*  val1 =  ((m1*16)+(l1/16)) ;  /*
                  /*getting value          */


              val =  ((m*16)+(l/16)-780) ;

                  fprintf(fptr1,"%ld\t%ld\n",num,val);
                   printf("%ld\t%ld\n",num,val);
                  val=0;
                  num+=1;
        }


        fclose(fptr1);

        printf("Done Hig !");
        getch();
}
```

---------- o ----------

"HIST.c"

This program sorts all of the data at a particular concentration and calculates the relevant statistics as well as storing the values in order for ease of plotting as a Histogram of distribution.

```
/* Averaging/Standard Deviation of samples of Laser System. */
/* Histogram Stats. Generation.  "Hist.c"              */
/*   Higgy,  Aug, 1992.       */


#include <conio.h>
#include <stdio.h>
#include <math.h>

int i,hist;
double num,num1;
double sdev,nval,tval,aval,nval2,tnval2,var;

char ch;

void main(void)
{


   FILE *fptr3;
   FILE *fptr4;



                fptr4= fopen("hist.dat","w");

   num = 0.15;

   for(i=0;i<40;i++)
   {

         fptr3= fopen("nval.dat","r");

         num1=(num+(0.01));

         fscanf(fptr3," %lf ",&nval);
```

```
    do{


            if( (nval<num1)&&(nval>num)  )
              {
                 hist += 1;

              }


            else
              {
              }


        }
        while(fscanf(fptr3," %lf ",&nval)!=EOF);

        fclose(fptr3);


        fprintf(fptr4,"%lf\t %d\n" ,num,hist);


  hist=0;
  num+=0.01;

  }




        fclose(fptr4);



        printf("/n  O.K. Finished !!!!  ");

ch= getch();


}
```

---------- o ----------

"DIV.c, DIV1.c and HIGAD.c "

The three programs which follow were used in the course of this work in the development of a full statistical analysis.

```
/* Averaging/Standard Deviation of samples of Laser System. */
/* hig.                */
/* Aug, 1992.          */


#include <conio.h>
#include <stdio.h>
#include <math.h>
int conc;
double valf,valp;
double sdev,sder,nval,tval,aval,nval2,tnval2,var;


char ch;

void main(void)
{

   FILE *fptr1;
   FILE *fptr2;
   FILE *fptr3;
   FILE *fptr4;


                    conc=50;
        fptr1= fopen("flur50dd.dat","r");
        fptr2= fopen("puls50dd.dat","r");
        fptr3= fopen("nval50dd.dat","w");
        fptr4= fopen("aval50dd.dat","w");


         fscanf(fptr1," %lf ",&valf);


      do{

         fscanf(fptr2," %lf ",&valp);
```

```
        nval  = ((valf)/(valp));

        fprintf(fptr3,"%lf\n",nval);

        tval += (nval);


      nval=0;


      }
      while(fscanf(fptr1," %lf ",&valf)!=EOF);

      aval = (tval/100);

      printf("\nConc..Int.ie. SumS1/S0./n = %d\t%lf \n",conc,aval);

      fprintf(fptr4,"%d\t%lf\n",conc,aval);



      fclose(fptr1);
      fclose(fptr2);
      fclose(fptr3);
      fclose(fptr4);




      printf("O.K. Finished !!!!  ");
ch= getch();

}
```

---------- o ----------

```
/* Averaging/Variance and Plotting of data. */
/* hig.                */
/* Aug, 1992.       */


#include <conio.h>
```

```
#include <stdio.h>
#include <math.h>

int   conc;
double valf,valp,ins;
double sdevp,sderp,tvalp,avalp,valp2,tvalp2,varp;
double sdevf,sderf,tvalf,avalf,valf2,tvalf2,varf;

char ch;




char ch;

void main(void)
{


   FILE *fptr1;
   FILE *fptr2;
   FILE *fptr3;
   FILE *fptr4;
   FILE *fptr5;
   FILE *fptr6;



                  conc=50;
        fptr1= fopen("flur050d.dat","r");
        fptr2= fopen("puls050d.dat","r");
        fptr3= fopen("tval050d.dat","w");
        fptr4= fopen("aval050d.dat","w");
         fptr5= fopen("int050d.dat","w");

         fscanf(fptr1," %lf ",&valf);


      do{

         fscanf(fptr2," %lf ",&valp);
```

```
        tvalf += (valf);
        tvalp += (valp);




    }
    while(fscanf(fptr1," %lf ",&valf)!=EOF);

      fprintf(fptr3,"%lf\n",tvalf);

      fprintf(fptr3,"%lf\n",tvalp);

    avalf = (tvalf/100);
    printf("\nAver.Val. flur. = %lf \n",avalf);
    fprintf(fptr4,"%lf\n",avalf);

    avalp = (tvalp/100);
    printf("\nAver.Val. puls. S1/S0 = %lf \n",avalp);
    fprintf(fptr4,"%lf\n",avalp);

    ins = (avalf/avalp);
    fprintf(fptr5,"%d\t%lf\n",conc,ins);
    printf("\nConc..Int.ie. Sum.avalf/Sum.avalp = %d\t%lf \n",conc,ins);



    fclose(fptr1);
    fclose(fptr2);
    fclose(fptr3);
    fclose(fptr4);
    fclose(fptr5);


     tvalf=0; valf=0; tvalp=0; valf=0;
     conc=0;




    printf("O.K. Finished !!!!  ");

ch= getch();
```

```
}
                ---------- o ----------


/*"HIGAD.c"
  Countdown Recorder and Plotter

  Hig. July '92      */

 #include <stdio.h>
 #include <dos.h>
 #include <math.h>
 #include <conio.h>
 #define BASE      640
 FILE  *fptr1;


 void main(void)
         {
              float volt[2][5];                  /* set up 2 dim array     */
              double num1;
              int num,m1,l1;
              int i,j,x,l,m,val,msb,lsb;
              i=0; x=0; num1=200;  num=200; msb=0; lsb=0;
              fptr1=fopen ("0100.dat","w");
              outportb(BASE + 7,146);               /* set up ports a and     */
              outportb(BASE + 3,48);                                          /*
b as inputs.          */

              clrscr();
           for (j=0;j<5;j++)
             {
              while (inportb(BASE+4)&1);          /*check A0 lo */

              while (!(inportb(BASE+4) & 1));  /*If A0 is HI proceed*/

              /*while (!(inportb(BASE+0) & 1));*/          /*check ctr0 low */
              /*printf("\nCnt Reg = %d \n",(inportb(BASE+0)&1));*/

              outportb(BASE +0,msb,);               /*send msb,lsb to cntr 0*/
              outportb(BASE +0,lsb);

                    m1 = inportb(BASE+0);            /*msb read in            */
                    l1 = inportb(BASE+0);           /*4lsb read in           */
                    printf("\tm1  = %d \t",m1);
                    printf("\tl1 = %d \n",l1);

              /*while ((inportb(BASE+0 )& 1)); */     /* check counter hi */
```

```
                                        /*terminal cnt. reached*/

        /*printf("\nCnt Reg = %d \n",(inportb(BASE+0)&1));*/

        outportb(BASE +16,0);           /*start a to d, channel 0 */

              while (!(inportb(BASE + 20)&1) );     /*eoc check
*/


              m = inportb(BASE+18);          /*msb read in          */
              l = inportb(BASE+19);          /*4lsb read in         */
              printf("\tm  = %d \t",m);
              printf("\tl = %d \n",l);

              val= ((m*16)+(l/16));          /*getting value        */
              fprintf(fptr1,"%d\t%d\n",num,val);

           printf("\t%d\t%d\n",num,val);
              num+=2;   num1+=2;
              msb= (num/256);
              lsb= (int)floor( (256*((num1/256)-msb)) );
           printf("\tmsb  = %d \t",msb);
           printf("\tlsb  = %d \n",lsb);
           printf("\tnum/256  = %lf \n",(num1/256));
     }
              fclose(fptr1);
              volt[x][i] = (((float)val/4095) * 10);/*change to volts  0 to 10*/
              printf("\nvalue  %d %d is  %f \n",i,x,volt[x][i]);



              printf("Done Hig !");
              getch();
}
```

---------- o ----------

APPENDIX H

14. Error, uncertainty of measurement and confidence level.

Every result of a measurement is afflicted with an uncertainty. No single result is absolutely accurate. More specific: one wishes to measure a value and uses a method to obtain an indication of that value. There will be no experimental method capable of returning the true value of the quantity to be measured. The indicated value will be in error with that value. The "International organization of legal metrology" (in PD 6461 "Vocabulary of legal metrology. Fundamental terms" §8.1) defines **error of measurement** to be:
"the discrepancy between the result of a measurement and the value of the quantity measured".
Since the value of the quantity measured (the true value) cannot be known, the error of measurement cannot be known either. Therefore one has developed a technique to estimate the error of measurement. This estimate is called the uncertainty of measurement. In order to make a thorough estimate of this uncertainty one has to be aware of all possible causes for the measured value to be in error. For all these causes one has to estimate (or evaluate) a value to express their contribution to the uncertainty.

Like for the error, the components that contribute to the uncertainty can be divided in two categories. The "Comité International des Poids et Mesures" recommended ("Rapport du Groupe Travail sur l'expression des uncertitudes" Procès-Verbaux des séances, Tome 49, 1981, A1 - A12) to indicate these **categories as A and B**. The committee has based this definition upon the method one uses to evaluate the uncertainty component. Components of type
A are those that are evaluated statistically.
Components of type
B are those that are evaluated by other methods.
From this one can conclude statistics to be a very important aspect of the uncertainty calculation, however the type B component will mostly be the largest part of the uncertainty. One has to realize that an important difference between the error and the uncertainty of a measurement is that:
the error is an absolute value and cannot be known, it characterizes one measurement only.
The uncertainty is a value which approaches the error; it is based upon and characterizes many measurementy

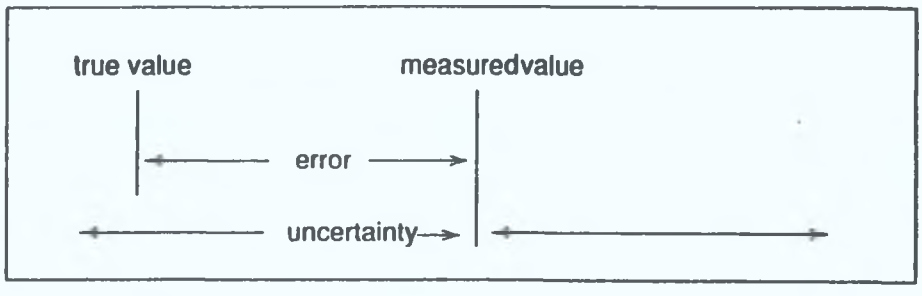

fig 14.1 The relation between error, uncertainty,true value and measured value

In other words: whereas the error is a theoretical value, too exact to be known, it can however be estimated by the uncertainty. Therefore from hereon we will focus on uncertainty only.

Type A components

If a measurement is performed a number of times, an average can be calculated and a spread will occur between the successive measurements. **Spread** is formally defined (PD 6461) as the difference between the maximum and the minimum of the measured values. It must therefore be a type A component. Is it a good indication of that component in the uncertainty? Metrologists feel not. If one calculates the spread from a certain number of measurements, there will always be a larger number of measurements after which there will be a measurement beyond the limit of the spread already defined. This makes spread a not unique value. A better and widely used measure for the type A components is the standard deviation. The **standard deviation** is defined (PD 6461) as:
the average of the differences between the results of a series of measurements and the arithmetic

mean of all the results of this series. In formula:

$$s = \sqrt{\left[\frac{\sum_{i=1}^{n} (\bar{x} - x_i)^2}{n-1} \right]}$$

The standard deviation s is an expectation value for the deviation of one measurement from the mean $\bar{x}$ of a series of n measurements represented, each of which is represented by x_i, i is any number from 1 to *n*. Quite often the standard deviation is referred to as **sigma**, σ.

It is obvious that the **standard deviation of the arithmetic mean of the series of measurements** (denoted by s_r) is less than the standard deviation of a single measurement s. In fact one can show (see any book on statistics e.g. HJ Larson, "Introduction to probability theory and statistical inference", John Whiley & Sons Inc, 1982) that

$$s_r = \frac{s}{\sqrt{n}}$$

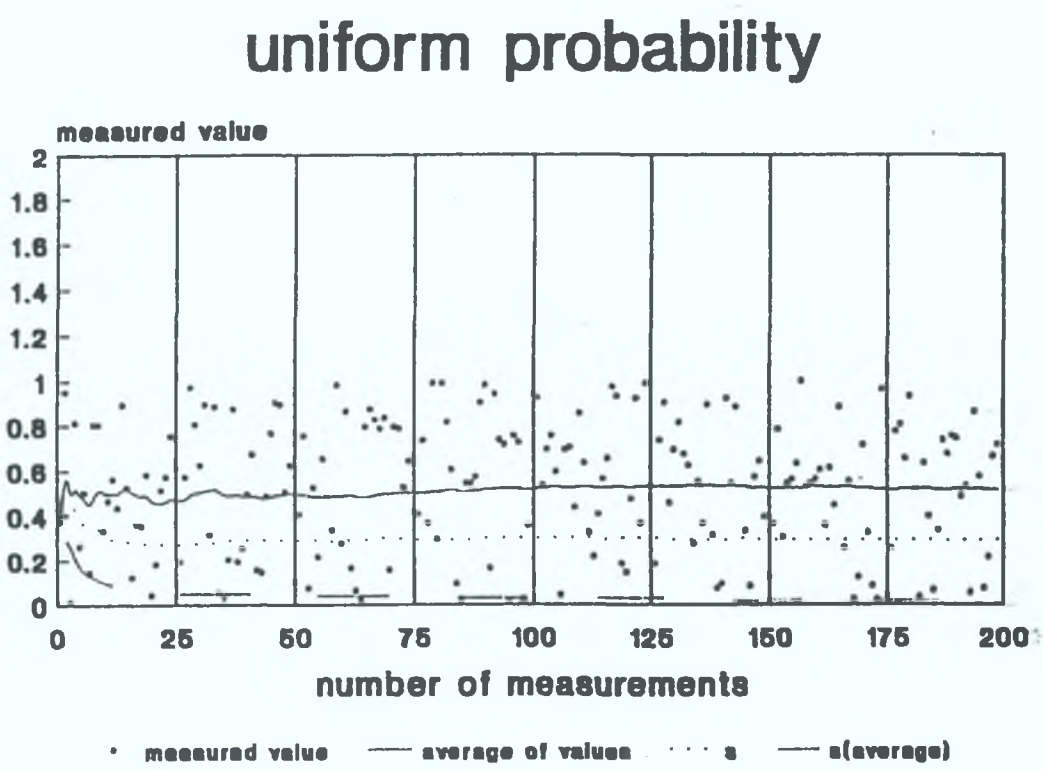

fig 14.2 For a number of measurements, increasing from 2 to 200, the mean and the standard deviations have been calculated. The probability distribution is uniform over the interval [0,1].

The figure shows a simulation of a series of measurements in which the measurement can result in any value between 0 and 1. That measurement satisfies a so-called uniform probability distribution. In the figure the mean, the standard deviation of a single measurement and the standard deviation of the mean, are displayed for the series of measurements from measurement number 1 to n. As the number of measurements in this series increases: the arithmetic mean approaches the value 0.5; the standard deviation decreases to $1/\sqrt{12}$; the standard deviation of the mean decreases to 0 as the number of measurements increases infinitely.

Confidence level and distribution functions

What does the standard deviation stand for? From theory so far, one can conclude the expectation value of this series of measurements (0.5) to lie within the interval $[x_i\text{-}s, x_i\text{+}s]$ for measurement x_i.

However, there is more information. The mean value $\bar{x}$ with its standard deviation s_r learn us that the expected value for the mean (0,5) must be found in the interval $[\bar{x}\text{-}s_r, \bar{x}\text{+}s_r]$. One can now take a closer look at the simulation. Figure 14.3 shows the measurements from number 91 to number 100 with bars representing the intervals just defined. For clarity the averages $\bar{x}$ have been drawn below the measurement number up and until which they were calculated.

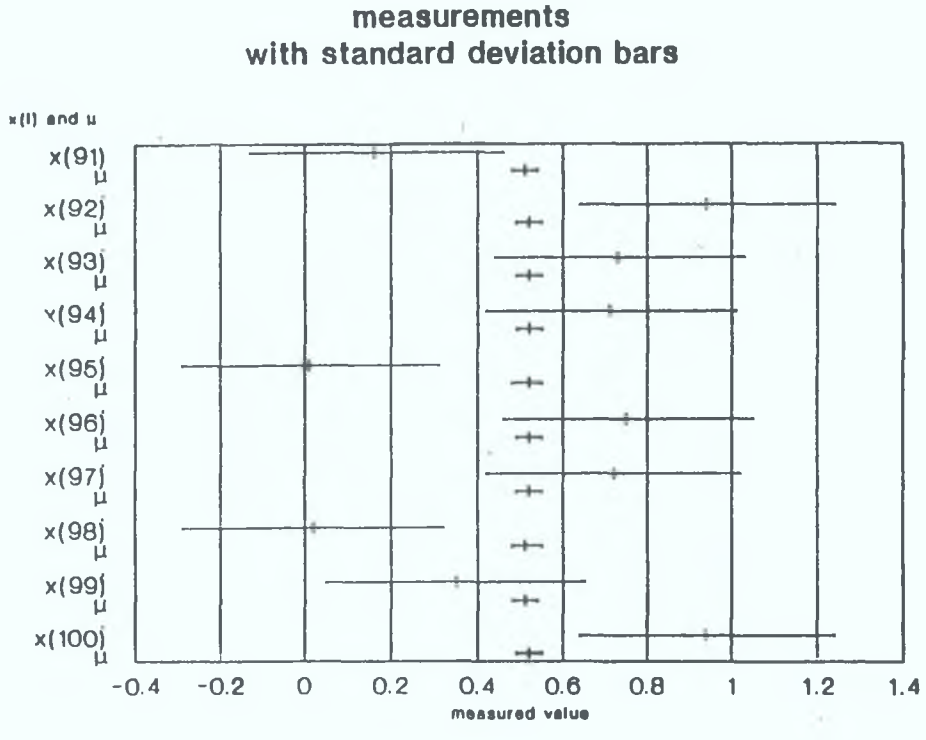

fig. 14.3 For the measurements 91 to 100 the intervals were drawn as described in the text.

For five out of ten measurements the interval around the measured value does not overlap the interval around the corresponding average. There is apparently no reason to be very **confident** in every measurement.

We recall spread here. Spread was intended to include every measured value and could not. For the standard deviation it is known that a certain fraction of the measured values does not lie in the intervals. For all the measurements in the simulation 135 out of 200 (67.5%) measured values satisfy this criterion. From calculation one can show (e.g. Larson, 1982) that *for an infinite series* of measurement this fraction will be 68.3%. This fraction is called the confidence level. The **confidence level** is:
the probability that the limits of a so-called **confidence interval** will not be exceeded by a measurement.

In the simulation the confidence interval is $[0.5\text{-}s_r, 0.5\text{+}s_r]$ for the mean values $\bar{x}$ and $[0.5\text{-}s, 0.5\text{+}s]$ for the measured values x_i.

There is a correlation between the confidence interval, the confidence level and the standard deviation: the confidence interval can be expressed in the standard deviation for a certain confidence level. For an infinite series of measurements the
following table applies:

confidence interval	confidence level
$\pm 1 \cdot s$	68.3 %
$\pm 1.96 \cdot s$	95 %
$\pm 2 \cdot s$	95 %
$\pm 2.58 \cdot s$	99 %
$\pm 3 \cdot s$	99.73 %

In general one can state that for a confidence level P (in %) the confidence interval is equal to $\pm t \cdot s$ around a single measurement x_i and $\pm t \cdot s_r$ around the arithmetic mean $\overline{x}$. The table is not valid for a situation in which a limited number of measurements is performed. One will be less confident in a standard deviation from two measurements than one from twenty measurements. So the multiplication factor t will increase with a decreasing number of measurements. So far t depends on P and the number of measurements. We will show that t depends on the probability distribution as well.

Probability distribution

For the simulation resulting in figures 14.2 and 14.3, a so-called uniform probability distribution was used: the measurement series this simulation represents, could result in any value in between 0 and 1 with the same probability.

One measures a standard resistor, the resistance of which is known to be 0.5 Ω with a negligible uncertainty. Even if the stability of the used measuring device is of the order of 0.5 Ω, one normally would not expect the simulation to represent this example. The measured values would be expected to be distributed around 0.5 Ω, such that there is a larger probability to find a measured value in an interval near 0.5 Ω than in an equal interval further away from it. And unless the used device were to have a range from 0 Ω to 1 Ω, one would expect some measurements beyond this range. The uniform distribution obviously does not describe this situation.

Statistics learns that there are several distribution functions, a few of which are displayed in figure 14.4:

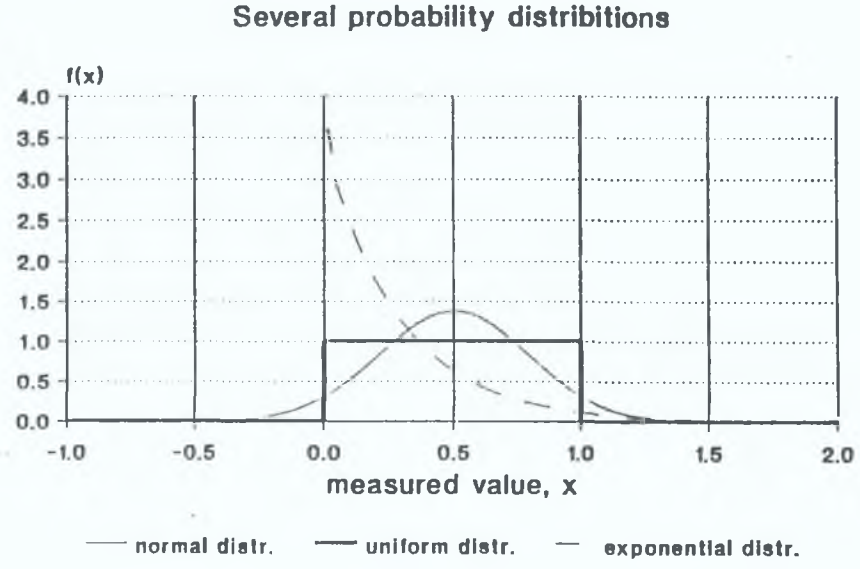

figure 14.4 Probability functions satisfy a few requirements

$$1 \qquad \int_{x-\Delta x}^{x+\Delta x} f(x)\,dx = P\,(x-\Delta x < x < x+\Delta x)$$

The integral is equal to the probability for the measured value to be found in the interval [x-Δx,x+Δx].

$$2 \qquad \int_{-\infty}^{+\infty} f(x)\,dx = 1$$

It should be very probable indeed to find a measured value anywhere.

Considering a few situations to which the probability functions of figure 14.4 could apply, one could take the example of the resistance measurement for the normal distribution.
If one measures a signal fluctuating randomly in a limited range, it will be measured like the simulation: a uniform distribution.
A zero value could be measured on a meter with a range starting at zero, as if the system behaves as an exponential distribution. Taking a limited number of measurements, the ratios of the then found standard deviations s and s_r to those found after infinite measurements, will not be independent of the sort of distribution. In other words: t depends on the sort of probability distribution function, describing the measurements.

Stability and drift

The standard deviation is only a measure for the type A contribution **during** the period in which the series of measurements take place. This type A contribution originates from the stability of the measured value on the one hand and the stability of the measurement equipment on the other hand. Since for a calibration only little time is available, the described procedure renders only a value for the **short time stability** of equipment and measured value. The short term stability of this system is a consequence of fluctuations on a short time scale. Information on the fluctuation of the system on a longer time scale can only be obtained by regular recalibration of that system. This **long term stability** will very often be a consequence of the drift of the components:
Take for instance a resistor: when manufactured the materials used for the resistor are stressed mechanically. Due to, amongst others, aging and thermal cycling these stresses may relax. This causes the resistance value to decrease. On the other hand oxidation may occur, to result in a slow decrease of the resistance value. For resistance thermometers these effects may be accounted for by thermal treatment during a calibration. In the case of a standard resistance this, for obvious reasons, is not very well possible.
In such clear cases one is able to forecast the drift of the system by regular calibration. When the system is new it has to be recalibrated with short time intervals in order to get sufficient information on the drift. These initial time intervals τ_i have to be chosen short in comparison with the required uncertainty u divided by the expectation value of the drift d:

$$\tau_i << u/d$$

When one has sufficient information on the drift one can make the recalibration interval longer. Evidently for a complex system the recalibration interval has to remain short always. Since drift or stability are usually not measured -or rather analyzed- statistically, one could call this component a type B component.

Type B components

In most measuring systems, the main contribution to the uncertainty is from not statistical (type B) components. Here we list a few of the possible type B contributions.

Temperature and pressure error

When an instrument is calibrated, it attains the temperature of the environment. If during use the environmental temperature is different, the instrument can be in error. Electrical components like resistances are temperature dependent, capacitors can be dependent of pressure. Sometimes the temperature dependence is specified by the manufacturer and can then be -partly- compensated for. In

other situations one has to estimate this error or test the instrument on its temperature and pressure dependence. Usually the temperature dependence of an instrument is of more influence than its pressure dependence.

frictional error
An indication of a mechanical instrument can be in error due to friction of its moving parts. The size of this error can be estimated during a calibration, by reading indicated values with both an increasing reference and a decreasing reference. The difference is a result of the frictional error of the instrument.

thermo-electricity
Like in a thermocouple, in any wire subjected to a temperature difference a thermo electrical voltage will occur. If improper connection wires are used this effect may cause error for both voltage measurements and resistance measurements, since resistance measurement consists of measuring a voltage resulting from a supplied current. This effect will be larger if different materials are used in an electrical circuit. This effect can partly be measured by interchanging connecting wires. It can be compensated for in a resistance measurement by using an instrument capable of alternating the measurement current. If one uses good copper leads and "low thermal connectors" these effects can be quite small (of the order of 1 μV). Worst case values can be reached of 0.1 mV for very badly designed systems.

Discontinuity error
Were one to measure a value equal to 30.5 with an instrument that does not indicate decimal figures, the discontinuity error would be 0.5.

Parallax error
If an index (needle) of an instrument is located at a certain distance of the scale, one could make reading errors. These errors can be prevented or minimized by looking under a fixed angle to the meter at all measurements. Many meters have a mirror on the scale. One than has to adjust the meter until the index covers its image.

Linearity error
If a meter has been calibrated in a range on one value only (apart from a zero check), the meter can have a different deviation from the calibration result, for other values in the range. The linearity usually will have to be checked during a calibration by taking more than one measurements on one scale.

Uncertainty
In order to be able to know the uncertainty with which one measures one has to know -or have estimated- all the components which contribute to that uncertainty. To do that one has to localize each and every uncertainty source in the measuring system (the above list can help to get started). Per source one has to measure or estimate the uncertainty contribution and express it in the same "unit" to be able to compare them. Unit then does not only mean that one has to express all uncertainties in millivolts for instance: they have to be expressed in one standard deviation. In practice this will be rather difficult or even impossible.
In those cases one estimates a contribution in such a way, that for more than about 70 % the measured values will not deviate (as a consequence of this contribution only!) more than the interval, produced by this estimate. Since one has to be "on the safe side" always this estimate will very often result in twice, or even more, the 70 % limits.

APPENDIX I

MPM 4007/ MPM 4000 Water Quality Measurement

ether used as a handheld lab-quality instrument for gle measurement analysis or configured to automatically file water quality conditions in harsh environments, the y portable MPM 4007, used with the MPM 4000 data- ger brings back datalogged information to be stored, alysed and displayed in report format.

- Six probe sockets as standard
- Single and multichannel measurements at the press of a button
- Expandable to 32 channels for simultaneous monitoring and logging
- Individual probes for Temperature, pH/ORP, Conductivity/Salinity/TDS, Dissolved Oxygen, Turbidity, Ion Concentration, or use the multichannel 803PS Water Quality Sonde
- 4–20mA/0–10V dc inputs for user sensors
- Custom calibration
- On-site or laboratory use

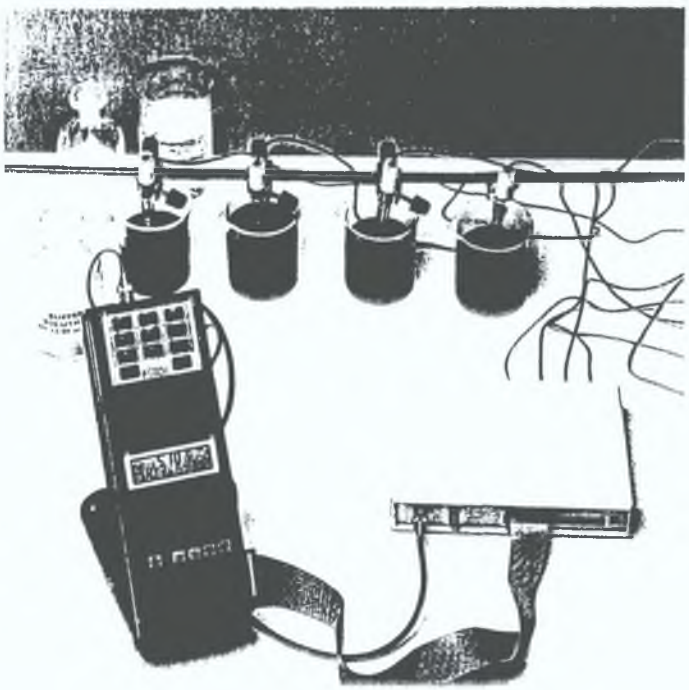

000 MiniLAB

e 4000 MiniLAB system incorporates the MPM 4000 alogger, MPM 4007 module and 803PS Sonde. A dura- , compact package, the MiniLAB may be left for months he most severe environments, where it will record or nsmit data following preset datalogging routines.

e MiniLAB is ideal for water quality surveys, effluent mit verification, bioassay validation, process monitoring l can be used in rivers, lakes, estuaries, oceanic sites, ver and wastewater systems, industrial discharge sites, undwater wells, fisheries and hatcheries and industrial cesses.

Water Quality Probes

803PS Sonde
Compact, immersible multichannel probe, measures pH, temperature, conductivity/salinity/TDS and dissolved oxygen, plus optional turbidity, ammonia/ammonium, depth, ORP and ion concentration.

pH & redox
A range of combination electrodes, complete with temperature sensor (Pt 100) to suit a variety of uses.

Conductivity & Salinity
For measurement of real and temperature compensated conductivity, salinity, TDS and resistance.

Dissolved Oxygen
For measurement of concentration (ppm) and % saturation.

Ion Concentration
A wide range of ion selective electrodes for measurement of ion concentration.

Ammonium
For measurement of NH_4/NH_3. The MPM 4000 can display/log calculated NH_3 from NH_4, pH and temperature inputs.

Turbidity
Direct measurement for highly turbid solutions and corrected Nephelometric technique for pure water determinations.

Temperature Pt 100
Wide range of probes including high temperature, laboratory, waterproof and air/gas.